



HAL
open science

Glasses and aging: A Statistical Mechanics Perspective

Francesco Arceri, François P. Landes, Ludovic Berthier, Giulio Biroli

► **To cite this version:**

Francesco Arceri, François P. Landes, Ludovic Berthier, Giulio Biroli. Glasses and aging: A Statistical Mechanics Perspective. Encyclopedia of Complexity and Systems Science (Living Reference), 2022, 10.1007/978-3-642-27737-5_248-2 . hal-02942375

HAL Id: hal-02942375

<https://inria.hal.science/hal-02942375>

Submitted on 1 Apr 2022

HAL is a multi-disciplinary open access archive for the deposit and dissemination of scientific research documents, whether they are published or not. The documents may come from teaching and research institutions in France or abroad, or from public or private research centers.

L'archive ouverte pluridisciplinaire **HAL**, est destinée au dépôt et à la diffusion de documents scientifiques de niveau recherche, publiés ou non, émanant des établissements d'enseignement et de recherche français ou étrangers, des laboratoires publics ou privés.

Glasses and aging: A Statistical Mechanics Perspective

Francesco Arceri,¹ François P. Landes,² Ludovic Berthier,^{3,4} and Giulio Biroli⁵

¹*Department of Physics, University of Oregon, Eugene, Oregon 97403, USA*

²*TAU, LRI, Université Paris Sud, CNRS, INRIA, Université Paris Saclay, Orsay 91405, France*

³*Laboratoire Charles Coulomb (L2C), Université de Montpellier, CNRS, 34095 Montpellier, France.*

⁴*Department of Chemistry, University of Cambridge,
Lensfield Road, Cambridge CB2 1EW, United Kingdom.*

⁵*Laboratoire de Physique de l'École normale supérieure, Université PSL,
CNRS, Sorbonne Université, Université Paris-Diderot, Paris, France*

(Dated: June 18, 2020)

CONTENTS

I. Glossary	1	C. Geometric frustration, avoided criticality, and locally preferred structures	25
II. Definition of the subject	2	1. Geometric frustration	25
III. Phenomenology	3	2. Coulomb frustrated theories	25
A. Basic facts	3	3. Locally preferred structures	26
B. Static and dynamic correlation functions	5	VIII. Mean-field theory of the amorphous phase	26
IV. Taxonomy of ‘glasses’ in science	6	A. Mean-field glassy phase diagrams	26
A. Colloidal glass transition	6	B. Jamming	28
B. Jamming transition	7	C. Vibrational properties	29
C. Granular glass transition	7	D. Rheology	29
D. Active glasses	7	IX. New computational methods	30
E. Random pinning glass transition	8	A. The Swap Monte-Carlo method	30
F. Ultrastable glasses	8	B. Franz-Parisi potential	31
G. Other glasses in physics, and beyond	9	C. Point-to-set lengthscale	32
V. Numerical simulations	9	D. s -ensemble and large deviations	33
VI. Dynamic heterogeneity	11	E. Machine Learning developments	34
A. Existence of spatio-temporal dynamic fluctuations	11	X. Aging and off-equilibrium dynamics	34
B. Multi-point correlation functions	13	A. Why aging?	34
C. Non-linear response function	15	B. Memory and rejuvenation effects	35
VII. Theory of the glass transition	16	C. Mean-field aging and effective temperatures	36
A. Random First Order Transition Theory	17	D. Beyond mean-field: Real Space	38
1. Mean-field models and a zest of replica theory	17	E. Beyond mean-field: Energy Landscape	40
2. Liquids and glasses in infinite dimensions	18	F. Driven glassy materials	40
3. Random first order transitions	18	XI. Future directions	41
4. Heterogeneous disorder and mapping to the Random Field Ising Model	21	Acknowledgments	41
5. Renormalization group for the glass transition	21	References	42
B. Free volume, defects, and facilitated models	22		
1. Lattice gases	22		
2. Free volume, dynamic criticality	22		
3. Defects: connection with Hamiltonian dynamics models	24		
4. Connection with other perspectives	24		

I. GLOSSARY

We start with a few concise definitions of the most important concepts discussed in this article.

Glass transition—For molecular liquids, the glass transition denotes a crossover from a viscous liquid to an amorphous solid. Experimentally, the crossover takes place at the glass temperature, T_g , conventionally defined as the temperature where the liquid’s viscosity reaches the arbitrary value of 10^{12} Pa.s. The glass transition

more generally applies to many different condensed matter systems where a crossover or, less frequently, a true phase transition, takes place between an ergodic phase and a frozen, amorphous glassy phase.

Aging—In the glass phase, disordered materials are characterized by relaxation times that exceed common observation timescales, so that a material quenched in its glass phase never reaches equilibrium (neither a metastable equilibrium). It exhibits instead an aging behaviour during which its physical properties keep evolving with time.

Dynamic heterogeneity—Relaxation spectra of dynamical observables, e.g. the dynamical structure factor, are very broad in supercooled liquids. This is associated to a spatial distribution of timescales: at any given time, different regions in the liquid relax at different rates. Since the supercooled liquid is ergodic, slow regions eventually become fast, and vice versa. Dynamic heterogeneity refers to the existence of these non-trivial spatio-temporal fluctuations in the local dynamical behaviour, a phenomenon observed in virtually all disordered systems with slow dynamics.

Effective temperature—An aging material relaxes very slowly, trying (in vain) to reach its equilibrium state. During this process, the system probes states that do not correspond to thermodynamic equilibrium, so that its thermodynamic properties can not be rigorously defined. Any practical measurement of its temperature becomes a frequency-dependent operation. A ‘slow’ thermometer tuned to the relaxation timescale of the aging system measures an effective temperature corresponding to the ratio between spontaneous fluctuations (correlation) and linear response (susceptibility). This corresponds to a generalized form of the fluctuation-dissipation theorem for off-equilibrium materials.

Frustration—Impossibility of simultaneously minimizing all the interaction terms in the energy function of the system. Frustration might arise from quenched disorder (as in the spin glass models), from competing interactions (as in geometrically frustrated magnets), or from competition between a ‘locally preferred order’, and global, e.g. geometric, constraints (as in hard spheres packing problems).

Marginal Stability—Systems are marginally stable when the number of external inputs controlling their stability is just enough to constrain all their degrees of freedom (think of a table with three legs). Marginally stable systems display an excess of zero-energy modes which makes them highly susceptible to external perturbations, and prone to extensive rearrangements.

II. DEFINITION OF THE SUBJECT

Glasses belong to a seemingly well-known state of matter: we easily design glasses with desired mechanical or optical properties on an industrial scale, they are widely present in our daily life. Yet, a deep microscopic under-

standing of the glassy state of matter remains a challenge for condensed matter physicists [1–3]. Glasses share similarities with crystalline solids (they are both mechanically rigid), but also with liquids (they both have similar disordered structures at the molecular level). It is mainly this mixed character that makes them fascinating objects, even to non-scientists.

A glass can be obtained by cooling the temperature of a liquid below its glass temperature, T_g . The quench must be fast enough, such that the more standard first order phase transition towards the crystalline phase is avoided. The glass ‘transition’ is not a thermodynamic transition at all, since T_g is only empirically defined as the temperature below which the material has become too viscous to flow on a ‘reasonable’ timescale (and it is hard to define the word ‘reasonable’ in any reasonable manner). Therefore, T_g cannot play a very fundamental role, as a phase transition temperature would. It is simply the temperature below which the material looks solid on the timescale of the observer. When quenched in the glass phase below T_g , liquids slowly evolve towards an equilibrium state they will never reach on experimental timescales. Physical properties are then found to evolve slowly with time in far from equilibrium states, a process known as ‘aging’ [4].

Describing theoretically and quantifying experimentally the physical mechanisms responsible for the viscosity increase of liquids approaching the glass transition and for aging phenomena below the glass transition certainly stand as central open challenges in condensed matter physics. Since statistical mechanics aims at understanding the collective behaviour of large assemblies of interacting objects, it comes as no surprise that it is a central tool in the glass field. We shall therefore summarize the understanding gained from statistical mechanics perspectives into the problem of glasses and aging.

The subject has quite broad implications. A material is said to be ‘glassy’ when its typical relaxation timescale becomes of the order of, and often much larger than, the typical duration of an experiment or a numerical simulation. Under this generic definition, a large number of systems can be considered as glassy [5]. One can be interested in the physics of liquids (window glasses are then the archetype), in ‘hard’ condensed matter (for instance type II superconductors in the presence of disorder such as high- T_c superconductors), charge density waves or spin glasses, ‘soft’ condensed matter with numerous complex fluids such as colloidal assemblies, emulsions, foams, but also granular materials, proteins, etc. All these materials exhibit, in a part of their phase diagrams, some sort of glassy dynamics characterized by a very rich phenomenology with effects such as aging, hysteresis, creep, memory, effective temperatures, rejuvenation, dynamic heterogeneity, non-linear response, etc.

This long list explains why this research field has received increasing attention from physicists in the last four decades. ‘Glassy’ topics now go much beyond the physics of simple liquids (glass transition physics) and

models and concepts developed for one system often find applications elsewhere in physics, from algorithmics to biophysics [6]. Motivations to study glassy materials are numerous. Glassy materials are everywhere around us and therefore obviously attract interest beyond academic research. At the same time, the glass conundrum provides theoretical physicists with deep fundamental questions since classical tools are sometimes not sufficient to properly account for the glass state. Moreover, numerically simulating the dynamics of microscopically realistic material on timescales that are experimentally relevant remains a difficult challenge, even with modern computers.

Studies on glassy materials constitute an exciting research area where experiments, simulations and theoretical calculations can meet, where both applied and fundamental problems are considered. How can one observe, understand, and theoretically describe the rich phenomenology of glassy materials? What are the fundamental quantities and concepts that emerge from these descriptions?

The outline of the article is as follows. In Sec. III the phenomenology of glass-forming liquids is discussed. In Sec. IV different types of glasses are described. We then describe how computer simulations can provide deep insights into the glass problem in Sec. V. The issue of dynamic heterogeneity is tackled in Sec. VI. The main theoretical perspectives currently available in the field are then summarized in Sec. VII. The mean-field analysis of the amorphous solid phase is reviewed in Sec. VIII. In Sec. IX, we discuss novel developments in computational studies. Aging and off-equilibrium phenomena occupy Sec. X. Finally, issues that seem important for future research are discussed in Sec. XI.

III. PHENOMENOLOGY

A. Basic facts

A vast majority of liquids (molecular liquids, polymeric liquids, etc) form a glass if cooled fast enough in order to avoid the crystallisation transition [1]. Typical values of cooling rate in laboratory experiments are 0.1 – 100 K/min. The metastable phase reached in this way is called ‘supercooled liquid’. In this regime the typical timescales increase in a dramatic way and they end up to be many orders of magnitudes larger than microscopic timescales at T_g , the glass transition temperature.

For example, around the melting temperature T_m , the typical timescale τ_α on which density fluctuations relax, is of the order of $\sqrt{ma^2/K_B T}$, which corresponds to few picoseconds (m is the molecular mass, T the temperature, K_B the Boltzmann constant and a a typical distance between molecules). At T_g , which as a rule of thumb is about $\frac{2}{3}T_m$, this timescale τ_α has become of the order of 100 s, i.e. 14 orders of magnitude larger! This phenomenon is accompanied by a concomitant increase

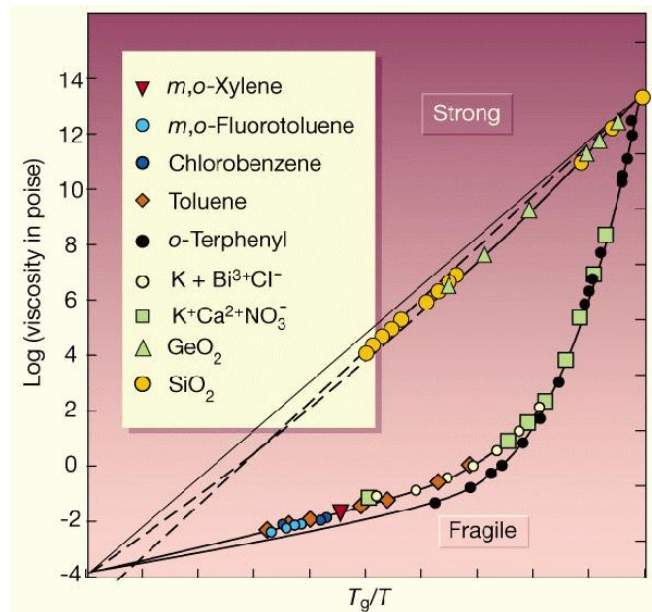


FIG. 1. Arrhenius plot of the viscosity of several glass-forming liquids approaching the glass temperature T_g [2]. For ‘strong’ glasses, the viscosity increases in an Arrhenius manner as temperature is decreased, $\log \eta \sim E/(K_B T)$, where E is an activation energy and the plot is a straight line, as for silica. For ‘fragile’ liquids, the plot is bent and the effective activation energy increases when T is decreased towards T_g , as for ortho-terphenyl.

of the shear viscosity η . This can be understood by a simple Maxwell model in which η and τ are related by $\eta = G_\infty \tau_\alpha$, where G_∞ is the instantaneous (elastic) shear modulus which does not vary considerably in the supercooled regime. In fact, viscosities at the glass transition temperature are of the order of 10^{12} Pa.s. In order to grasp how viscous this is, recall that the typical viscosity of water (or wine) at ambient temperature is of the order of 10^{-2} Pa.s. How long would one have to wait to drink a glass of wine with a viscosity 10^{14} times larger?

As a matter of fact, the temperature at which the liquid does not flow anymore and becomes an amorphous solid, called a ‘glass’, is protocol dependent. It depends on the cooling rate and on the patience of the person carrying out the experiment: solidity is a timescale-dependent notion. Pragmatically, T_g is defined as the temperature at which the shear viscosity is equal to 10^{13} Poise (also 10^{12} Pa.s).

The increase of the relaxation timescale of supercooled liquids is remarkable not only because of the large number of decades involved but also because of its temperature dependence. This is vividly demonstrated by plotting the logarithm of the viscosity (or of the relaxation time) as a function of T_g/T , as in Fig. 1. This is called the ‘Angell’ plot [1], which is very helpful in classifying supercooled liquids. A liquid is called strong or fragile depending on its position in the Angell plot. Straight lines correspond to ‘strong’ glass-formers and to an Arrhenius

Substance	o-terphenyl	2-methyltetra-hydrofuran	n-propanol	3-bromopentane
T_g	246	91	97	108
T_0	202.4	69.6	70.2	82.9
T_K	204.2	69.3	72.2	82.5
T_K/T_0	1.009	0.996	1.028	0.995

TABLE I. Values of glass transition temperature, VFT singularity and Kauzmann temperatures for four supercooled liquids [7].

behaviour. In this case, one can extract from the plot an effective activation energy, suggesting quite a simple mechanism for relaxation, for instance by ‘breaking’ locally a chemical bond. The typical relaxation time is then dominated by the energy barrier to activate this process and, hence, has an Arrhenius behaviour. Window glasses fall in this category [8]. If one tries to define an effective activation energy for fragile glass-formers using the slope of the curve in Fig. 1, then one finds that this energy scale increases when the temperature decreases, a ‘super-Arrhenius’ behaviour. This increase of energy barriers immediately suggests that glass formation is a collective phenomenon for fragile supercooled liquids. Support for this interpretation is provided by the fact that a good fit of the relaxation time or the viscosity is given by the Vogel-Fulcher-Tamman law (VFT):

$$\tau_\alpha = \tau_0 \exp \left[\frac{DT_0}{(T - T_0)} \right], \quad (1)$$

which suggests a divergence of the relaxation time, and therefore a phase transition of some kind, at a finite temperature T_0 . A smaller D in the VFT law corresponds to a more fragile glass. Note that there are other comparably good fits of these curves, such as the Bässler law [9],

$$\tau_\alpha = \tau_0 \exp \left(K \left(\frac{T_*}{T} \right)^2 \right), \quad (2)$$

that only lead to a divergence at zero temperature. Actually, although the relaxation time increases by 14 orders of magnitude, the increase of its logarithm, and therefore of the effective activation energy is very modest, and experimental data do not allow one to unambiguously determine the true underlying functional law without any reasonable doubt. For this and other reasons, physical interpretations in terms of a finite temperature phase transition must always be taken with a grain of salt.

However, there are other experimental facts that shed some light and reinforce this interpretation. Among them is an empirical connection found between kinetic and thermodynamic behaviours. Consider the part of the entropy of liquids, S_{exc} , which is in excess compared to the entropy of the corresponding crystal. Once this quantity, normalized by its value at the melting temperature, is plotted as a function of T , a remarkable connection with the dynamics emerges. As for the relaxation time one cannot follow this curve below T_g in thermal equilibrium. However, extrapolating the curve below T_g apparently indicates that the excess entropy vanishes at

some finite temperature, called T_K , which is very close to zero for strong glasses and, generically, very close to T_0 , the temperature at which a VFT fit diverges. This coincidence is quite remarkable: for materials with glass transition temperatures that vary from 50 K to 1000 K the ratio T_K/T_0 remains close to 1, up to a few percents. Examples reported in Ref. [7] are provided in Table I.

The chosen subscript for T_K stands for Kauzmann [10], who recognized T_K as an important temperature scale for glasses. Kauzmann further claimed that some change of behaviour (phase transition, crystal nucleation, etc.) must take place above T_K , because below T_K the entropy of the liquid, a disordered state of matter, becomes less than the entropy of the crystal, an ordered state of matter. The situation that seemed paradoxical at that time is actually not a serious conceptual problem [3, 11]. There is no general principle that constrains the entropy of the liquid to be larger than that of the crystal. As a matter of fact, the crystallisation transition for hard spheres takes place precisely because the crystal becomes the state with the largest entropy at sufficiently high density [12].

On the other hand, the importance of T_K stands, partially because it is experimentally very close to T_0 . Additionally, the quantity S_{exc} which vanishes at T_K , is thought to be a proxy for the so-called configurational entropy, S_c , which quantifies the number of metastable states. A popular physical picture due to Goldstein [13] is that close to T_g the system explores a part of the energy landscape (or configuration space) which is full of minima separated by barriers that increase when temperature decreases. The dynamic evolution in the energy landscape would then consist in a rather short equilibration inside a minimum followed by infrequent ‘jumps’ between different minima. At T_g the barriers between states become so large that the system remains trapped in one minimum, identified as one of the possible microscopic amorphous configurations of a glass. Following this interpretation, one can split the entropy into two parts. A first contribution is due to the fast relaxation inside one minimum and a second one, called the ‘configurational’ entropy, counts the number of metastable states: $S_c = \log N_{\text{metastable}}$. Assuming that the contribution to the entropy due to the ‘vibrations’ around an amorphous glass configuration is not very different from the entropy of the crystal, one finds that $S_{\text{exc}} \approx S_c$. In that case, T_K would correspond to a temperature at which the configurational entropy vanishes. This in turn would lead to a discontinuity (a downward jump) of the specific heat

and would truly correspond to a thermodynamic phase transition.

B. Static and dynamic correlation functions

At this point the reader might have reached the conclusion that the glass transition may not be such a difficult problem: there are experimental indications of a diverging timescale and a concomitant singularity in the thermodynamics. It simply remains to find static correlation functions displaying a diverging correlation length related to the emergence of ‘amorphous order’, which would indeed classify the glass transition as a standard second order phase transition. Remarkably, this conclusion remains an open and debated question despite several decades of research. Simple static correlation functions are quite featureless in the supercooled regime, notwithstanding the dramatic changes in the dynamics. A simple static quantity is the structure factor defined by

$$S(q) = \left\langle \frac{1}{N} \delta\rho_{\mathbf{q}} \delta\rho_{-\mathbf{q}} \right\rangle, \quad (3)$$

where the Fourier component of the density reads

$$\delta\rho_{\mathbf{q}} = \sum_{i=1}^N e^{i\mathbf{q}\cdot\mathbf{r}_i} - \frac{N}{V} \delta_{\mathbf{q},0}, \quad (4)$$

with N is the number of particles, V the volume, and \mathbf{r}_i is the position of particle i . The structure factor measures the spatial correlations of particle positions, but it does not show any diverging peak in contrast to what happens, for example, at the liquid-gas critical point where there is a divergence at small \mathbf{q} . More complicated static correlation functions have been studied [14], especially in numerical work, but until now there are no strong indications of a diverging, or at least substantially growing, static lengthscale [15–17]. A snapshot of a supercooled liquid configuration in fact just looks like a glass configuration, despite their widely different dynamic properties [11]. What happens then at the glass transition? Is it a transition or simply a dynamic crossover? A more refined understanding can be gained by studying dynamic correlations or response functions.

A dynamic observable studied in light and neutron scattering experiments is the intermediate scattering function,

$$F(\mathbf{q}, t) = \left\langle \frac{1}{N} \delta\rho_{\mathbf{q}}(t) \delta\rho_{-\mathbf{q}}(0) \right\rangle. \quad (5)$$

Different $F(\mathbf{q}, t)$ measured by neutron scattering in supercooled glycerol [18] are shown for different temperatures in Fig. 2. These curves show a first, rather fast, relaxation to a plateau followed by a second, much slower, relaxation. The plateau is due to the fraction of density fluctuations that are frozen on intermediate timescales,

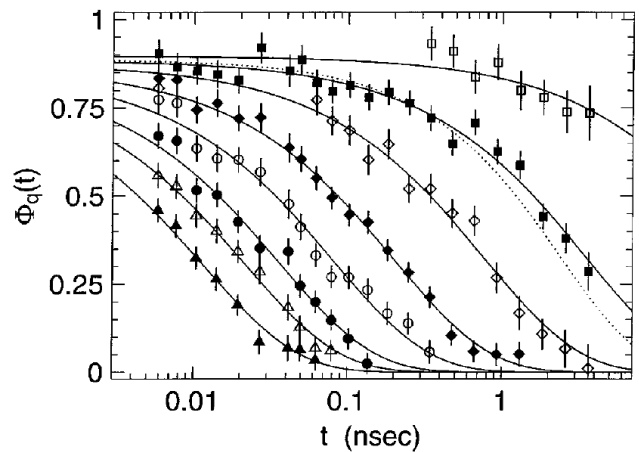


FIG. 2. Temperature evolution of the intermediate scattering function normalized by its value at time equal to zero for supercooled glycerol [18]. Temperatures decrease from 413 K to 270 K from right to left. The solid lines are fit with a stretched exponential with exponent $\beta = 0.7$. The dotted line represents another fit with $\beta = 0.82$.

but eventually relax during the second relaxation. The latter is called ‘alpha-relaxation’, and corresponds to the structural relaxation of the liquid. This plateau is akin to the Edwards-Anderson order parameter q_{EA} defined for spin glasses, which measures the fraction of frozen spin fluctuations [19]. Note that q_{EA} continuously increases from zero at the spin glass transition. Instead, for structural glasses, a finite plateau value already appears above any transition.

The intermediate scattering function can be probed only on a relatively small regime of temperatures. In order to track the dynamic slowing down from microscopic to macroscopic timescales, other correlators have been studied. A popular one is obtained from the dielectric susceptibility, which is related by the fluctuation-dissipation theorem to the time correlation of polarization fluctuations. It is generally admitted that different dynamic probes reveal similar temperature dependencies of the relaxation time. The temperature evolution of the imaginary part of the dielectric susceptibility, $\epsilon''(\omega)$, is shown in Fig. 3 which covers a very wide temperature window [20]. At high temperature, a good representation of the data is given by a Debye law, $\epsilon(\omega) = \epsilon(\infty) + \Delta\epsilon/(1 + i\omega\tau_\alpha)$, which corresponds to an exponential relaxation in the time domain. When temperature is decreased, however, the relaxation spectra become very broad and strongly non-Debye. One particularly well-known feature of the spectra is that they are well fitted, in the time domain, for times corresponding to the alpha-relaxation with a stretched exponential, $\exp(-(t/\tau_\alpha)^\beta)$. In the Fourier domain, forms such as the Havriliak-Negami law are used, $\epsilon(\omega) = \epsilon(\infty) + \Delta\epsilon/(1 + (i\omega\tau_\alpha)^\alpha)^\gamma$, which generalizes the Debye law. The exponents β , α and γ depend in general on temperature and on the particular dynamic probe chosen, but they capture the fact that

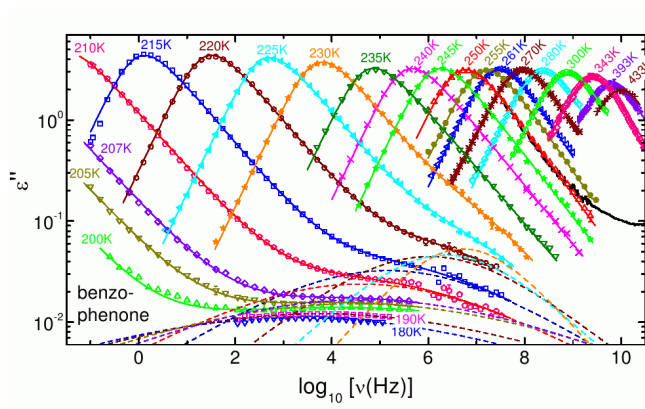


FIG. 3. Temperature evolution of the dielectric susceptibility of the glass-former benzophenone measured over more than 10 decades of relaxation times [20]. Dynamics slows down dramatically as temperature is decreased and relaxation spectra become very broad at low temperature.

relaxation is increasingly non-exponential when T decreases towards T_g . A connection was empirically established between fragility and degree of non-exponentiality, more fragile liquids being characterized by broader relaxation spectra [2].

To sum up, there are many remarkable phenomena that take place when a supercooled liquid approaches the glass transition. Striking ones have been presented, but many others have been left out for lack of space [1, 2, 14, 19, 21]. We have discussed physical behaviours, relationships or empirical correlations observed in a broad class of materials. This is quite remarkable and suggests that there is some physics (and not only chemistry) to the problem of the glass transition, which we see as a collective (critical?) phenomenon which should be relatively independent of microscopic details. This justifies our statistical mechanics perspective on this problem.

IV. TAXONOMY OF ‘GLASSES’ IN SCIENCE

We now introduce a wider range of systems whose phenomenological behaviour is close or related to the one of glass-forming liquids, showing that glassiness is truly ubiquitous. It does not only appear in many different physical situations but also in more abstract contexts, such as computer science.

A. Colloidal glass transition

Colloidal suspensions consist of large particles suspended in a solvent [22]. The typical radii of the particles are in the range $R = 1 - 500$ nm. The solvent, which is at equilibrium at temperature T , renders the short-time dynamics of the particles Brownian. The microscopic timescale for this diffusion is given by $\tau = R^2/D$ where D

is the short-time self-diffusion coefficient. A typical value is of the order of $\tau \sim 1$ ms, which is thus much larger than microscopic timescales for molecular liquids (in the picosecond regime). The interaction potential between particles depends on the systems, and this large tunability makes colloids very attractive objects for technical applications. A particularly relevant case, on which we will focus in the following, is a purely hard sphere potential, which is zero when particles do not overlap and infinite otherwise. In this case the temperature scale becomes an irrelevant number, apart from a trivial rescaling of the microscopic timescale. Colloidal hard sphere systems have been intensively studied [22] in experiments, simulations and theory, varying their density ρ , or their volume fraction $\varphi = \frac{4}{3}\pi R^3\rho$. Hard spheres display a fluid phase from $\varphi = 0$ to intermediate volume fractions, a freezing-crystallisation transition at $\varphi \simeq 0.494$, and a melting transition at $\varphi \simeq 0.545$. Above this latter value the system can be compressed until the close packing point $\varphi \simeq 0.74$, which corresponds to the FCC crystal. Interestingly for our purposes, a small amount of size polydispersity can suppress crystallization. In this case, the system can be ‘supercompressed’ above the freezing transition without nucleating the crystal, at least on experimental timescales. In this regime the relaxation timescale increases very fast [23]. At a packing fraction $\varphi_g \simeq 0.58 - 0.60$ it becomes so large compared to typical experimental timescales that the system does not relax anymore: it is frozen. This ‘colloidal glass transition’ is obviously reminiscent of the glass transition of molecular systems. In particular, the location φ_g of the colloidal glass transition is as ill-defined as the glass temperature T_g .

Actually, the phenomena that take place when increasing the volume fraction are analogous to the ones seen in molecular supercooled liquid when decreasing temperature: the relaxation timescales increases very fast and can be fitted [24, 25] by a VFT law in density similar to Eq. (1), dynamical correlation functions display a broad spectrum of timescales and develop a plateau, no static growing correlation length has been found, etc. Also the phenomenon of dynamic heterogeneity that will be addressed in Sec. VI is also observed in colloids [26, 27]. However, it is important to underline a major difference: because the microscopic timescale for colloids is so large, experiments can only track the first 5 decades of slowing down. A major consequence is that the comparison between the glass and colloidal transitions must be performed by focusing in both cases on the first 5 decades of the slowing down, which corresponds to relatively high temperatures in molecular liquids [28]. Understanding how much and to what extent the glassiness of colloidal suspensions is related to the one of molecular liquids remains an active domain of research. Recently, by using colloids of smaller size and hence decreasing the microscopic timescale τ , it has been possible to explore a larger range of relaxation times [29]. This is a very promising research direction to explore the colloidal glassy regime.

B. Jamming transition

Every day life offers many examples of jammed solids. Grains and beans poured into a container, foams and emulsions produced by a large shear stress, sand and colloidal particles under very high pressure. Depending on how compressed they are, these materials behave as fluids or solids: a handful of sand will flow from our open hand, while we experience rigidity when closing the fist. Formally, the jamming transition is reached at infinite pressure when all the droplets, bubbles or colloids are forced to come into enduring kissing contact with one another [30, 31]. All these systems share a fundamental feature: they can be considered athermal in the sense that thermal fluctuations at room-temperature are, by far, not able to allow the system to explore its phase space.

As an immediate consequence, the glass and jamming transitions are of a very different nature. The former describes a fluid-to-solid transition in a system controlled by thermal fluctuations, and its location depends on the cooling or compression rate. The latter is a purely geometrical transition happening at $T = 0$ in the absence of any dynamics, but it also corresponds to the change between a viscous liquid to a solid mechanical response [32]. In recent years, the connection between the two phenomena has been elucidated [33], and both transitions can be observed under different physical conditions in the hard spheres model.

C. Granular glass transition

Driven granular media represent another family of systems that have recently been studied from the point of view of their glassiness. Grains are macroscopic objects and, as a consequence, are not affected by thermal fluctuations. A granular material is therefore frozen in a given configuration if no energy is injected into the system [34]. However, it can be forced in a steady state by an external drive, such as shearing or tapping. The dynamics in this steady state shows remarkable similarities (and differences) with simple fluids. The physics of granular materials is a very wide subject [34]. In the following we only address briefly what happens to a polydisperse granular fluid at very high packing fractions. As for colloids, the timescales for relaxation or diffusion increase very fast when density is increased, without any noticeable change in structural properties. It is now established [35–37] that many phenomenological properties of the glass and jamming transitions also occur in granular assemblies. Going beyond the mere analogy and understanding how much colloids and granular materials are related is a very active domain of research.

D. Active glasses

Active matter has recently emerged as a new field in physics [38, 39], fueled by the observation that systems such as a school fish, bacterial colonies and biological tissues display physical properties and phase transitions which can be described by statistical physics tools, and captured by simplified theoretical models. Physical systems mimicking the behaviour of natural systems have also been developed to perform controlled experiments on model systems of active materials. In particular, colloidal particles and macroscopic objects similar to the systems displaying a granular glass transition have also been developed so that these particles can become ‘active’ [40–42], i.e. self-motile objects that can move in the absence of thermal fluctuations, similar to animals, cells or bacteria.

It is natural to expect that dense assemblies of active particles will undergo some form of dynamic arrest [43, 44]. As human beings, we are well aware that it becomes difficult to walk very fast in a dense crowd, as observed in the streets of large cities or in subway corridors at peak times. Indeed, there are several indications from experimental observations that a transition from a fluid-like state to an arrested glassy state can be observed in active materials [44–47].

From a conceptual viewpoint, the main difference between these observations and the glass transition observed in molecular and colloidal systems is that the driving force for single particle motion is not of thermal origin, but is instead chemical, mechanical, or biological. This means that any theoretical model for dense active materials must include some sort of non-equilibrium sources of microscopic motion and consequently the glassy phenomena that will be described must necessarily occur far from equilibrium [48]. In that sense, the situation is conceptually not very different from the phenomenon of the granular glass transition discussed in the previous paragraph. The difference between the two essentially lies in the details of the driving motion, which very much resembles a quasi-equilibrium thermal bath in granular glasses [37].

Several numerical and theoretical studies of the glass transition in active materials have been recently published, see Refs. [49] for a specific review on this topic. In particular, the glassy dynamics of so-called self-propelled particles have received considerable attention [50–55]. In these models, particles interacting with simple pair interactions (similar to the ones studied to model the equilibrium glass transition) are driven by active forces that tend to displace the particles in straight lines over a finite persistence length.

It is now understood that for dense active fluids, due to these non-equilibrium driving forces both the structure and the dynamics are very different from their equilibrium counterparts [49]. It is observed that a large persistence length has a profound influence on the static correlations of the fluid since both density-density (as in

Eq. (3)) and velocity-velocity correlation functions develop non trivial non-equilibrium features [54]. As particle crowding is increased, slow dynamics develop and is accompanied by a phenomenology similar to that of equilibrium glassy materials, with motion becoming gradually arrested at large enough density or small enough activity. Dynamic arrest in dense active materials is therefore called a non-equilibrium glass transition [48]. Understanding this new class of glassy dynamics is an exciting new direction for research.

E. Random pinning glass transition

The standard control parameters used to induce a glass transition are temperature and pressure. A new way introduced in the 2000s is ‘random pinning’ [56, 57], which consists in freezing the positions of a fraction c of particles from an equilibrium configuration of a supercooled liquid. Theoretical arguments [58] and numerical simulations [59, 60] suggested that the dynamics of the remaining free particles slow down and undergo a glass transition by increasing c . The study of the random pinning glass transition has been the focus of several theoretical analyses [61–70] and numerical simulations [59, 71–82] in the decade 2005-2015. It has also been studied in experiments, in particular in colloidal glasses by optical microscopy [83–86].

The interest in the ‘random-pinning glass transition’ has been twofold. First, it represents a new way to test theories of the glass transition. In fact, RFOT theory and MCT (see Sec. VII) predict that it should have the same properties as the usual glass transition [58, 63], i.e. increasing the pinned fraction c plays the same role as lowering the temperature. This phenomenon was studied and confirmed in Ref. [71], where the equilibrium phase diagram of a randomly pinned glass-former was fully characterized. The dynamical behavior is not as well understood. Although it is clear that dynamics dramatically slows down when increasing c , hence the name ‘random-pinning glass transition’, it has proven difficult to disentangle trivial effects due to steric constraints from collective ones. In consequence, numerical simulations could not validate or disprove the competing predictions from dynamical facilitation theories [87] and RFOT theory [58]. The other reason for the random pinning procedure was to produce configurations equilibrated very close to the glass transition (just after pinning, the remaining unpinned particles are in an equilibrium configuration for the constrained systems [88]). This allowed to perform the first computational study of ultrastable glasses [89], see below.

The random pinning procedure has interesting connections, similarities and differences with other ways to constrain the dynamics of glassy liquids introduced in recent years. Those can be grouped in three main categories: modifications of the Hamiltonian (ϵ -coupling, see Sec. IX B), in the dynamical rules (s -ensemble dynamics,

see Sec. IX D), and in the space available to the system (liquids in quenched environments [90]).

F. Ultrastable glasses

Glassy materials are typically prepared by slowly cooling or compressing a dense fluid across the glass transition described above. The glass transition temperature or density is set by the competition between an extrinsic time scale imposed by the experimentalist (for instance the duration of the experiment, or the cooling rate), and an intrinsic timescale of the material, such as the structural relaxation time. The degree of supercooling observed in most glassy materials is then set by the typical duration of an experiment, which corresponds to an intrinsic timescale of about 100 s in molecular liquids.

It has recently become possible to prepare ‘ultrastable’ glasses [91, 92], namely glassy materials which reach a degree of supercooling which is equivalent to cooling glasses at rates that are $10^5 - 10^{10}$ times slower than usual. Ultrastable glasses are not prepared by cooling bulk liquids across the glass transition, but using a completely different route called physical vapor deposition. In this procedure, the glassy material is prepared directly at the desired temperature (there is no cooling involved) by the slow deposition of individual molecules suspended in a gas phase onto a glassy film whose height increases slowly as more molecules are deposited.

The degree of supercooling that can be achieved by physical vapor deposition is again set by the competition between two timescales [91, 93]. The extrinsic timescale is now related to the deposition rate of the molecules, whereas the intrinsic timescale is set by the relaxation time of molecules diffusing at the free surface of the glassy film. It is known that bulk and surface dynamics may differ by many orders of magnitude in glasses [94], because the molecular mobility at a free surface is much less constrained than in the bulk. Therefore, for a similar extrinsic timescale imposed by the experimental setup, a much deeper degree of supercooling is achieved by the vapor deposition process.

Ultrastable glasses prepared using physical vapor deposition are thus expected to behave as extraordinarily-slowly cooled supercooled liquids, with a cooling rate or a preparation time that is impractically large. As such, these glasses have physical properties that can differ rather drastically from ordinary glassy materials. In particular, it was shown that their mechanical, thermodynamic and kinetic properties differ quantitatively from ordinary glasses, and display specific dynamic phenomena [95–100]. As such, they are currently the subject of intense theoretical investigations as well [101–108]. The goal is to better understand the deposition process itself, but also to better characterise the physical properties of ultrastable glasses in view of their many potential practical applications. Also, since ultrastable glasses offer a way to access much deeper supercooled states, it can be

hoped that they can be used to shed new light on the glass transition phenomenon itself.

G. Other glasses in physics, and beyond

There are many other physical contexts in which glassiness plays an important role [5]. One of the most famous examples is the field of spin glasses. Real spin glasses are magnetic impurities interacting by quenched random couplings. At low temperatures, their dynamics become extremely slow and they freeze in amorphous spin configuration dubbed a ‘spin glass’ by Anderson. There are many other physical systems, often characterized by quenched disorder, that show glassy behavior, like Coulomb glasses, Bose glasses, etc. In many cases, however, one does expect quite a different physics from structural glasses: the similarity between these systems is therefore only qualitative.

Quite remarkably, glassiness also emerges in other branches of science [6]. In particular, it has been discovered recently that concepts and techniques developed for glassy systems turn out to apply and be very useful tools in the field of computer science. Problems like combinatorial optimization display phenomena completely analogous to phase transitions, and actually, to glassy phase transitions. *A posteriori*, this is quite natural, because a typical optimization problem consists in finding a solution in a presence of a large number of constraints. This can be defined, for instance, as a set of N Boolean variables that satisfies M constraints. For N and M very large at fixed $\alpha = M/N$, this problem very much resembles finding a ground state in a statistical mechanics problem with quenched disorder. Indeed one can define an energy function (a Hamiltonian) as the number of unsatisfied constraints, that has to be minimized, as in a $T = 0$ statistical mechanics problem. The connection with glassy systems originates from the fact that in both cases the energy landscape is extremely complicated, full of minima and saddles. The fraction of constraints per degree of freedom, α , plays a role similar to the density in a hard sphere system. For instance, a central problem in optimization, random k -satisfiability, has been shown to undergo a glass transition when α increases, analogous to the one of structural glasses [109].

Glassiness also plays an important role in machine learning and signal processing. In those cases, one wants to learn a specific task from many examples or retrieve a specific signal from a huge amount of data. This is done in practice by minimizing a cost function. For example, imagine that one is given a tensor $T_{i_1, i_2, i_3} = v_{i_1} v_{i_2} v_{i_3}$, constructed from a vector v_i ($i = 1, \dots, N$) of norm \sqrt{N} , and that this tensor is corrupted by noise J_{i_1, i_2, i_3} , which for simplicity we take independent and Gaussian for each triple (i_1, i_2, i_3) . The problem called tensor PCA, which appears in image and video analysis [110], consists in retrieving the signal v_i from the noisy tensor $T_{i_1, i_2, i_3} + J_{i_1, i_2, i_3}$. The simplest procedure to solve this

problem is to find the vector x_i minimizing the following cost function:

$$H(\{x_i\}) = \sum_{i_1, i_2, i_3} (v_{i_1} v_{i_2} v_{i_3} + J_{i_1, i_2, i_3} - x_{i_1} x_{i_2} x_{i_3})^2.$$

By developing the square, one finds that the cost function H is identical to the one of a 3-spin spherical glass mean-field model with quenched random couplings J_{i_1, i_2, i_3} and a term favoring configurations in the direction of v_i [111]. These two contributions are competing for determining the ground-state properties, the strength of the latter with respect to the former is proportional to the signal-to-noise ratio. This example illustrates one way in which glassiness plays an important role in machine learning: one has to find a signal (the v_i 's) buried in a rough landscape (induced by the J_{i_1, i_2, i_3} 's). Practical algorithms, such as gradient descent and its stochastic version, lead to dynamics which are very similar to the ones of physical systems after a quench to low temperature. One of the main questions in this area is characterizing the algorithmic threshold, i.e. the critical value of the signal-to-noise ratio such that the original signal can be recovered with some given accuracy. Glassy dynamics plays a central role: it is the main obstacle for recovering the signal, as the dynamics can be lost and trapped in bad minima instead of converging toward the good one correlated with the signal [112].

Finally, hunting for a signal in a rough landscape [113] is not the only context in which glassiness emerged in machine learning in recent years. In fact, more generally, there has been a lot of work aimed at characterizing the landscapes over which optimization dynamics take places in general machine learning problems (from high-dimensional statistics to deep neural networks), and at assessing to which extent glassy dynamics and rough landscapes play a relevant role [114, 115].

V. NUMERICAL SIMULATIONS

Studying the glass transition of molecular liquids at a microscopic level is in principle straightforward since one must answer a very simple question: how do particles move in a liquid close to T_g ? It is of course a daunting task to attempt answering this question experimentally because one should then resolve the dynamics of single molecules to be able to follow the trajectories of objects that are a few Angstroms large on timescales of tens or hundreds of seconds, which sounds like eternity when compared to typical molecular dynamics usually lying in the picosecond regime. In recent years, such direct experimental investigations have been developed using time and space resolved techniques such as atomic force microscopy [116] or single molecule spectroscopy [117, 118], but this remains a very difficult task.

In numerical simulations, by contrast, the trajectory of each particle in the system can, by construction, be

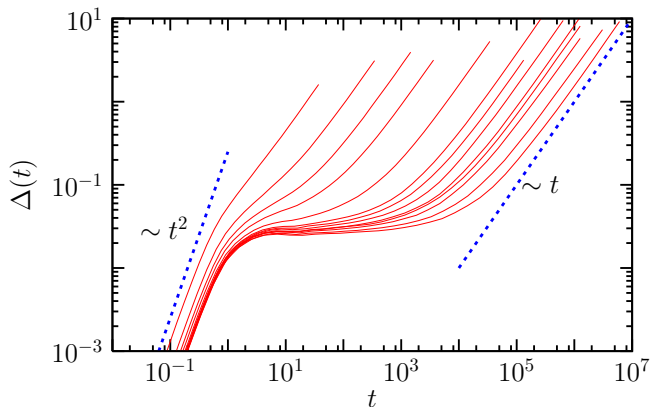


FIG. 4. Mean-squared displacements of individual particles in a simple model of a glass-forming liquid composed of Lennard-Jones particles observed on a wide time window. When temperature decreases (from left to right), the particle displacements become increasingly slow with several distinct time regimes corresponding to (in this order) ballistic, localized, and diffusive regimes.

followed at all times. This allows one to quantify easily single particle dynamics, as proved in Fig. 4 where the averaged mean-squared displacement $\Delta(t)$ measured in a simple Lennard-Jones glass-former is shown and is defined as

$$\Delta(t) = \left\langle \frac{1}{N} \sum_{i=1}^N |\mathbf{r}_i(t) - \mathbf{r}_i(0)|^2 \right\rangle, \quad (6)$$

where $\mathbf{r}_i(t)$ represents the position of particle i at time t in a system composed of N particles and the brackets indicate an ensemble average. The particle displacements considerably slow down when T is decreased and the self-diffusion constant decreases by orders of magnitude, mirroring the behaviour of the viscosity shown in Fig. 1 for real systems. Moreover, a rich dynamics is observed, with a plateau regime at intermediate timescales, corresponding to an extended time window during which particles vibrate around their initial positions, exactly as in a crystalline solid. The difference with a crystal is of course that this localization is only transient, and all particles eventually escape and diffuse at long times with a diffusion constant D_s , so that $\Delta(t) \sim 6D_s t$ when $t \rightarrow \infty$.

In recent years, computer experiments have played an increasingly important role in glass transition studies. It could almost be said that particle trajectories in numerical work have been studied under so many different angles that probably very little remains to be learnt from such studies in the regime that is presently accessible using present day computers. Unfortunately, this does not imply complete knowledge of the physics of supercooled liquids. As shown in Fig. 4, it is presently possible to follow the dynamics of a simple glass-forming liquid over more than eight decades of time, and over a temperature window in which average relaxation timescales increase by more than five decades. This might sound impressive,

but a quick look at Fig. 1 shows, however, that at the lowest temperatures studied in the computer, the relaxation timescales are still orders of magnitude faster than in experiments performed close to the glass transition temperature. They can be directly compared to experiments performed in this high temperature regime, but this also implies that simulations focus on a relaxation regime that is about eight to ten decades of times faster than in experiments performed close to T_g . Whether numerical works are useful to understand the kinetics of the glass transition itself at all is therefore an open, widely debated, question. We believe that it is now possible to numerically access temperatures which are low enough that many features associated to the glass transition physics can be observed: strong decoupling phenomena, clear deviations from fits to the mode-coupling theory (which are experimentally known to hold only at high temperatures), and crossovers towards truly activated dynamics. In Sec. IX, we discuss recent developments in the field of computational studies that are able to address novel challenges regarding the static properties of supercooled liquids over a broad temperature range.

Classical computer simulations of supercooled liquids usually proceed by solving a cleverly discretized version of Newton's equations for a given potential interaction between particles [119]. If quantitative agreement with experimental data on an existing specific material is sought, the interaction must be carefully chosen in order to reproduce reality, for instance by combining classical to *ab-initio* simulations. From a more fundamental perspective one rather seeks the simplest model that is still able to reproduce qualitatively the phenomenology of real glass-formers, while being considerably simpler to study. The implicit, but quite strong, hypothesis is that molecular details are not needed to explain the behaviour of supercooled liquids, so that the glass transition is indeed a topic for statistical mechanics, not for chemistry. A considerable amount of work has therefore been dedicated to studying models such as hard spheres, soft spheres, or Lennard-Jones particles. More realistic materials are also studied focusing for instance on the physics of network forming materials, multi-component ones, anisotropic particles, or molecules with internal degrees of freedom. Connections to experimental work can be made by computing quantities that are experimentally accessible such as the intermediate scattering function, static structure factors, $S(\mathbf{q})$, or thermodynamic quantities such as specific heat or configurational entropy, which are directly obtained from particle trajectories and can be measured in experiments as well. As an example we show in Fig. 5 the intermediate scattering function $F(\mathbf{q}, t)$ obtained from a molecular dynamics simulation of a classical model for SiO_2 as a function of time for different temperatures [120].

An important role is played by simulations also because a large variety of dynamic and static quantities can be simultaneously measured in a single model system. As we shall discuss below, there are scores of different theoret-

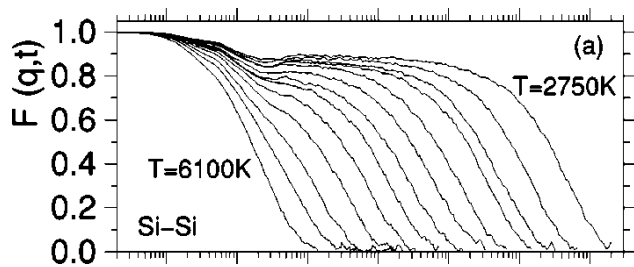


FIG. 5. Intermediate scattering function at wavevector 1.7 \AA^{-1} for the Si particles at $T = 2750 \text{ K}$ obtained from molecular dynamics simulations of a model for silica [120].

ical approaches to describe the physics of glass-formers, and sometimes they have their own set of predictions that can be readily tested by numerical work. Indeed, quite a large amount of numerical papers have been dedicated to testing in detail the predictions formulated by the mode-coupling theory of the glass transition, as reviewed in Ref. [121]. Here, computer simulations are particularly well-suited as the theory specifically addresses the relatively high temperature window that is studied in computer simulations.

While Newtonian dynamics is mainly used in numerical work on supercooled liquids, a most appropriate choice for these materials, it can be interesting to consider alternative dynamics that are not deterministic, or which do not conserve the energy. In colloidal glasses and physical gels, for instance, particles undergo Brownian motion arising from collisions with molecules in the solvent, and a stochastic dynamics is more appropriate. Theoretical considerations might also suggest the study of different sorts of dynamics for a given interaction between particles, for instance, to assess the role of conservation laws and structural information. Of course, if a given dynamics satisfies detailed balance with respect to the Boltzmann distribution, all structural quantities remain unchanged, but the resulting dynamical behaviour might be very different. Several papers [122–124] have studied in detail the influence of the chosen microscopic dynamics on the dynamical behaviour in glass-formers using either stochastic dynamics (where a friction term and a random noise are added to Newton’s equations, the amplitude of both terms being related by a fluctuation-dissipation theorem), Brownian dynamics (in which there are no momenta, and positions evolve with Langevin dynamics), or Monte-Carlo dynamics (where the potential energy between two configurations is used to accept or reject a trial move). Quite surprisingly, the equivalence between these three types of stochastic dynamics and the originally studied Newtonian dynamics was established at the level of the averaged dynamical behaviour [122–124], except at very short times where obvious differences are indeed expected. This strongly suggests that an explanation for the appearance of slow dynamics in these materials originates from their amorphous structure. However, important differences were found when

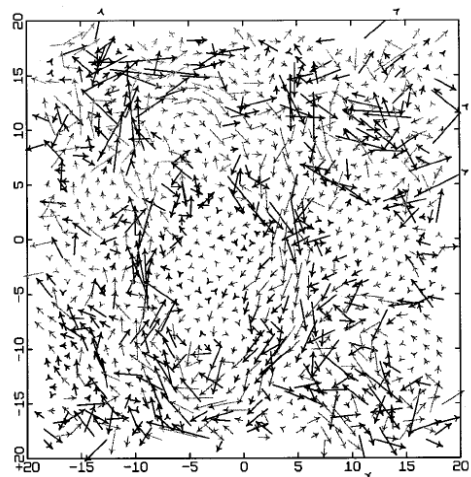


FIG. 6. Spatial map of single particle displacements in the simulation of a binary mixture of soft spheres in two dimensions [127]. Arrows show the displacement of each particle in a trajectory of length about 10 times the structural relaxation time. The map reveals the existence of particles with different mobilities during relaxation, but also the existence of spatial correlations between these dynamic fluctuations.

dynamic fluctuations were considered [124–126], even in the long-time regime comprising the structural relaxation.

Another crucial advantage of molecular simulations is illustrated in Fig. 6. This figure shows a spatial map of single particle displacements recorded during the simulation of a binary soft sphere system in two dimensions [127]. This type of measurement that study the liquid state, reveals that dynamics might be very different from one particle to another. More importantly, Fig. 6 also unambiguously reveals the existence of spatial correlations between these dynamic fluctuations. The presence of non-trivial spatio-temporal fluctuations in supercooled liquids is now called ‘dynamic heterogeneity’ [128], as we now discuss.

VI. DYNAMIC HETEROGENEITY

A. Existence of spatio-temporal dynamic fluctuations

A new facet of the relaxational behaviour of supercooled liquids has emerged in the last two decades thanks to a considerable experimental and theoretical effort. It is called ‘dynamic heterogeneity’ (DH), and now plays a central role in modern descriptions of glassy liquids [128, 129]. As anticipated in the previous section, the phenomenon of dynamic heterogeneity is related to the spatio-temporal fluctuations of the dynamics. Initial motivations stemmed from the search of an explanation for the non-exponential nature of relaxation pro-

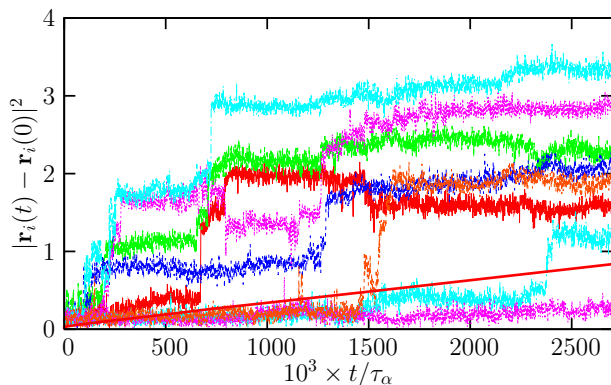


FIG. 7. Time resolved squared displacements of individual particles in a simple model of a glass-forming liquid composed of Lennard-Jones particles. The average is shown as a smooth full line. Trajectories are composed of long periods of time during which particles vibrate around well-defined positions, separated by rapid jumps that are widely distributed in time, underlying the importance of dynamic fluctuations.

cesses in supercooled liquids, related to the existence of a broad relaxation spectrum. Two natural but fundamentally different explanations can be put forward. (1) The relaxation is locally exponential, but the typical relaxation timescale varies spatially. Hence, global correlation or response functions become non-exponential upon spatial averaging over this spatial distribution of relaxation times. (2) The relaxation is complicated and inherently non-exponential, even locally. Experimental and theoretical works [128] suggest that both mechanisms are likely at play, but definitely conclude that relaxation is spatially heterogeneous, with regions that are faster and slower than the average. Since supercooled liquids are ergodic materials, a slow region will eventually become fast, and vice-versa. A physical characterization of DH entails the determination of the typical lifetime of the heterogeneities, as well as their typical lengthscale.

A clear and more direct confirmation of the heterogeneous character of the dynamics also stems from simulation studies. For example, whereas the simulated average mean-squared displacements are smooth functions of time, time signals for individual particles clearly exhibit specific features that are not observed unless dynamics is resolved both in space and time. These features are displayed in Fig. 7. What do we see? We mainly observe that particle trajectories are not smooth but rather composed of a succession of long periods of time where particles simply vibrate around well-defined locations, separated by rapid ‘jumps’. Vibrations were previously inferred from the plateau observed at intermediate times in the mean-squared displacements of Fig. 4, but the existence of jumps that are clearly statistically widely distributed in time cannot be guessed from averaged quantities only. The fluctuations in Fig. 7 suggest, and direct measurements confirm, the importance played by fluctuations around the averaged dynamical behaviour.

A simple type of such fluctuations has been studied in much detail. When looking at Fig. 7, it is indeed natural to ask, for any given time, what is the distribution of particle displacements. This is quantified by the self-part of the van-Hove function defined as

$$G_s(\mathbf{r}, t) = \left\langle \frac{1}{N} \sum_{i=1}^N \delta(\mathbf{r} - [\mathbf{r}_i(t) - \mathbf{r}_i(0)]) \right\rangle. \quad (7)$$

For an isotropic Gaussian diffusive process, one gets $G_s(\mathbf{r}, t) = \exp(-|\mathbf{r}|^2/(4D_s t))/(4\pi D_s t)^{3/2}$. Simulations reveal instead strong deviations from Gaussian behaviour on the timescales relevant for structural relaxation [130]. In particular they reveal ‘fat’ tails in the distributions that are much wider than expected from the Gaussian approximation. These tails are in fact better described by an exponential decay rather than a Gaussian one, in a wide time window comprising the structural relaxation, such that $G_s(\mathbf{r}, t) \sim \exp(-|\mathbf{r}|/\lambda(t))$ [131]. Thus, they reflect the existence of a population of particles that moves distinctively further than the rest and appears therefore to be much more mobile. This observation implies that relaxation in a viscous liquid qualitatively differs from that of a normal liquid where diffusion is close to Gaussian, and that a non-trivial single particle displacements statistics exists.

A long series of questions immediately follows this seemingly simple observation. Answering them has been the main occupation of many workers in this field over the last decade. What are the particles in the tails effectively doing? Why are they faster than the rest? Are they located randomly in space or do they cluster? What is the geometry, time and temperature evolution of the clusters? Are these spatial fluctuations correlated to geometric or thermodynamic properties of the liquids? Do similar correlations occur in all glassy materials? Can one predict these fluctuations theoretically? Can one understand glassy phenomenology using fluctuation-based arguments? Can these fluctuations be detected experimentally?

Another influential phenomenon that was related early on to the existence of DH is the decoupling of self-diffusion (D_s) and viscosity (η). In the high temperature liquid self-diffusion and viscosity are related by the Stokes-Einstein relation [132], $D_s \eta/T = \text{const}$. For a large particle moving in a fluid the constant is equal to $1/(6\pi R)$ where R is the particle radius. Physically, the Stokes-Einstein relation means that two different measures of the relaxation time R^2/D_s and $\eta R^3/T$ lead to the same timescale up to a constant factor. In supercooled liquids this phenomenological law breaks down, as shown in Fig. 8 for ortho-terphenyl [133]. It is commonly found that D_s^{-1} does not increase as fast as η so that, at T_g , the product $D_s \eta$ has increased by 2-3 orders of magnitude as compared to its Stokes-Einstein value. This phenomenon, although less spectacular than the overall change of viscosity, is a significant indication that different ways to measure relaxation times lead to different

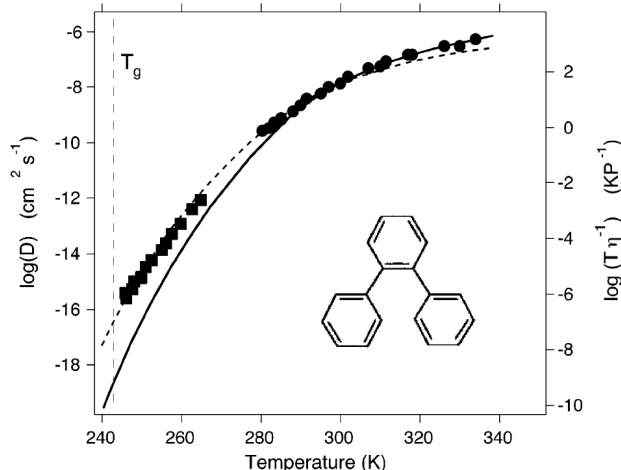


FIG. 8. Decoupling between viscosity (full line) and self-diffusion coefficient (symbols) in supercooled orthoterphenyl [133]. The dashed line shows a fit with a ‘fractional’ Stokes-Einstein relation, $D_s \sim (T/\eta)^\zeta$ with $\zeta \sim 0.82$.

answers and thus is a strong hint of the existence of a distribution of relaxation timescales.

Indeed, a natural explanation of this effect is that different observables probe the underlying distribution of relaxation times in different ways [128]. For example, the self-diffusion coefficient of tracer particles is dominated by the more mobile particles whereas the viscosity or other measures of structural relaxation probe the timescale needed for every particle to move. An unrealistic but instructive example is a model where there is a small, non-percolative subset of particles that are blocked forever, coexisting with a majority of mobile particles. In this case, the structure never relaxes but the self-diffusion coefficient is non-zero because of the mobile particles. Of course, in reality all particles move, eventually, but this shows how different observables are likely to probe different moments of the distribution of timescales, as explicitly shown within several theoretical frameworks [134, 135].

The phenomena described above, although certainly an indication of spatio-temporal fluctuations, do not allow one to study how these fluctuations are correlated in space. This is however a fundamental issue both from the experimental and theoretical points of view. How large are the regions that are faster or slower than the average? How does their size depend on temperature? Are these regions compact or fractal? These important questions were first addressed in pioneering works using four-dimensional NMR [136], or by directly probing fluctuations at the nanoscopic scale using microscopy techniques. In particular, Vidal Russel and Israeloff using Atomic Force Microscopy techniques [116] measured the polarization fluctuations in a volume of size of few tens of nanometers in a supercooled polymeric liquid (PVAc) close to T_g . In this spatially resolved measurement, the

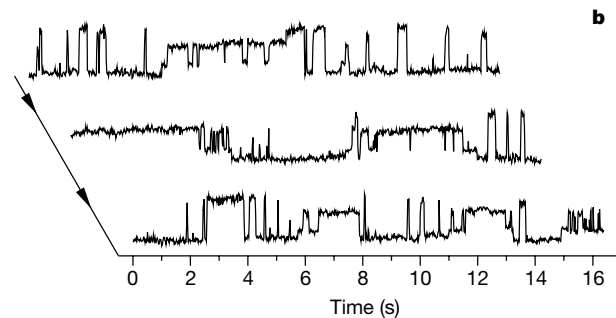


FIG. 9. Time series of polarization in the AFM experiment performed by Vidal Russell and Israeloff [116] on PVAc at $T = 300$ K. The signal intermittently switches between periods with fast or slow dynamics, suggesting that extended regions of space indeed transiently behave as fast and slow regions.

hope is to probe a small enough number of dynamically correlated regions, and detect their dynamics. Indeed, the signal shown in Fig. 9 shows a dynamics which is very intermittent in time, switching between periods with intense activity and other periods with no dynamics at all, suggesting that extended regions of space indeed transiently behave as fast or slow regions. A much smoother signal would be measured if such dynamically correlated ‘domains’ were not present. Spatially resolved and NMR experiments are quite difficult. They give undisputed information about the typical lifetime of the DH, but their determination of a dynamic correlation lengthscale is rather indirect and/or performed on a small number of liquids in a small temperature window. Nevertheless, the outcome is that a non-trivial dynamic correlation length emerges at the glass transition, where it reaches a value of the order of 5 – 10 molecule diameters [128].

B. Multi-point correlation functions

More recently, substantial progress in characterizing spatio-temporal dynamical fluctuations was obtained from theoretical [125, 126, 137, 138] and numerical results [127, 139–143]. In particular, it is now understood that dynamical fluctuations can be measured and characterized through the use of four-point correlation functions. These multi-point functions can be seen as a generalization of the spin glass susceptibility measuring the extent of amorphous long-range order in spin glasses. In this subsection, we introduce these correlation functions and summarize the main results obtained using them.

Standard experimental probes of the averaged dynamics of liquids give access to the time-dependent auto-correlation function of the spontaneous fluctuations of

some observable $O(t)$, $F(t) = \langle \delta O(0) \delta O(t) \rangle$, where $\delta O(t) = O(t) - \langle O \rangle$ represents the instantaneous value of the deviation of $O(t)$ from its ensemble average $\langle O \rangle$ at time t . One can think of $F(t)$ as being the average of a two-point quantity, $C(0, t) = \delta O(0) \delta O(t)$, characterizing the dynamics. A standard example corresponds to O being equal to the Fourier transform of the density field. In this case $F(t)$ is the dynamical structure factor as in Eq. (5). More generally, a correlation function $F(t)$ measures the global relaxation in the system. Intuitively, in a system with important dynamic correlations, the fluctuations of $C(0, t)$ are stronger. Quantitative information on the amplitude of those fluctuations is provided by the variance

$$\chi_4(t) = N \langle \delta C(0, t)^2 \rangle, \quad (8)$$

where $\delta C(0, t) = C(0, t) - F(t)$, and N is the total number of particles in the system. The associated spatial correlations show up more clearly when considering a ‘local’ probe of the dynamics, like for instance an orientational correlation function measured by dielectric or light scattering experiments, which can be expressed as

$$C(0, t) = \frac{1}{V} \int d^3r c(\mathbf{r}; 0, t), \quad (9)$$

where V is the volume of the sample and $c(\mathbf{r}; 0, t)$ characterizes the dynamics between times 0 and t around point \mathbf{r} . For example, in the above mentioned case of orientational correlations, $c(\mathbf{r}; 0, t) \propto \frac{V}{N} \sum_{i,j=1}^N \delta(\mathbf{r} - \mathbf{r}_i) Y(\Omega_i(0)) Y(\Omega_j(t))$, where Ω_i denotes the angles describing the orientation of molecule i , $\mathbf{r}_i(0)$ is the position of that molecule at time 0, and $Y(\Omega)$ is some appropriate rotation matrix element. Here, the ‘locality’ of the probe comes from the fact that it is dominated by the self-term involving the same molecule at times 0 and t , or by the contribution coming from neighboring molecules. The dynamic susceptibility $\chi_4(t)$ can thus be rewritten as

$$\chi_4(t) = \rho \int d^3r G_4(\mathbf{r}; 0, t), \quad (10)$$

where

$$G_4(\mathbf{r}; 0, t) = \langle \delta c(\mathbf{0}; 0, t) \delta c(\mathbf{r}; 0, t) \rangle, \quad (11)$$

and translational invariance has been taken into account ($\rho = N/V$ denotes the mean density). The above equations show that $\chi_4(t)$ measures the extent of spatial correlation between dynamical events at times 0 and t at different points, *i.e.* the spatial extent of dynamically heterogeneous regions over a time span t .

The function $\chi_4(t)$ has been measured by molecular dynamics, Brownian and Monte Carlo simulations in different liquids [140–145]. An example is shown in Fig. 10 for a Lennard-Jones liquid. The qualitative behaviour is similar in all cases [125, 137, 138]: as a function of time $\chi_4(t)$ first increases, it has a peak on a timescale that tracks the structural relaxation timescale and then

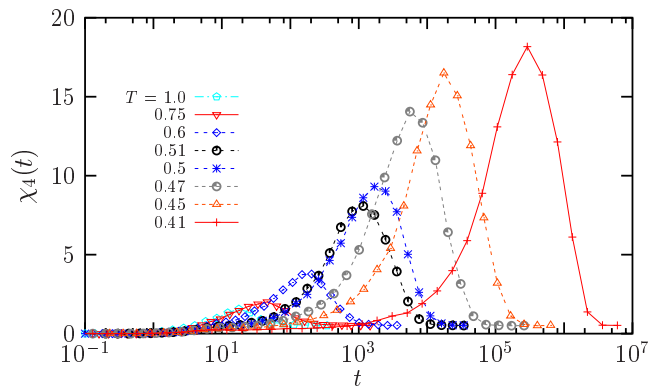


FIG. 10. Time dependence of $\chi_4(t)$, quantifying the spontaneous fluctuations of the intermediate scattering function in a Lennard-Jones supercooled liquid. For each temperature, $\chi_4(t)$ has a maximum, which shifts to larger times and has a larger value when T is decreased, revealing the increasing lengthscale of dynamic heterogeneity in supercooled liquids approaching the glass transition.

it decreases [146]. Thus the peak value measures the volume on which the structural relaxation processes are correlated. It is found to increase when the temperature decreases and the dynamics slows down. By measuring directly $G_4(\mathbf{r}; 0, t)$ it has also been checked that the increase of the peak of $\chi_4(t)$ corresponds, as expected, to a growing dynamic lengthscale ξ [125, 141–143], although these measurements are much harder in computer simulations, because very large systems need to be simulated to determine ξ unambiguously. Note that if the dynamically correlated regions were compact, the peak of χ_4 would be proportional to ξ^3 in three dimensions, directly relating χ_4 measurements to that of the relevant lengthscale of DH.

These results are also relevant because many theories of the glass transition assume or predict, in a way or another, that the dynamics slows down because there are increasingly large regions on which particles have to relax in a correlated or cooperative way. However, this lengthscale remained elusive for a long time. Measures of the spatial extent of dynamic heterogeneity, in particular $\chi_4(t)$ and $G_4(\mathbf{r}; 0, t)$, seem to provide the long-sought evidence of this phenomenon. This in turn suggests that the glass transition is indeed a critical phenomenon characterized by growing timescales and lengthscales. A clear and conclusive understanding of the relationship between the lengthscale obtained from $G_4(\mathbf{r}; 0, t)$ and the relaxation timescale is still the focus of an intense research activity.

One major issue is that obtaining information on the behaviour of $\chi_4(t)$ and $G_4(\mathbf{r}; 0, t)$ from experiments is difficult. Such measurements are necessary because numerical simulations can only be performed rather far from T_g , see Sec. V. Up to now, direct experimental measurements of $\chi_4(t)$ have been restricted to colloidal [147] and granular materials [37, 148] close to the jamming transi-

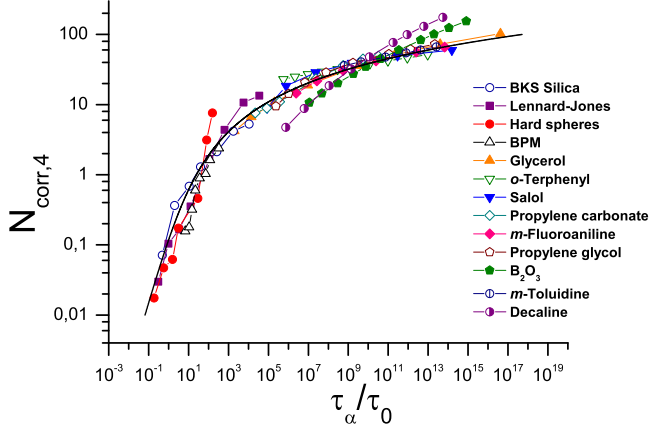


FIG. 11. Universal dynamic scaling relation between number of dynamically correlated particles, $N_{\text{corr},4}$, and relaxation timescale, τ_α , for a number of glass-formers [150], determined using Eq. (12).

tion, because dynamics is more easily spatially resolved in those cases. Unfortunately, similar measurements are currently not available in molecular liquids.

Recently, an approach based on fluctuation-dissipation relations and rigorous inequalities has been developed in order to overcome this difficulty [125, 126, 149, 150]. The main idea is to obtain a rigorous lower bound on $\chi_4(t)$ using the Cauchy-Schwarz inequality $\langle \delta H(0) \delta C(0, t) \rangle^2 \leq \langle \delta H(0)^2 \rangle \langle \delta C(0, t)^2 \rangle$, where $H(t)$ denotes the enthalpy at time t . By using fluctuation-dissipation relations the previous inequality can be rewritten as [149]

$$\chi_4(t) \geq \frac{k_B T^2}{c_P} [\chi_T(t)]^2, \quad (12)$$

where the multi-point response function $\chi_T(t)$ is defined by

$$\chi_T(t) = \left. \frac{\partial F(t)}{\partial T} \right|_{N,P} = \frac{N}{k_B T^2} \langle \delta H(0) \delta C(0, t) \rangle. \quad (13)$$

In this way, the experimentally accessible response $\chi_T(t)$ which quantifies the sensitivity of average correlation functions $F(t)$ to an infinitesimal temperature change, can be used in Eq. (12) to yield a lower bound on $\chi_4(t)$. Moreover, detailed numerical simulations and theoretical arguments [125, 126] strongly suggest that the right hand side of (12) actually provides a good estimation of $\chi_4(t)$, not just a lower bound.

Using this method, Dalle-Ferrier *et al.* [150] have been able to obtain the evolution of the peak value of χ_4 for many different glass-formers in the entire supercooled regime. In Fig. 11 we show some of these results as a function of the relaxation timescale. The value on the y -axis, the peak of χ_4 , is a proxy for the number of molecules, $N_{\text{corr},4}$ that have to evolve in a correlated

way in order to relax the structure of the liquid. Note that χ_4 is expected to be equal to $N_{\text{corr},4}$ only up to a proportionality constant that is not known from experiments, which probably explains why the high temperature values of $N_{\text{corr},4}$ are smaller than one. Figure 11 also indicates that $N_{\text{corr},4}$ grows faster when τ_α is not very large, close to the onset of slow dynamics, and a power law relationship between $N_{\text{corr},4}$ and τ_α fits this regime well ($\tau_\alpha/\tau_0 < 10^4$). The growth of $N_{\text{corr},4}$ becomes much slower closer to T_g . A change of 6 decades in time corresponds to a mere increase of a factor about 4 of $N_{\text{corr},4}$, suggesting logarithmic rather than power law growth of dynamic correlations. This is in agreement with several theories of the glass transition which are based on activated dynamic scaling [151–153].

Understanding quantitatively this relation between timescales and lengthscales is one of the main recent topics addressed in theories of the glass transition, see Sec. VII. Furthermore, numerical works are also devoted to characterizing better the geometry of the dynamically heterogeneous regions [154–156].

C. Non-linear response function

Diverging responses are characteristic signatures of phase transitions. Linear static responses measuring the change in the order parameter due to external fields diverge at second order phase transitions [157]. By using fluctuation-dissipation relations one can show that such divergence is intimately related to the divergence of the correlation length emerging in two point-functions. Spin-glasses, the archetypal example of disordered systems, display a diverging static magnetic non-linear cubic response [158, 159]. In Ref. [160] it was argued that the counterpart of these phenomena for supercooled liquids can be found in non-linear dynamical susceptibilities, which should grow approaching the glass transition, thus providing a complementary way (compared to χ_4) to reveal its collective nature. In experiments on molecular liquids, non-linear dielectric susceptibility are a natural probe to unveil this phenomenon.

The simplest explanation [161] for this scenario is based on the assumption that $N_{\text{corr}} = (\ell/a)^{d_f}$ molecules are amorously ordered over the lengthscale ℓ , where a is the molecular size and d_f is the fractal dimension of the ordered clusters. In consequence, their dipoles, which are oriented in apparently random positions, are essentially locked together during a time τ_α . In the presence of an external electric field E oscillating at frequency $\omega \geq \tau_\alpha^{-1}$, the dipolar degrees of freedom of these molecules contribute to the polarisation per unit volume as

$$p = \mu_{dip} \frac{\sqrt{(\ell/a)^{d_f}}}{(\ell/a)^d} F \left(\frac{\mu_{dip} E \sqrt{(\ell/a)^{d_f}}}{kT} \right) \quad (14)$$

where μ_{dip} is an elementary dipole moment, F is an odd scaling function, and $d = 3$ the dimension of space. This

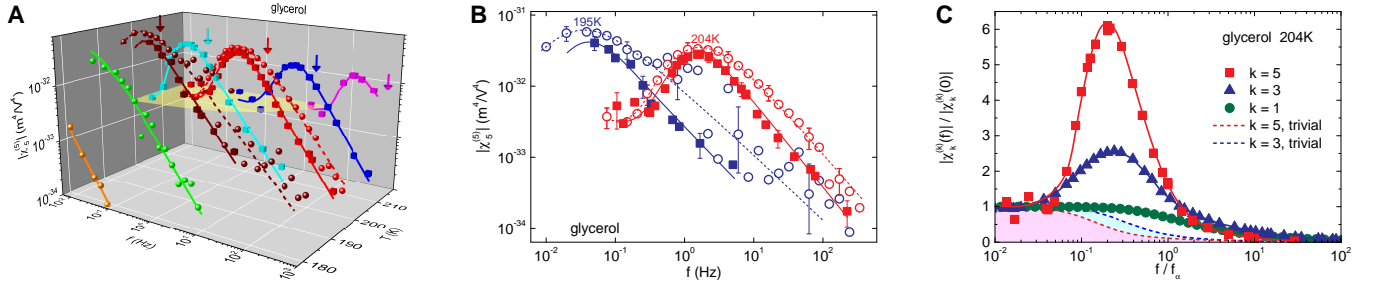


FIG. 12. Modulus of the fifth-order susceptibility in super-cooled glycerol as a function of frequency (from [161]). (A) The susceptibilities $\chi_5^{(5)}$ reported are obtained directly by monitoring the response of the sample at 5ω , when applying an electric field E at angular frequency ω . Two independent setups were used. Lines are guides for the eyes. (B) Projection onto the susceptibility-frequency plane of the data of panel A at 204K and at 195K. (C) Comparison of the fifth-order, cubic, and linear susceptibilities. Symbols, with line to guide the eyes. The higher the order k , the stronger the hump of $|\chi_k^{(k)}|$.

states that randomly locked dipoles have an overall moment $\sim \sqrt{N_{\text{corr}}}$, and that we should compare the thermal energy with the energy of this ‘super-dipole’ in a field.

Expanding Eq. 14 in powers of E , one finds the ‘glassy’ contribution to p :

$$\begin{aligned} \frac{p}{\mu_{dip}} &= F'(0) \left(\frac{\ell}{a}\right)^{d_f-d} \left(\frac{\mu_{dip}E}{kT}\right) + \\ &+ \frac{1}{3!} F^{(3)}(0) \left(\frac{\ell}{a}\right)^{2d_f-d} \left(\frac{\mu_{dip}E}{kT}\right)^3 + \\ &+ \frac{1}{5!} F^{(5)}(0) \left(\frac{\ell}{a}\right)^{3d_f-d} \left(\frac{\mu_{dip}E}{kT}\right)^5 + \dots \end{aligned} \quad (15)$$

Because $d_f \leq d$, the first term, contributing to the usual linear dielectric susceptibility, $\chi_1(\omega)$, cannot grow as ℓ increases. This simple theoretical argument explains why spatial glassy correlations does not show up in $\chi_1(\omega)$, in experiments. The second term, contributing to the third-order dielectric susceptibility $\chi_3(\omega)$, does grow with ℓ provided $d_f > d/2$. Several theories indeed suggest that ordered domains are compact, $d_f = d$ [153, 162]. The third term leads to the fifth-order susceptibility $\chi_5(\omega)$, which should diverge as ℓ^{3d_f-d} (higher n -order susceptibilities diverge as $\ell^{(n+1)d_f/2-d}$). This line of arguments shows that measuring non-linear susceptibilities is a way to probe and characterize the collective dynamical behavior associated to glassy dynamics.

This challenge was taken up in the series of works [161, 163–165]. The main outcomes of these experiments have been: (i) to show that indeed a growth of the non-linear responses goes along with the glass transition, (ii) to measure in a new way the number of correlated molecules close to T_g , (iii) to estimate that $d_f \simeq d$ (for $d = 3$). As an example, we reproduce the results of [161] in Fig. 12, which shows the increase of the fifth-order susceptibility with temperature (panel A), its humped shape in frequency (panel B), and the stronger singularity of the fifth-order susceptibility compared to the third-order one (panel C), as expected for a collective phenomenon.

Another set of experiments on non-linear responses was

performed in colloids: non-linear mechanical susceptibilities were probed approaching the colloidal glass transition [166] and shown to grow approaching it. Differently from the dielectric case, third-harmonic shear responses have a peak at a frequency associated to the β -relaxation, and not to the α -relaxation. The reason is related to the fact that a very slow shear-strain does not affect the relaxation time-scale, whereas an external electric field (even a static one) does, see Ref. [166].

Finally, a word about theories. Given that the growth of non-linear dynamical susceptibility is a relatively newly established fact in the glass-physics arena, one can wonder how the different theoretical framework developed to explain the glass transitions cope with it. Thermodynamic theories based on the increases of some kind of medium range order naturally do, as explained above. Mode-Coupling-Theory also predicts diverging dynamical non-linear susceptibility at the MCT transition [166, 167]. Purely local theory are instead at odds. Dynamical facilitation theory was argued to be compatible with such findings in Ref. [168], even though the general arguments put forward in Ref. [161] indicate the opposite conclusion.

VII. THEORY OF THE GLASS TRANSITION

We now present some theoretical approaches to the glass transition. It is impossible to cover all of them in a brief review, simply because there are way too many of them, perhaps the clearest indication that the glass transition remains an open problem. We choose to present approaches that are keystones and have a solid statistical mechanics basis. Loosely speaking, they have an Hamiltonian, can be simulated numerically, or studied analytically with statistical mechanics tools. Of course, the choice of Hamiltonians is crucial and contains very important assumptions about the nature of the glass transition. All these approaches have given rise to unexpected results. One finds more in them than what was supposed at the beginning, which leads to new, testable predic-

tions. Furthermore, with models that are precise enough, one can test (and hopefully falsify!) these approaches by working out all their predictions in great detail, and comparing the outcome to actual data. This is not possible with ‘physical pictures’, or simpler approaches of the problem which we therefore do not discuss.

Before going into the models, we would like to state the few important questions that theoreticians face.

- Why do the relaxation time and the viscosity increase when T_g is approached? Why is this growth super-Arrhenius?
- Can one understand and describe quantitatively the average dynamical behaviour of supercooled liquids, in particular broad relaxation spectra, non-exponential behaviour, and their evolution with fragility?
- Is there a relation between kinetics and thermodynamics (like $T_0 \simeq T_K$), and why?
- Can one understand and describe quantitatively the spatio-temporal fluctuations of the dynamics? How and why are these fluctuations related to the dynamic slowing down?
- Is the glass transition a collective phenomenon? If yes, of which kind? Is there a finite temperature or zero temperature ideal glass transition?
- Is the slowing down of the dynamics driven by the growth of amorphous order and a static length? Or is its origin purely dynamic?
- Is there a geometric, real space explanation for the dynamic slowing down that takes into account molecular degrees of freedom?

The glass transition appears as a kind of ‘intermediate coupling’ problem, since for instance typical growing lengthscales are found to be at most a few tens of particle large close to T_g . It would therefore be difficult to recognize the correct theory even if one bumped into it. To obtain quantitative, testable predictions, one must therefore be able to work out also preasymptotic effects. This is particularly difficult, especially in cases where the asymptotic theory itself has not satisfactorily been worked out. As a consequence, at this time, theories can only be judged by their overall predictive power and their theoretical consistency.

A. Random First Order Transition Theory

1. Mean-field models and a zest of replica theory

In the last three decades, three independent lines of research, Adam-Gibbs theory [169], mode-coupling theory [121] and spin glass theory [170], have merged to

produce a theoretical ensemble that now goes under the name of Random First Order Transition theory (RFOT), a terminology introduced by Kirkpatrick, Thirumalai and Wolynes [171, 172] who played a major role in this unification. Instead of following the rambling development of history, we summarize it in a more modern and unified way.

A key ingredient of RFOT theory is the existence of a chaotic or complex free energy landscape with a specific evolution with temperature and/or density. Analysing it in a controlled way for three dimensional interacting particles is an impossible task. This can be achieved, however, in simplified models or using mean-field approximations, that have therefore played a crucial role in the development of RFOT theory.

A first concrete example is given by ‘lattice glass models’ [173]. These are models of hard particles sitting on a lattice. The Hamiltonian is infinite either if there is more than one particle on a site or if the number of occupied neighbors of an occupied site is larger than a parameter m , but is zero otherwise. Tuning the parameter m , or changing the type of lattice, in particular its connectivity, yields different models. Lattice glasses are constructed as simple statmech models to study the glassiness of hard sphere systems. The constraint on the number of occupied neighbors mimicks the geometric frustration [174] encountered when trying to pack hard spheres in three dimensions. Numerical simulations show that their phenomenological glassy behavior is indeed analogous to the one of supercooled liquids [175–177]. Other models with a finite energy are closer to molecular glass-formers, and can also be constructed [178]. These models can be solved exactly on a Bethe lattice [179], which reveals a rich physical behaviour [180]. In particular their free energy landscape can be analyzed in full details and turns out to have the properties that are also found in several ‘generalized spin glasses’. Probably the most studied example of such spin glasses is the p -spin model, defined by the Hamiltonian [181]

$$H = - \sum_{i_1, \dots, i_p} J_{i_1, \dots, i_p} S_{i_1} \dots S_{i_p}, \quad (16)$$

where the S_i ’s are N Ising or spherical spins, $p > 2$ is the number of interacting spins in a single term of the sum, and J_{i_1, \dots, i_p} quenched random couplings extracted from a distribution which, with no loss of generality, can be taken as the Gaussian distribution with zero mean and variance $p!/(2N^{p-1})$. In this model, the couplings J_{i_1, \dots, i_p} play the role of self-induced disorder in glasses, and promotes a glass phase at low temperature.

All these models can be analyzed using the so-called replica theory [170]. Given its importance in setting the foundations of the theory of glasses at the mean-field level, we now present its main technical steps. To keep the discussion as simple as possible, we focus on p -spin models. Note that the theory holds for more complex models but it is technically more involved. The starting point is the computation of the free-energy which is

obtained as an average over the distribution of couplings:

$$F = \lim_{N \rightarrow \infty} -\frac{1}{\beta N} \overline{\log Z_J}, \quad (17)$$

where $\overline{\dots}$ represents the average over the disorder. Performing this average is possible thanks to the replica trick

$$\overline{\log Z_J} = \lim_{n \rightarrow 0} \frac{1}{n} \log \overline{Z^n}, \quad (18)$$

where n is the index of replicas, i.e. clones of the same system with different couplings J_{i_1, \dots, i_p} extracted from the same distribution. The use of the replica trick may seem purely mathematical, yet it has a profound physical sense. If the system is ergodic, averages of thermodynamical observables for two replicas of the same system (with identical disorder) coincide, whereas they differ if ergodicity is broken. We can define the overlaps between two replicas a, b as Q_{ab} , which defines the $n \times n$ overlap matrix:

$$Q_{ab} = \frac{1}{N} \sum_{i=1}^N S_i^a S_i^b, \quad (19)$$

where the product between spins represents a dot product for spherical spins [182]. After some computations, the free energy can be expressed as a function of Q_{ab} , which therefore plays the role of the order parameter. In the ergodic phase one expects symmetry between replicas [183], and the so-called replica-symmetric (RS) parametrization of Q_{ab} is adopted: all the off-diagonal elements of Q_{ab} are equal to $q_0 < 1$ and the diagonal elements are $Q_{aa} = 1$. The parametrization that corresponds to the glass phase, when ergodicity is broken, is the so-called one-step replica symmetry breaking (1RSB) solution. Here, the overlap matrix is divided into blocks of dimension $m \times m$; elements belonging to blocks far from the diagonal are equal to q_0 , while off-diagonal elements of blocks along the diagonal are equal to q_1 with $1 > q_1 > q_0$. On the diagonal $Q_{aa} = 1$. This parametrization encodes the existence of many thermodynamically equivalent basins, hence two replicas can either fall in the same basin and have overlap q_1 , or fall in two different basins and have overlap q_0 . The crucial simplification introduced by the mean-field approximation is that barriers between basins have a free energy cost which grows exponentially with N , so that truly metastable states can be defined in the thermodynamic limit [184]. At high temperature (or low density) the RS solution has a lower free energy. Below the ideal glass transition temperature the 1RSB solution instead becomes dominant.

2. Liquids and glasses in infinite dimensions

A major theoretical breakthrough of the last years is the analysis of the glass transition for interacting particle systems in the limit of infinite dimensions [185–187]. The

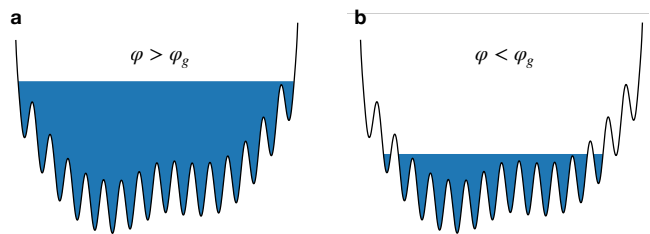


FIG. 13. Sketch of the evolution of free-energy landscape of hard spheres across the glass transition. In the liquid phase (a) at low packing fractions $\varphi < \varphi_g$, every portion of the phase space is accessible. For $\varphi > \varphi_g$ the system is in the glass phase (b) and remains trapped in one of the many equivalent basins.

starting point approach is the definition of a pair interaction potential with a proper scaling with dimension d to ensure a non trivial thermodynamic limit:

$$v(r) = \tilde{v}[d(r/\ell - 1)] \quad (20)$$

where ℓ defines the range of the interaction. Many different potentials used to model glasses can be written in this way by using a suitable function $\tilde{v}(x)$, such as hard spheres, Lennard-Jones, Yukawa, square-well, harmonic, and Weeks-Chandler-Andersen potentials [187]. In the limit of infinite space dimension, $d \rightarrow \infty$, and using the scaling above, the thermodynamics and the dynamics of liquids and glasses can be analyzed exactly [188]. The resulting theory is qualitatively very similar to the one obtained from the simple models discussed in the previous section (both for the statics, in terms of replica formalism, and for the dynamics, in terms of self-consistent Langevin equations).

In fact, all these models belong to the universality class of 1RSB systems [189], with a free-energy landscape evolving as in the sketch in Fig. 13. At low densities or high enough temperatures, they all describe an ergodic liquid phase, analogous to the paramagnetic phase of a spin glass. Under cooling or application of an external pressure, the free energy breaks up into many different minima which eventually trap the dynamics, and the system enters the glass phase, as described further below.

The merit of the infinite dimensional theory is that it offers quantitative results and applies directly to microscopic models of liquids and glasses. Moreover, it directly reveals the nature of ‘mean-field’ theories and approximations, such as the diagrammatic liquid theory and Mode-Coupling Theory. Last but not least, it establishes once and for all that the 1RSB phase and associated physics and phase transition is the correct and universal mean-field theory of glass-forming models.

3. Random first order transitions

We now discuss the physics associated to the 1RSB phase transition, and more generally to RFOT. The free

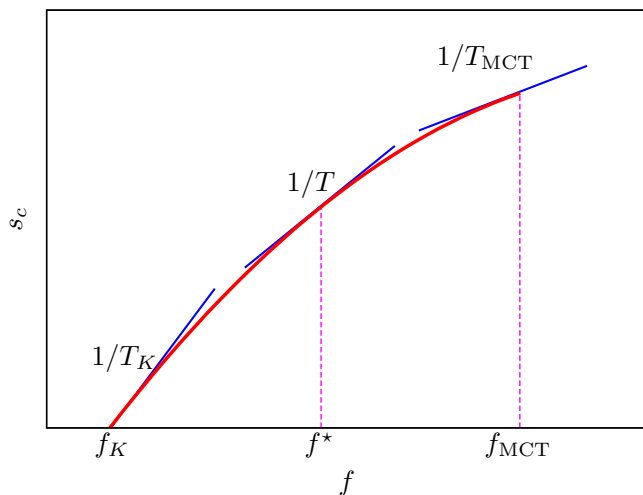


FIG. 14. Typical shape of the configurational entropy, s_c , as a function of free energy density, f in the range $T_k < T < T_{MCT}$ for random first order landscapes. A graphical solution of Eq. (22) is obtained by finding the value of f at which the slope of the curve is $1/T$. Note that s_c is also a function of temperature, so this curve changes with T .

energy landscape of glassy systems is ‘rugged’, as shown in Fig. 13. It is characterized by many minima and saddle points of various order. Actually, the number of stationary points is so large that in order to count them one has to introduce an entropy, called configurational entropy or complexity, $s_c = \frac{1}{N} \log \mathcal{N}(f)$, where $\mathcal{N}(f)$ is the number of stationary points with a given free energy density f . The (real space) density profile corresponding to one given minimum is amorphous and lacks any type of periodic long-range order, and different minima are very different from one another. Defining a similarity measure between them, an ‘overlap’ Q (see Eq. (39) below for a precise definition), one typically finds that two minima with the same free energy f have zero overlap. The typical shape of the configurational entropy as a function of f is shown in Fig 14.

At high temperature, there is typically a single minimum, the high temperature liquid state. There is a temperature below which an exponentially large (in the system size) number of minima appears. Within mean-field models, corresponding to Bethe lattices, completely connected lattices, and interacting particles for $d \rightarrow \infty$ these minima correspond to macroscopic physical states analogous to the periodic minimum corresponding to the crystal [190]. Once the system is in one of these states it remains trapped there forever, since the barriers separating states diverge with the system size. However, when transposed to finite dimensional systems, these states become metastable and have a finite lifetime. As a consequence, in order to compute thermodynamic properties, one has to sum over all of them using the Boltzmann

weight $\exp(-\beta N f_\alpha)$ for each state α [191]:

$$Z = \sum_{\alpha} e^{-\beta N f_{\alpha}} = \int df \exp[N s_c(f; T)] e^{-\beta N f}, \quad (21)$$

where $\beta = 1/(K_B T)$. Evaluating this sum by saddle point method yields three regimes. At high temperature, $T > T_{MCT}$, the liquid corresponding to a flat density profile dominates the sum. The landscape is simple and has a single minimum. This is followed by an intermediate temperature regime, $T_K < T < T_{MCT}$, where the sum is dominated by all terms with free energy density satisfying

$$\left. \frac{\partial s_c(f, T)}{\partial f} \right|_{f=f^*} = \beta. \quad (22)$$

There are many of them, the logarithm of their number being given by $N s_c(f^*, T)$, see Fig. 14 for a graphical solution of Eq. (22). Upon decreasing the temperature, $s_c(f^*, T)$ decreases until a temperature, T_K , below which the sum in Eq. (21) becomes dominated by only few terms corresponding to states with free energy density f_K given by $s_c(f_K, T) = 0$, see Fig. 14. The entropy in the intermediate temperature range above T_K has two contributions: the one counting the number of minima, given by s_c , and the intra-state entropy, s_{in} , counting the number of configurations inside each state. At T_K , the configurational entropy vanishes, $s_c(T_K) = 0$. As a consequence the specific heat undergoes a jump towards a smaller value across T_K , an exact realization of the ‘entropy vanishing’ mechanism conjectured by Kauzmann [10].

Let us discuss the dynamical behaviour which results from the above analysis. We have already mentioned that relaxation processes do not occur below T_{MCT} because states have an infinite lifetime. The stability of these states can be analyzed by computing the free energy Hessian in the minima [182]. One finds that states become more fragile when $T \rightarrow T_{MCT}^-$, are marginally stable at $T = T_{MCT}$, unstable for $T > T_{MCT}$. The relaxation dynamics of these models can be analyzed exactly [192, 193]. Coming from high temperature, the dynamics slows down and the relaxation time diverges at T_{MCT} in a power law manner,

$$\tau_{\alpha} \sim \frac{1}{(T - T_{MCT})^{\gamma}}, \quad (23)$$

where γ is a critical exponent. The physical reason is the incipient stable states that appear close to T_{MCT} . The closer the temperature is to T_{MCT} , the longer it takes to find an unstable direction to relax.

Amazingly, the dynamical transition that appears upon approaching T_{MCT} in random first order landscapes is completely analogous to the one predicted for supercooled liquids by the Mode-Coupling Theory (MCT) of the glass transition, and developed independently by

Leuthesser, Bengtzelius, Götze, Sjölander and coworkers [121]. Actually, MCT can be considered as an approximation which becomes controlled and exact for these mean-field models. Originally, MCT was developed using projector operator formalism [194, 195] and field-theory methods [196] to yield closed integro-differential equations for the dynamical structure factor in supercooled liquids. These approaches were recently generalized [197, 198] to deal with dynamic heterogeneity and make predictions for the multi-point susceptibilities and correlation functions discussed in Sec. VI. Within MCT, the relaxation timescale diverges in a power law fashion at T_{MCT} , as in Eq. (23). This divergence is accompanied by critical behaviour that appears both in space (long range spatial dynamic correlations), and in time (time-dependent power laws).

Comparing Eqs. (1) and (23) makes it clear that MCT cannot be used to describe viscosity data close to T_g since it does not predict activated behaviour. It is recognized that an MCT transition at T_{MCT} does not occur in real materials, so that T_{MCT} is, at best, a dynamical crossover. A central advantage of MCT, compared to many other theories is that it can yield quantitative predictions from microscopic input obtained for a particular material. As such it has been applied to scores of different systems, with predictions that can be directly confronted to experimental or numerical measurements. A major drawback is the freedom offered by the ‘crossover’ nature of the MCT transition, so that ‘negative’ results can often be attributed to corrections to asymptotic predictions rather than deficiencies of the theory itself. Nevertheless, MCT has proven to be useful and continues to be developed, applied and generalized to study many different physical situations [121], including aging systems and non-linear rheology of glassy materials [199–201], see also Sec. X.

What happens below T_{MCT} in a finite dimensional system if the relaxation time does not diverge as predicted in Eq. (23)? Why is the transition avoided? In fact, the plethora of states that one finds in mean-field are expected to become (at best) metastable in finite dimension, with a finite lifetime, even below T_{MCT} . What is their typical lifetime, and how these metastable states are related to the structural relaxation are issues that still await for a complete microscopic analysis.

There exist, however, phenomenological arguments [151, 202, 203], backed by microscopic computations [204, 205] that yield a possible solution dubbed ‘mosaic state’ by Kirkpatrick, Thirumalai and Wolynes [202]. Schematically, the mosaic picture states that, in the regime $T_K < T < T_{MCT}$, the liquid is composed of domains of linear size ξ . Inside each domain, the system is in one of the mean-field states. The length of the domains is fixed by a competition between energy and configurational entropy. A state in a finite but large region of linear size l can be selected by appropriate boundary conditions that decrease its free energy by an amount which scales as Υl^θ with $\theta \leq 2$. On the other

hand, the system can gain entropy, which scales as $s_c l^3$, if it visits the other numerous states. Entropy obviously gains on large lengthscales, the crossover length ξ being obtained by balancing the two terms,

$$\xi = \left(\frac{\Upsilon}{T s_c(T)} \right)^{1/(3-\theta)}. \quad (24)$$

In this scenario, the configurational entropy on scales smaller than ξ is too small to stir the configurations efficiently and win over the dynamically generated pinning field due to the environment, while ergodicity is restored at larger scale. Hence, the relaxation time of the system is the relaxation time, $\tau(\xi)$, of finite size regions. Barriers are finite, unlike in the mean-field treatment. Smaller length scales are faster but unable to decorrelate, whereas larger scales are orders of magnitude slower. Assuming thermal activation over energy barriers which are supposed to grow with size as ξ^ψ , one finally predicts, using Eq. (24), that [203]

$$\log \left(\frac{\tau_\alpha}{\tau_0} \right) = c \frac{\Upsilon}{k_B T} \left(\frac{\Upsilon}{T s_c(T)} \right)^{\psi/(3-\theta)}, \quad (25)$$

where c is a constant.

The above argument is rather generic and therefore not very predictive. There exist microscopic computations [204–206] aimed at putting these phenomenological arguments on a firmer basis and computing the exponents θ and ψ . The results are not yet fully conclusive because they involve replica calculations with some assumptions, but they do confirm the phenomenological scenario presented above and suggest that $\theta = 2$. Some other phenomenological arguments suggest the value of $\theta = 3/2$ [202]. There are no computation available for ψ , only the suggestion that $\psi = \theta$ [202].

Note that using the value $\theta = 3/2$ with $\theta = \psi$ simplifies Eq. (25) into a form that is well-known experimentally and relates $\log \tau_\alpha$ directly to $1/S_c$, which is the celebrated Adam-Gibbs relation [169] between relaxation time and configurational entropy that is in rather good quantitative agreement with many experimental results [207–210]. The Random First Order Transition theory can be considered, therefore, as a microscopic theory that reformulates and generalizes the Adam-Gibbs mechanism. Furthermore, using the fact that the configurational entropy vanishes linearly at T_K , a VFT divergence of the relaxation time as in Eq. (1) is predicted, with the identification that

$$T_0 = T_K. \quad (26)$$

The equality (26) between two temperatures that are commonly used in the description of experimental data certainly constitutes a central achievement of RFOT theory since it accounts for the empirical relation found between the kinetics and the thermodynamics of supercooled liquids. Furthermore RFOT theory naturally contains MCT, which can be used to describe the first

decades of the dynamical slowing down, while the spin glass side of RFOT theory qualitatively explains the dynamics in terms of the peculiar features of the free energy landscape that have been detailed above. Dynamics first slows down because there appears incipient metastable states, and once these metastable states are formed, the dynamics becomes dominated by the thermally activated barrier crossing from one metastable state to another, which is consistent with the relation between dynamical correlation length and timescale discussed in Sec. VI. Quite importantly, microscopic computations of T_{MCT} and T_0 for realistic models of liquids are possible [187, 211].

Probably the most serious weakness of the RFOT theory construction is that the theory, although worked out in full details within mean-field models or the large dimensionality limit, is based for finite dimensions on asymptotic results valid, e.g., for $T \rightarrow T_K$. The application of RFOT theory to temperatures accessible in experiments (hence not very close to T_K) requires additional phenomenological assumptions. Moreover, the dynamical processes leading to the VFT law are not understood completely. Although the ultimate consequences of the theory are sometimes in very good agreement with experiments, as Eq. (26), direct tests of the mosaic state picture are rare and difficult [17, 212].

4. *Heterogeneous disorder and mapping to the Random Field Ising Model*

The study of second-order phase transitions shows that field theory provides a natural framework to go beyond mean-field theory [157]. With this in mind, researchers in glass physics have also gone down this route in recent years. One of their main achievements has been to identify fluctuations that are neglected by mean-field theory and play a very important role in shaping the physical behavior of supercooled liquids. These fluctuations have been related to the notion of ‘self-induced disorder’ in Ref. [213]. In the following, we may prefer the name ‘self-induced heterogeneity’ [214] to make the distinction with the ‘self-induced disorder’ discussed in Sec. IX B. The main idea is that when observing equilibrium relaxation from time t to time $t + \tau_\alpha$, the state of the system at time t is spatially heterogeneous: for instance it can have higher density in one region and lower density in another. Actually, theoretical analysis shows [215–217] that even key mean-field quantities, such as the configurational entropy, are heterogeneously distributed in space. Since the amount of slowing down is directly linked to those quantities (at least within RFOT theory), these static fluctuations induce strong dynamical fluctuations, leading in particular to dynamical heterogeneities [213]. From the theoretical point of view, they play a key role in changing properties of the MCT transition and the ideal glass transition. In fact, even though the MCT transition is like a spinodal instability within

mean-field theory [218], one finds that once these fluctuations are included, MCT enters the universality class of a disordered spinodal, like, e.g. the spinodal of the Random Field-Ising Model [213]. Using results obtained on this problem, this connection implies that even in the absence of activated hopping, the MCT transition changes nature in any finite dimension: it is either wiped out by non-perturbative fluctuations [219] or it becomes dominated by rare and non-perturbative events, as happens for the spinodal of the RFIM [220]. One nevertheless expects that the higher the spatial dimension, the more obvious an echo of the MCT mean-field transition should persist [193, 221, 222].

Finally, the role of heterogeneous disorder on the ideal glass transition has been investigated in Refs. [215–217]. The main outcome of these studies is an effective model for the glass transition that takes the form of an RFIM with extra long-range anti-ferromagnetic and multi-body interactions. These new couplings depress the ideal glass transition temperature but do not lead to qualitative changes. The strength of the disorder is, however, crucial: a strong enough disorder (a system-dependent feature) can destroy the ideal glass transition, as may happen for the RFIM. Another relation with the RFIM was also found in Ref. [221], where it was shown that amorphous interfaces between rearranging regions behave statistically as the ones of domain walls in the RFIM.

Let us conclude with a word of caution: not everything is understood about self-induced heterogeneity. Since the disorder is strongly linked to the state of the system, it is also to a large extent renewed after a time τ_α , thus it evolves and at the same time it affects the dynamics, i.e. it is not truly quenched. This is a first difficulty in assessing precisely its role for glassy relaxation [223]. A second one is that although for static properties, such as configurational entropy or the Franz-Parisi potential, one can establish a mapping to the RFIM, for the dynamics the situation is more intricate and no mapping has been found up to now [224].

5. *Renormalization group for the glass transition*

In parallel with the efforts described in the previous section, developing a renormalization group (RG) analysis of the glass transition has been a new important theoretical activity in the last decade. Different methods have been used, and were applied on lattice disordered models and replica lattice field theories which display a glass transition. Given that the ideal glass transition has a mixed character, intermediate between first and second-order phase transition, usual perturbative RG techniques developed for continuous phase transitions do not work. Therefore researchers had to focus on non-perturbative methods. In Ref. [225] the hierarchical Dyson RG method was employed to analyse the Random Energy Model in finite dimension. The authors found an ideal glass phase transition similar to the one

taking place within mean-field but with a non-analytical behavior of the free-energy at T_K , leading in particular to a specific heat exponent different from one, as assumed within RFOT theory. The real-space properties, correlation length and energy barrier, and the nature of the fixed-point were first studied in [226, 227] by Migdal-Kadanoff RG. A complete and more advanced analysis was performed in [228], in which it was shown that the ideal glass transition is associated to a so-called zero temperature fixed point [229]. The main implication is that the correlation length and the typical energy barrier have power law divergences with non-trivial exponents, hence implying a super-Arrhenius behavior. However, such a fixed point was found only in dimensions higher than three. In consequence, this RG treatment predicts that in three dimensions the glass transition is actually an avoided phase transition [230]: glassy behavior is still driven by the RG fixed point present in higher dimension, but the correlation length and the timescale do not truly diverge (arguably an irrelevant fact since one cannot approach the transition close enough, but an important conceptual one).

The RG approaches we reviewed above offer a new perspective on the nature of the glass transition. They provide important guidelines for more controlled non-perturbative RG treatments. Ideally, one would like to tackle directly interacting particle systems in the continuum and use methods that have been proved to be precise and reliable in previous studies, such as the one developed by Wetterich [231]. This is a formidable challenge as those techniques do not seem to be able to handle the kind of rare and localized non-perturbative events that are relevant for glassy dynamics [232].

B. Free volume, defects, and facilitated models

1. Lattice gases

In this subsection we motivate and briefly summarize studies of a different family of statistical mechanics models that turns out to yield a rich variety of physical behaviors. Their starting point are physical assumptions that might seem similar to the models described in Sec. VII A, but the outcome yields a different physical explanation of the glass transition. Although the two theoretical approaches cannot be simultaneously correct, they both have been influential and very instructive in order to develop a theoretical understanding of glassy phenomena.

As in Sec. VII A, we first consider hard sphere systems. We follow the lattice gas description introduced by Kob and Andersen [233], and work on a three dimensional cubic lattice. As in a hard sphere system, we assume no interaction between particles beyond the hard-core constraint that the occupation number n_i at site i is at most equal to 1,

$$H[\{n_i\}] = 0, \quad n_i = 0, 1. \quad (27)$$

In contrast to the lattice glass model, all configurations respecting the hard-core constraint are allowed and are equally probable. Geometric frustration is instead introduced at the level of the kinetic rules, that are defined as constrained local moves. Namely, a particle can jump to a nearest neighbor site only if that site is empty (to satisfy the hard-core constraint), but, additionally, only if the sites occupied before and after the move have less than m neighbors, m being an adjustable parameter, which Kob and Andersen choose as $m = 4$ for $d = 3$ ($m = 6$ corresponds to the unconstrained lattice gas). The model captures the idea that if the liquid is locally very dense, no movement is possible while regions with low density move more easily.

Of course, such kinetically constrained lattice gases have been studied in various spatial dimensions, for different values of m , for different constraints, or even different lattice geometries [234]. These models capture the idea of a ‘cage’ effect in a strict sense, meaning that a particle with a dense neighbor shell cannot diffuse. Although the cage seems a purely local concept, it turns out that diffusion in constrained lattice gases arises from cooperative rearrangements, so that slow dynamics can be directly shown to be driven by the growth of dynamic lengthscales for these cooperative moves [235–237]. This strongly suggests that such cooperative moves most probably have a role in the dynamics of real liquids.

2. Free volume, dynamic criticality

In the lattice gas picture, the connection with the liquid is not obvious because it is the density (‘free volume’) rather than the temperature that controls the dynamics. Thermal models with similar features can in fact be defined along the following lines. In a liquid, low temperature implies a very small probability to find a location with enough free volume to move. The idea of a small concentration of ‘hot spots’ is in fact reminiscent of another picture of the glass transition based on the idea of ‘defects’ which is captured by the defect model proposed by Glarum [238] in the 60’s, where relaxation proceeds via the diffusion of a low concentration of independent defects. In the mid-80’s, using both ideas of kinetic constraints and rare defects, Fredrickson and Andersen defined a family of kinetic Ising models for the glass transition [239]. They studied an assembly of non-interacting spins,

$$H[\{n_i\}] = \sum_{i=1}^N n_i, \quad n_i = 0, 1, \quad (28)$$

where $n_i = 1$ represents the defects, whose concentration becomes exponentially small at low temperature, $\langle n_i \rangle \approx \exp(-1/T)$. As for the Kob-Andersen lattice gas, the non-trivial ingredient lies in the chosen rates for the kinetic transitions between states. The kinetic rules stipulate that a transition at site i can happen with

a usual Glauber rate, but only if site i is surrounded by at least k defects ($k = 0$ corresponds to the unconstrained limit). Again, one can easily imagine studying such models in different spatial dimensions, on different lattices, and with slightly different kinetic rules, yielding a large number of possible behaviors [234, 240]. The similarity between those spin facilitated models and the kinetically constrained lattice gases is striking. Altogether, they form a large family of models generically called kinetically constrained models (KCMs) [234].

The connection between KCMs and the much older concept of free volume is obvious from our presentation. Free volume models are among the most widely used models to analyze experimental data, especially in polymeric systems. They have been thoroughly reviewed before [14, 241], and the main prediction is that dynamic slowing down occurs because the free volume available to each particle, v_f , vanishes at some temperature T_0 as $v_f \approx \alpha(T - T_0)$. Statistical arguments then relate relaxation timescales to free volume assuming that a movement is possible if locally there is ‘enough’ available free volume, more than a typical value v_0 . This is clearly reminiscent of the above idea of a kinetic constraint for local moves in lattice gases. An appealing VFT divergence is then predicted:

$$\frac{\tau_\alpha}{\tau_0} \sim \exp\left(\gamma \frac{v_0}{v_f}\right) \sim \exp\left(\frac{\gamma v_0/\alpha}{[T - T_0]^\mu}\right), \quad (29)$$

where γ is a numerical factor and $\mu = 1$. Predictions such as Eq. (29) justify the wide use of free volume approaches, despite the many (justified) criticisms that have been raised.

Initially it was suggested that KCMs would similarly display finite temperature or finite density dynamic transitions similar to the one predicted by the mode-coupling theory of supercooled liquids [239], but it was soon realized [242, 243] that most KCMs do not display such singularity, and timescales in fact only diverge in the limit of zero temperature ($T = 0$) or maximal density ($\rho = 1$). Models displaying a $T_c > 0$ or $\rho_c < 1$ transition have also been introduced and analyzed [244]. They provide a microscopic realization, based on well-defined statistical mechanics models, of the glass transition predicted by free volume arguments. Their relaxation timescale diverges with a VFT-like form but with an exponent $\mu \simeq 0.64$. Understanding their universality classes or the degree of generality of the mechanism leading to the transition is still an open problem [245–247]; the most recent results on this front come from mathematical physicists who have been able to classify many of the different possible behaviors on the basis of the microscopic dynamical rules [248–251].

Extensive studies have shown that KCMs have a macroscopic behavior which resembles the phenomenology of supercooled liquids, displaying in particular an Arrhenius or super-Arrhenius increase of relaxation timescales upon decreasing temperature, and non-exponential relaxation functions at equilibrium [234].

Early studies also demonstrated that, when suddenly quenched to very low temperatures, the subsequent non-equilibrium aging dynamics of these models compares well with experimental observations on the aging of liquids [242]. The diverse definitions of such models suggest a broad variety of different behaviors. This feature is both positive and negative: on the one hand one can explore various scenarios to describe glass transition phenomena, but on the other hand, one would like to be able to decide what particular model should be used to get a quantitative description for a particular liquid. It is not straightforward to perform microscopic predictions using the framework of KCMs, since there is no direct observable parameter to use as input of the theory (unlike $g(r)$, for MCT). An operative definition of KCMs’ defects was provided (see next section and [252, 253]), however this does not allow to directly choose which KCM (which rules) are appropriate for a given liquid.

Despite this caveat, it is quite useful to use KCMs as theoretical tools to define concepts and obtain new ideas. It is precisely in this perspective that interest in KCMs has increased, in large part since it was realized that their dynamics is spatially heterogeneous [235, 243, 254], a central feature of supercooled liquids dynamics. In particular, virtually all the aspects related to dynamic heterogeneity mentioned in Sec. VI can be investigated and rationalized, at least qualitatively, in terms of KCMs. The dynamics of these systems can be understood by considering where ‘relaxation’ happens and then propagate, which is dictated by the underlying defect motion [234]. Depending on the particular model, defects can diffuse or have a more complicated motion. Furthermore, they can be point-like or ‘cooperative’ (formed by point-like defects moving in a cooperative way). A site can relax only when it is visited by a defect. As a consequence, the heterogeneous character of the dynamics is entirely encoded in the defect configuration and defect motion [254]. For instance, a snapshot similar to Fig. 6 in a KCM shows clusters which have relaxed within the time interval t [255, 256]. These are formed by all sites visited by a defect between 0 and t . The other sites are instead frozen in their initial state. In these models the dynamics slows down because the defect concentration decreases. As a consequence, in the regime of slow dynamics there are few defects and strong dynamic heterogeneity. Detailed numerical and analytical studies have indeed shown that in these systems, non-exponential relaxation patterns do stem from a spatial, heterogeneous distribution of timescales, directly connected to a distribution of dynamic lengthscales [236, 237, 244, 254, 255, 257]. Decoupling phenomena also appear naturally in KCMs and can be shown to be very direct, quantifiable, consequences of the dynamic heterogeneity [135], which also deeply affects the process of self-diffusion in a system close to its glass transition [258]. More fundamentally, multi-point susceptibilities and multi-point spatial correlation functions such as the ones defined in Eqs. (8) and (11), can be studied in much greater detail than in molecu-

lar systems, relating their evolution to time and length scales [126, 138, 237, 259, 260]. This type of scaling behavior has been observed close to $T = 0$ and $\rho = 1$ in spin models and lattice gases without a transition [261]. Different theoretical approaches have shown that these particular points of the phase diagram correspond to genuine critical points where timescales and dynamic lengthscales diverge with well-defined critical laws [257, 260]. Such ‘dynamic criticality’ implies the existence of universal scaling behavior in the physics of supercooled liquids, of the type reported for instance in Fig. 11.

3. Defects: connection with Hamiltonian dynamics models

A central criticism about the free volume approach, that is equally relevant for KCMs, concerns the identification, at the molecular level, of the vacancies (in lattice gases), mobility defects (in spin facilitated models), or of the free volume itself. The attempts to provide reasonable coarse-graining from molecular models with continuous degrees of freedom to lattice models with kinetic rules have been, for a very long time, quite limited and not fully convincing [144, 262].

For molecular models, this issue was first attacked in 2010, with a definition of the cumulated dynamical activity K , an extensive quantity characterizing the frequency of state changes (from excited to non-excited and vice versa) [246, 263]. This definition was made more concrete and studied in models of supercooled liquids in [253], where an appropriate functional is explicitly designed as a recorder of excitations (or defects). Defects or excitations are not to be mistaken with displacements. Indeed, some locations providing opportunities for structural reorganization do coincide with defects, and their presence can be inferred by observing nontrivial particle displacements associated with transitions between relatively long-lived configurations. Displacements instead refer to dynamical moves in short segments of a trajectory, while defects refer to underlying configurations. The explicit definition of defects has since been used to estimate the role of facilitation in glassy dynamics, to provide a microscopic validation of KCMs [264, 265], to explain dynamical heterogeneities in glassy materials, or to compute the dynamical facilitation volume [247].

The conceptual proof that kinetic rules emerge effectively and induce a slow dynamics has been obtained for simple lattice spin models [266], with a dynamics that directly maps onto constrained models. A deeper study of this kind of model was performed more recently [267]. Several examples are available but here we only mention the simple case of the bidimensional plaquette model defined by a Hamiltonian of a p -spin type on a square lattice of linear size L ,

$$H = -J \sum_{i=1}^{L-1} \sum_{j=1}^{L-1} S_{i,j} S_{i+1,j} S_{i,j+1} S_{i+1,j+1}, \quad (30)$$

where $S_{i,j} = \pm 1$ is an Ising variable lying at node (i, j) of the lattice. Contrary to KCMs, the Hamiltonian in Eq. (30) contains genuine interactions, which are no less (or no more) physical than p -spin models discussed in Sec. VII A. Interestingly the dynamics of this system is (trivially) mapped onto that of a KCM by analyzing its behavior in terms of plaquette variables, $p_{i,j} \equiv S_{i,j} S_{i+1,j} S_{i,j+1} S_{i+1,j+1}$, such that the Hamiltonian becomes a non-interacting one, $H = -J \sum_{i,j} p_{i,j}$, as in Eq. (28). More interestingly, the analogy also applies to the dynamics [266]. The fundamental moves are spin-flips, but when a single spin is flipped the states of the four plaquettes surrounding that spin change. Considering the different types of moves, one quickly realizes that excited plaquettes, $p_{i,j} = +1$, act as sources of mobility, since the energetic barriers to spin flips are smaller in those regions. This observation allows to identify the excited plaquettes as defects, by analogy with KCMs. Spatially heterogeneous dynamics, diverging lengthscales accompanying diverging timescales and scaling behavior sufficiently close to $T = 0$ can be established by further analysis [268], providing a simple but concrete example of how an interacting many body system might effectively behave as a model with kinetic constraints [269].

4. Connection with other perspectives

An essential drawback of facilitated models is that among the microscopic ‘details’ thrown away to arrive at simple statmech models such as the ones in Eqs. (27) and (28), information on the thermodynamical behavior of the liquids has totally disappeared. In particular, a possible coincidence between VFT and Kauzmann temperatures, T_0 and T_K is not expected, nor can the dynamics be deeply connected to thermodynamics, as in Adam-Gibbs relations. The thermodynamical behavior of KCMs appears different from the one of real glassformers close to T_g [270]. This is probably the point where KCMs and RFOT approaches differ most obviously. Even though the dynamics of KCMs shares similarities with systems characterized with a complex energy landscape [271, 272], thermodynamical behaviors are widely different in both cases, as has been recently highlighted in Ref. [273] by focusing on the concrete examples of plaquette models such as in Eq. (30).

Finally, when KCMs were first defined, they were argued to display a dynamical transition of a very similar nature to the one predicted by MCT [239]. Although the claim has been proven wrong [274], it bears some truth: both approaches basically focus on the kinetic aspects of the glass transition and they both predict the existence of some dynamic criticality with diverging lengthscales and timescales. This similarity is even deeper, since a mode-coupling singularity is present when (some) KCMs are studied on the Bethe lattice [236], but is ‘avoided’ when more realistic lattice geometries are considered [275].

C. Geometric frustration, avoided criticality, and locally preferred structures

In all of the above models, ‘real space’ was present in the sense that special attention was paid to different lengthscales characterizing the physics of the models that were discussed. However, apart from the ‘packing models’ with hard-core interactions, no or very little attention was paid to the geometric structure of local arrangements in molecular liquids close to a glass transition. This slight oversight is generally justified using concepts such as ‘universality’ or ‘simplicity’, meaning that one studies complex phenomena using simple models, a typically statistical mechanics perspective. However, important questions remain: what is the liquid structure within mosaic states? How do different states differ? What is the geometric origin of the defects invoked in KCMs? Are they similar to defects found in crystalline materials (disclinations, dislocations, vacancies, etc.)? Some lines of research attempt to provide answers to these questions, making heavy use of the concept of geometric frustration.

1. Geometric frustration

Broadly speaking, frustration refers to the impossibility of simultaneously minimizing all the interaction terms in the energy function of a system. Frustration might arise from quenched disorder (as in the spin glass models described above), but liquids have no quenched randomness. In liquids, instead, frustration has a purely geometrical origin. It is attributed to a competition between a short-range tendency for the extension of a ‘locally preferred order’, and global constraints that prevent the periodic tiling of space with this local structure.

This can be illustrated by considering once more the packing problem of spheres in three dimensions. In that case, locally the preferred cluster of spheres is an icosahedron. However, the 5-fold rotational symmetry characteristic of icosahedral order is not compatible with translational symmetry, and formation of a periodic icosahedral crystal is impossible [276]. The geometric frustration that affects spheres in three dimensional Euclidean space can be relieved in curved space [174]. In Euclidian space, the system possesses topological defects (disclination lines), as the result of forcing the ideal icosahedral ordering into a ‘flat’ space. Nelson and coworkers developed a solid theoretical framework based on this picture to suggest that the slowing down of supercooled liquids is due to the slow wandering of these topological defects [174], but their treatment remains too abstract to obtain quantitative, explicit results. Further theoretical work extended the integral-equation approach to calculate the pair correlation function in hyperbolic geometry, making it easier to compare predictions and simulation data [277]. MCT was also re-derived in curved space (on a sphere), showing that it still cannot capture quantitatively the transition [278, 279]. Explicit numerical

results were also obtained recently [280], showing a clear first-order like transition from liquid to ordered solid in an appropriately curved space, becoming avoided as Euclidean space is retrieved.

2. Coulomb frustrated theories

The picture of sphere packing disrupted by frustration has been further developed in simple statistical models characterized by geometric frustration, in a pure statistical mechanics approach [153]. To build such a model, one must be able to identify, then capture, the physics of geometric frustration. Considering a locally ordered domain of linear size L , Kivelson *et al.* [230] suggest that the corresponding free energy scales as

$$F(L, T) = \sigma(T)L^2 - \phi(T)L^3 + s(T)L^5. \quad (31)$$

The first two terms express the tendency of growing locally preferred order and represent respectively the energy cost of having an interface between two phases and a bulk free energy gain inside the domain. Geometric frustration is encoded in the third term which represents the strain free energy resulting from frustration. The remarkable feature of Eq. (31) is the super-extensive scaling of the energy cost due to frustration which opposes the growth of local order. The elements in Eq. (31) can then be directly incorporated into ferromagnetic models where ‘magnetization’ represents the local order, ferromagnetic interactions represent the tendency to local ordering, and Coulombic antiferromagnetic interactions represent the opposite effect, coming from the frustration. The following Hamiltonian possesses these minimal ingredients:

$$H = -J \sum_{\langle i, j \rangle} \mathbf{S}_i \cdot \mathbf{S}_j + K \sum_{i \neq j} \frac{\mathbf{S}_i \cdot \mathbf{S}_j}{|\mathbf{x}_i - \mathbf{x}_j|}, \quad (32)$$

where the spin \mathbf{S}_i occupies the site i at position \mathbf{x}_i . Such Coulomb frustrated models have been studied in great detail, using various approximations to study models for various space and spin dimensions [153].

The general picture is that the ferromagnetic transition occurring at $T = T_c^0$ in the pure model with no frustration ($K = 0$) is either severely displaced to lower temperatures for $K > 0$, sometimes with a genuine discontinuity at $K \rightarrow 0$, yielding the concept of ‘avoided criticality’. For the simple case of Ising spins in $d = 3$, the situation is different since the second order transition becomes first-order between a paramagnetic phase and a spatially modulated phase (stripes). For $K > 0$ and $T < T_c^0$ the system is described as a ‘mosaic’ of domains corresponding to some local order, the size of which increases (but does not diverge!) when T decreases. Tarjus, Kivelson and co-workers clearly demonstrated that such a structuration into mesoscopic domains allows one to understand most of the fundamental phenomena occurring in supercooled liquids [153]. Their picture as a whole is very appealing because it directly addresses the physics

in terms of the ‘real space’, and the presence of domains of course connects to ideas such as cooperativity, dynamic heterogeneity and spatial fluctuations, that directly explains, at least qualitatively, non-exponential relaxation, decoupling phenomena or super-Arrhenius increase of the viscosity. However, as for the RFOT mosaic picture, direct confirmations of this scenario are rare [281], or difficult to obtain.

3. Locally preferred structures

Going back to the geometric structure of local arrangements in real space, a line of research has emerged that is based upon some kind of local order [282–285]. Icosahedral order was initially shown to be linked to the dynamics of some binary mixtures. But more generally, for simple enough glass-formers, a broader variety of locally ordered structures can be defined [283], such as, e.g., defective icosahedron [286]. A vast body of literature has shown that these locally preferred structures (LPS) seem to correlate with structural relaxation. Using trajectory path sampling (see Sec. IX D), it was found that LPS and dynamic activity play equivalent roles, and are therefore strongly correlated [287, 288]. The increased number of LPS has also been linked to hindered crystallization [289]. These multiple effects suggest the LPS impacts the dynamics in various ways.

For several systems in $d = 2, 3$, simple local order parameters measuring the distance from sterically favored structures (sixfold symmetry, angles and closeness to local tetrahedron) have been spatially coarse-grained [290], thus revealing a clear structure-dynamics relationship. The interpretation in Ref. [290] is that these LPS represent an indirect measurement of the true amorphous order. The very simple and widespread tetrahedral order has been observed in a variety of materials [291]. The LPS-dynamics correlation has also been confirmed recently in experiments on colloids [29, 292], providing further evidence of the important role of LPS in glassy behavior.

Despite these important advances, the concrete application of LPS-based techniques on any particular realistic glass-forming material is hindered by the lack of a universal operative definition of the LPS. For relatively simple systems, an operative scheme was designed to automatically find these LPS [283, 293].

A natural alternative to this tedious exercise is the use of modern machine learning techniques. In particular, one may consider the unsupervised learning task of grouping together similar local structures (this is called clustering). Once clusters (corresponding to automatically-found LPS) are found, any local environment may be assigned to its most similar group (LPS), but without the burden of defining the LPS’s one by one [294, 295].

VIII. MEAN-FIELD THEORY OF THE AMORPHOUS PHASE

The phase transition between liquid and glass is not the only interesting phenomenon characterising the phase diagram of glassy materials. Since the transition occurs at finite pressure and temperature, glasses can be further compressed or cooled within the glass phase itself [185, 186, 296]. How do physical properties of glasses change in this context? In mean-field theory, this question has been widely investigated by using the hard spheres glass model [297, 298], a favorite canonical example of a glass-former system because of its analytical simplicity. Eventually, by compressing a hard sphere glass, the system undergoes the jamming transition in the limit of infinite pressure [31]. In this section, we briefly survey recent progress in the development of an analytic theory of the glass phase in the large d limit, with a particular emphasis on hard spheres [187].

A. Mean-field glassy phase diagrams

When a glass-forming liquid undergoes the glass transition, it becomes confined into a single free energy minimum and the timescale to explore different minima becomes infinite. It is formally possible to define thermodynamic properties by restricting the available statistical configurations to a single free energy minimum. This can be enforced in the replica formalism by considering two copies of the system and constraining the distance between them [33]. First, an equilibrium reference configuration \underline{Y} at $(T_g, \hat{\varphi}_g)$ is introduced, where $\hat{\varphi}$ is the scaled packing fraction $\hat{\varphi} = 2^d \varphi / d$. Second, a copy of the equilibrium configuration $\underline{X}(t)$ is created and evolved in time. Let us define now the mean-squared displacement (MSD) between the two copies as $\overline{\Delta(\underline{X}, \underline{Y})} = \Delta_r$. The properties of $\underline{X}(t)$ are sampled in a restricted region of phase space close to the equilibrium configuration. Within this state following construction, the system at $(T_g, \hat{\varphi}_g)$ with initial configuration \underline{Y} can be adiabatically followed anywhere in the glass phase diagram.

Concretely, for the glass state selected by \underline{Y} and followed until $(T, \hat{\varphi})$, we can write the restricted partition function as:

$$Z[T, \hat{\varphi} | \underline{Y}, \Delta_r] = \int d\underline{X} e^{-\beta V(\underline{X})} \delta(\Delta_r - \Delta(\underline{X}, \underline{Y})), \quad (33)$$

where $V(\underline{X})$ is the potential energy of the configuration \underline{X} , and the delta function enforces the restricted average. In order to obtain the glass free energy, we need to compute its average over the chosen reference configuration \underline{Y} , which acts as a source of quenched disorder:

$$f_g(T, \hat{\varphi} | T_g, \hat{\varphi}_g, \Delta_r) = -\frac{T}{N} \int \frac{d\underline{Y}}{Z[T_g, \hat{\varphi}_g]} e^{-\beta_g V(\underline{Y})} \times \ln Z[T, \hat{\varphi} | \underline{Y}, \Delta_r] \quad (34)$$

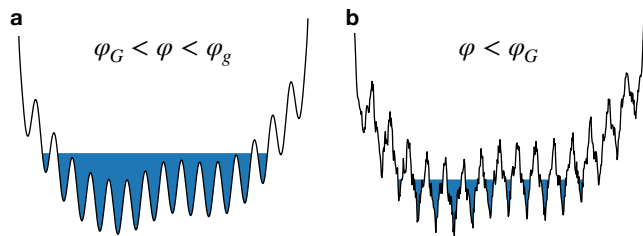


FIG. 15. (a) Sketch of the free energy structure deep in the hard sphere glass phase, where each basin breaks down in sub-basins corresponding to secondary relaxations. At the Gardner transition in (b), the sub-basins become fractal and ergodicity is broken.

where $Z[T_g, \hat{\varphi}_g] = \int dY \exp^{-\beta_g V(\underline{Y})}$ is the partition function at $(T_g, \hat{\varphi}_g)$. Mathematically, the quenched disorder is handled using the replica method. We then introduce $(n + 1)$ replicas of the original system, with the initial glass at $(T_g, \hat{\varphi}_g)$ being the master replica, while the n other slave replicas describe the glass at $(T, \hat{\varphi})$. The glass free energy is finally expressed in terms of the average MSD between the slave replicas and the master replica Δ_r , and the average distance between the slave replicas Δ . At this step, we assume that the symmetry between slave replicas is not broken, which corresponds to the 1RSB ansatz described in Sec. VII A.

By choosing the state point at $(T, \hat{\varphi}) = (T_g, \hat{\varphi}_g)$, the recursive equations for Δ and Δ_r have to satisfy $1/\hat{\varphi} = \mathcal{F}_\beta(\Delta)$, where $\mathcal{F}_\beta(\Delta)$ is a positive function which vanishes for both $\Delta \rightarrow \infty$ and $\Delta \rightarrow 0$, with an absolute maximum in between. This equation can then be satisfied only if

$$\frac{1}{\hat{\varphi}_d} \leq \max_{\Delta} \mathcal{F}_\beta(\Delta). \quad (35)$$

This condition occurs for volume fractions larger than a critical value $\hat{\varphi}_d(\beta_g)$, which corresponds to the dynamical glass transition.

We can explore the glass phase following the glass prepared at the glass transition $(T_g, \hat{\varphi}_g)$ at different temperatures and packing fractions. At low T and high $\hat{\varphi}$ one eventually meets another phase transition, where the 1RSB assumption fails [170] and the more complex full-replica symmetry breaking (fullRSB) solution is necessary to compute the glass free energy, the so-called Gardner phase transition [299, 300]. Here, the fullRSB solution corresponds to a hierarchical organisation of the distances between the slave replicas and the glass becomes marginally stable [301, 302]. The emergence of a complex free energy landscape gives rise to non-trivial dynamical processes [303–305]. A pictorial representation of the Gardner transition is shown in Fig. 15.

It is worth noting that the derivation sketched above is completely general and can be used for any glassy pair potential mentioned in Sec. VII A. In the following we will apply this formalism to the hard spheres model, for which several implications from the mean field pic-

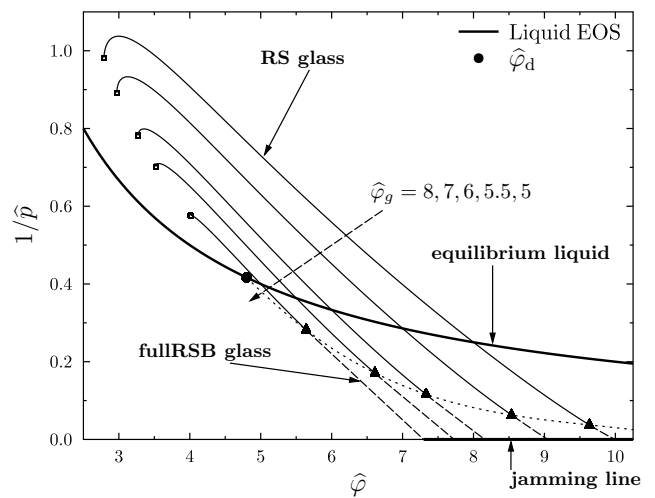


FIG. 16. Phase diagram of hard spheres in the inverse reduced pressure – reduced packing fraction $(1/\hat{p}, \hat{\varphi})$ plane. The glass transition is marked by a full circle. The glass equations of state are reported as full lines in the region where the replica symmetric solution is stable. The Gardner transition is marked by triangles, beyond which the fullRSB solution is stable (dashed lines). The glass equations of state end at the jamming transition. Upon decompression, glasses are stable until a spinodal instability arises (open squares).

ture have been successfully tested numerically [189, 306]. Here, the relevant state parameter is the scaled reduced pressure $\hat{p} \equiv \beta P/\rho d$. We refer to Refs. [296, 300, 305, 307] for more results regarding systems made of soft potentials.

Starting from an equilibrated hard sphere liquid configuration at $\hat{\varphi}_g$, we can apply the state following formalism to explore the hard sphere phase diagram in Fig. 16. The reduced pressure can be computed from the equation of state of an infinite dimensional hard sphere liquid $\hat{p} \sim \hat{\varphi}/2$, derived from a Virial expansion of the free energy [193]. Starting from $\hat{\varphi}_g$ and decompressing the system, the glass eventually undergoes a melting transition: the 1RSB solution becomes unstable and the glass melts into the liquid via a spinodal instability [186]. Upon compression instead, the glass enters deeper into the glass phase and remains dynamically arrested. Numerically, this has been proven by measuring Δ as the long-time limit of the MSD $\Delta(t)$ between the system at time t and the initial configuration at $t = 0$. The order parameter of the transition Δ_r is instead computed as the long-time limit of the distance $\Delta_{AB}(t)$ between two copies A and B of the same initial system evolved with different initial velocities:

$$\Delta_{AB} = \left\langle \frac{1}{N} \sum_{i=1}^N |\mathbf{r}_i^A - \mathbf{r}_i^B|^2 \right\rangle. \quad (36)$$

Upon further compression, the glass eventually undergoes the Gardner transition at a finite pressure \hat{p}_G . Here, the relation between Δ_r and Δ breaks down and $\Delta(t)$ is

characterized by a logarithmic growth in time, suggesting the emergence of a complex free energy landscape [306]. The copies A and B cannot occupy the same sub-basin and are no longer able to explore the entire metabasin. Due to the fractal nature of the free energy landscape, the excitations required to move around the fractal states correspond to soft modes [305]. The correlation length of these modes can be estimated by measuring the dynamical susceptibility, computed as the variance of Δ_{AB} , which indeed shows a divergence at the Gardner transition [306].

Compressing further within the Gardner phase, the pressure eventually diverges as the system reaches its jamming density $\hat{\varphi}_J$, which depends explicitly on the selected initial condition $(T_g, \hat{\varphi}_g)$. In particular, there exists a range of jamming points, or a ‘jamming line’ [308], whose extension increases with d [185].

B. Jamming

During the last two decades, a large research effort has shed light on the critical behavior characterizing the jamming transition [309]. Jamming can be seen from two different perspectives. An assembly of Brownian hard spheres under compression becomes rigid at a finite density, at which point the pressure diverges. On the other hand, athermal packings of soft repulsive spheres reach the jamming point under decompression when the pressure vanishes. In both situations, each particle is constrained by enduring contacts with the neighbor particles and the system is rigid. In particular, at jamming the average number of contacts per particle Z reaches the critical value $Z_c = 2d$, which represents the lower limit for mechanical stability [310] (Maxwell’s criterion for rigidity). From the hard spheres side, Z jumps from zero to Z_c at the transition, while from the soft spheres side, as the pressure decreases toward zero the excess number of contacts scales as [311, 312]:

$$\Delta Z \equiv Z - Z_c \sim \Delta\varphi^{1/2}, \quad (37)$$

where $\Delta\varphi = \varphi - \varphi_J$ is the amount of compression above the jamming threshold. A connection between hard and soft spheres at jamming is observed in the pair correlation function [30, 311], confirming that allowed configurations of hard and soft spheres are identical at jamming.

When $\Delta Z = 0$ the system is isostatic, i.e. there are just enough contacts to ensure mechanical stability and the system is marginally stable: breaking a bond between contacts can lead to an excitation that causes a collective motion throughout the whole system [313]. Not surprisingly, this critical behavior fits well into the free energy picture of marginal glasses reported above.

Marginality in athermal jammed solids can be explained in real space by the so-called cutting argument [314]. Imagine removing the contacts between a subsystem of linear size l and the rest of the system. If we slightly compress the system, this cutting will lead

to a competition between the overall excess contacts ΔZ created by the compression, and the missing contacts at the boundary of the subsystem. If the total number of contacts is below the isostatic value $N_{iso} = NZ/2$, then there are modes with no energetic cost, i.e. soft modes. The number of soft modes N_{soft} then corresponds to the difference between the number of contacts at the boundary, proportional to l^{d-1} , and the number of extra contacts created by the compression, which scales as $\Delta Z l^d$. There is then a critical length $l^* \sim \Delta\varphi^{-1/2}$ for which the system looks isostatic and for $l = l^*$, soft modes correlate over the whole subsystem. These extended anomalous modes correspond to random excitations over all the system, profoundly different from acoustic modes proper of crystalline solids.

Other anomalies of jammed solids are observed in the scaling of the elastic moduli near the transition. These critical behaviors have been successfully described within a force network picture, for which an effective medium theory has been developed [315, 316]. In particular, a jammed soft sphere configuration can be mapped onto a network of springs with elastic contacts k_{eff} , computed as second derivatives of the pairwise interaction between particles. The resulting scaling behaviors for the bulk modulus $B \sim k_{eff}$ and the shear modulus $G \sim k_{eff}\Delta\varphi^{1/2}$ suggest that the Poisson ratio $G/B \sim \Delta\varphi^{1/2}$ vanishes at the jamming transition [311]. This criticality reflects on the frequency of normal modes which is directly related to the elastic moduli ($B(\omega), G(\omega)$) by the dispersion relation $\omega^* = ck^*$, where $k^* \sim 1/l^*$ and c is the speed of sound. Since sound propagates either longitudinally (B) or transversely (G), two different length scales can be defined: the longitudinal length scale $l^* \sim \Delta\varphi^{-1/2}$, which matches the cutting length scaling behavior and is indeed attributed to extended soft modes, and the transverse length scale which follows the scaling $l_t \sim \Delta\varphi^{-1/4}$.

Other critical scaling laws have been predicted both by replica mean field calculations and effective medium theory for a spring network, with good consistency with numerical results in finite dimensions. In particular, the distributions of interparticle voids and interparticle forces follow universal power-laws [317–320]. Contact forces can be either extended or localized, with distributions defined by power law exponents θ_e and θ_l respectively. Extended forces are predicted from the infinite dimensional exact solution, whereas the localized forces likely result from the presence of localised defects, such as rattling particles, which only exist in finite dimensions. Remarkably, the numerical value of the critical exponents associated to scaling laws near jamming can be predicted analytically in the mean-field approach [187], and their value is confirmed by numerical simulations in dimensions $d \geq 2$.

The influence of temperature on the jamming criticality has also been studied [316, 321]. These works show that above jamming there exists a region in the plane $T - \varphi$ where the harmonic approximation of the soft sphere potential holds, and the vibrational spec-

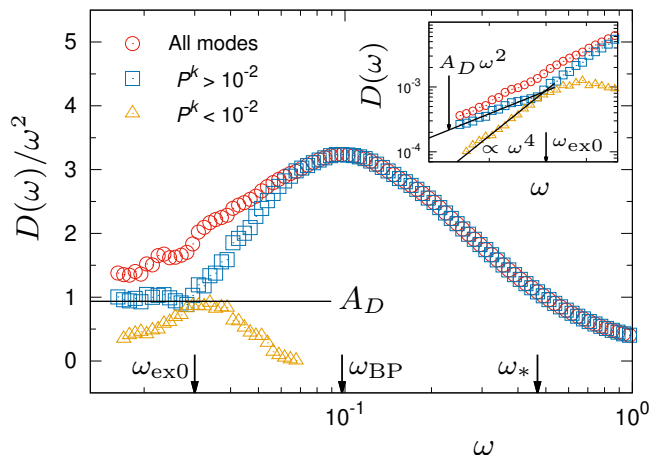


FIG. 17. Adapted from [324]. Vibrational density of states of jammed harmonic soft spheres scaled by the Debye law ω^{d-1} in $d = 3$. Modes with index k are classified as extended (blue) or localized (yellow) by their participation ratio P^k . Below the boson peak frequency ω_{BP} , the density of states is the superposition of anomalous extended modes eventually obeying Debye scaling, and a population of quasi-localised modes scaling as ω^4 , as confirmed in the inset.

trum converges to its zero temperature limit, provided that $T < T^*(\varphi)$. The value of $T^*(\varphi)$ decreases with $\Delta\varphi \rightarrow 0$ with a trivial scaling exponent. A similar result holds below jamming for hard sphere glasses [322]. For $T > T^*(\varphi)$, the harmonic approximation breaks down, defining an anharmonic critical regime, controlled by non-analyticities in the interparticle potential. Physically, strong anharmonicities stem from the constant breaking and reformation of particle contacts in the presence of thermal fluctuations [323].

C. Vibrational properties

The anomalous thermal properties of low temperature glasses can be related to the structure of the free energy landscape of glassy states. Amorphous solids behave very differently from crystalline solids. In terms of heat capacity and thermal conductivity, crystals are dominated by phononic excitations with a low-frequency density of states (DOS) $D(\omega)$ given by the Debye scaling law $D(\omega) \sim \omega^{d-1}$. Instead, the thermal properties of glasses are dominated by an excess of vibrational modes referred to as the boson peak and by an anomalous low-frequency scaling of $D(\omega)$. This excess of anomalous vibrations reflects, within mean-field theory, the existence of multiple free energy barriers in glassy states. In fact, when the glass enters the Gardner phase, the system becomes marginal and even infinitesimal perturbations lead to excitations that can bring the system to a different glassy state.

The mean-field theory of glasses has been explored using soft spheres in the jamming limit [325]. The the-

ory predicts the low-frequency scaling of the vibrational density of states (vDOS) to be $D(\omega) \sim \omega^2$ in any dimension [298, 315, 326], quite differently from the Debye scaling. The same result was previously obtained within the effective medium theory [319].

Numerically, the nature of the low-frequency vibrational spectrum has been widely studied using soft spheres packings close to jamming. Early studies suggested the existence of the $D(\omega) \sim \omega^2$ scaling [189, 325] for a wide range of dimensions d , reinforcing the relevance of the mean-field description for finite dimensional systems [327]. The modes giving rise to this scaling form have been found to be extended anomalous modes. A more recent study established that the ω^2 scaling is only observed over a finite frequency range, which seems to increase systematically with the space dimension d , which is consistent with a pure quadratic scaling when $d = \infty$. However, for any finite d , the density of states eventually obeys Debye scaling for sufficiently low frequencies.

Finally, recent numerical works show that for frequencies lower than the boson peak, an additional family of soft modes due to marginal instabilities can be observed [324, 328]. As Fig. 17 shows, the vibrational density of these additional modes scales as ω^4 . A spatial analysis of such modes shows that they correspond to quasi-localised modes, which are again absent from the large d analytic description.

D. Rheology

Once the glass is created, it can be adiabatically cooled or compressed, but it can also be deformed by applying an external mechanical constraint. The rheology of amorphous solids is a very broad research field. Here, we present recent results in this field obtained using the mean field glass theory, including implications regarding elasticity, yielding and shear jamming [301, 329, 330].

We report results obtained from the same state following formalism applied to study the amorphous phase along a compression in the $d \rightarrow \infty$ limit. If the master replica \underline{Y} is in the dynamically arrested region, the system reacts elastically to a small applied strain γ . We can then obtain the stress-strain curve as a function of the state point (T, φ) of the slave replica \underline{X} . The stress for an elastic medium increases linearly with strain, which defines the shear modulus $\hat{\mu} = \frac{d\hat{\sigma}}{d\gamma}$ computed at zero strain, where stress and shear modulus are scaled such that the $d \rightarrow \infty$ limit remains finite. In the small strain limit one finds

$$\hat{\mu} = \frac{1}{\Delta} \quad (38)$$

where Δ is the long time limit of the MSD. The MSD $\Delta(\underline{X}, \underline{Y})$ is the superposition of an affine component due to the strain, and of a non-affine contribution defined by the particular shear protocol. At the glass transition, the shear modulus jumps from a zero value (liquid state) to

a finite value at $\hat{\varphi}_d$ (glass state). In finite dimensions, this sharp discontinuity becomes a crossover [187].

When the system is confined within a glass state, it is able to sustain a shear strain on a time scale which corresponds to the diverging time scale for which the dynamics becomes diffusive. One can then follow adiabatically the slave replica until a state point $(T, \hat{\varphi})$ and study the linear response to shear for the different phases of the glass. This corresponds to exploring the strain vs volume fraction phase diagram of the system. Upon decompression, the shear modulus decreases and displays a square root singularity at the melting spinodal point [187, 329].

Increasing the strain and/or the volume fraction, the glass phase may undergo a Gardner transition and transform into a marginal glass, for which all non-linear elastic moduli diverge and standard elasticity theory does not hold anymore [331]. As for a simple compression without shear, the boundary of the Gardner phase transition explicitly depends on the selected glass state.

Once the Gardner phase is entered, upon further compression or strain, two kinds of transition may occur in hard sphere glasses. First, the shear modulus may increase and eventually diverge when a jamming point is reached. At zero strain, this is the ordinary jamming transition. In that case, the power law scaling of the MSD directly implies a similar behaviour for the shear modulus. In the presence of a finite strain, this corresponds to the phenomenon of shear jamming, observed in the context of granular materials [332, 333].

A second type of instability can occur when increasing the strain of a hard sphere glass. Here, the shear stress reaches a maximum followed by a spinodal instability where the fullRSB solution for Δ and Δ_r is no longer stable. The spinodal point $\gamma_Y(\hat{\varphi}_g)$ corresponds to the glass yielding transition [332, 334]. The yielding transition in glasses has been studied for a variety of models and under different physical conditions [335, 336]. In particular, it has been suggested that the yielding transition belongs to the same universality class as the RFIM, i.e. a spinodal transition with disorder.

IX. NEW COMPUTATIONAL METHODS

In the last decade, a number of new numerical techniques have allowed to attack the challenges presented in the above theoretical sections. These techniques typically make use of tools that go beyond the realm of standard computer simulations to either sample phase space more efficiently, or access information and observables that are not directly stored in particle trajectories.

A. The Swap Monte-Carlo method

To sample deeply supercooled states in equilibrium, one needs to run computer simulations over a duration that scales with the equilibrium structural relaxation

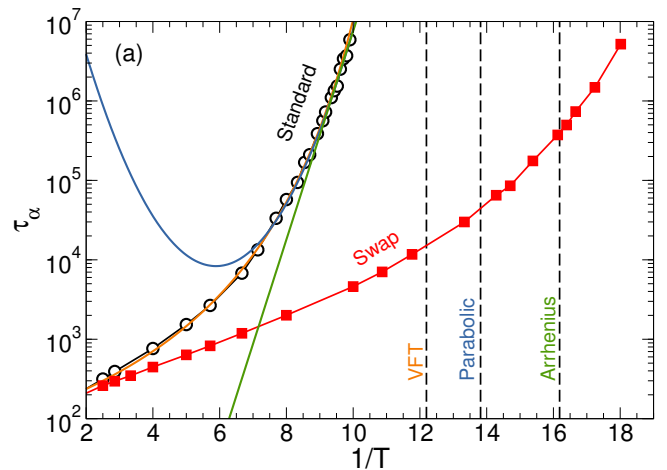


FIG. 18. From [338]. Relaxation times for standard (open symbols) and swap (closed symbols) Monte Carlo dynamics. The standard dynamics is fitted with the VFT, parabolic, and Arrhenius laws, which are then used to estimate the location of the experimental glass temperature T_g (vertical dashed lines). The swap dynamics efficiently equilibrates the system at temperatures below T_g .

time τ_α . Because τ_α grows rapidly as the system approaches the glass transition, ordinary computer simulations are limited to a rather high temperature regime much above the experimental glass transition T_g .

The swap Monte Carlo algorithm is an efficient way to produce equilibrium configurations of a supercooled liquid on the computer [337, 338]. Here, ‘efficient’ means that the equilibration time of the swap Monte Carlo algorithm increases much less than τ_α as temperature decreases. Actually, it was shown that for several three dimensional model systems, the equilibration speedup can be larger than a factor 10^{11} , as illustrated in Fig. 18. For this particular model of soft spheres, the swap algorithm continues to reach thermal equilibrium below the experimental glass transition T_g .

The swap algorithm was introduced long ago [339], and it was first used in the context of the glass transition by Grigera and Parisi [340]. Its ability to reach equilibrium at extremely low temperatures was established more recently [337, 338, 341]. By comparison with ordinary computer simulations, the swap Monte Carlo algorithm introduces unphysical particle moves, where the identity of a pair of randomly chosen particles is exchanged. Provided the swap moves are constructed to satisfy detailed balance, the algorithm is guaranteed to reach thermal equilibrium. The swap Monte Carlo algorithm can be implemented in a molecular dynamics setting, replacing the swap moves by an exchange between the system and a reservoir of particles [342–344]. Typically, increasing the frequency of swap moves speeds up the dynamics but there are practical limits to the maximal allowed frequency [344]. The swap algorithm was shown to work well from $d = 2$ up to at least $d = 8$ dimensions [345].

A decisive step to increase the efficiency of the swap

Monte Carlo algorithm was the development of models for supercooled liquids that were tailored to increase the swap efficiency. However, and perhaps more importantly, many models that were previously thought to be good glass-formers were in fact crystallizing very easily when swap was employed. Thus, a key step was also the development of more robust glass-forming models, using size polydispersity and non-additive interaction parameters to prevent structural ordering [338, 346].

In summary, the swap Monte Carlo algorithm easily and rapidly produces a large number of independent equilibrium configurations of a glass-former over a very broad range of temperatures, from the high temperature liquid, down to the mode-coupling crossover, and even below the experimental glass transition temperature. The latter regime can be explored experimentally only using physical vapor deposition, see Sec. IV F. Therefore, many physical properties of glassy materials can now be measured over a temperature regime that is extremely broad, and may be compared directly to experiments with no extrapolation. This has led to an important activity to address several problems related to glassy materials: the Gardner transition in finite dimensional glass-formers [304–306], the link between glass and jamming transitions [337, 347], the measurement of the configurational entropy in deeply supercooled liquids [348, 349], the analysis of point-to-set lengthscales [350, 351] and of the Franz-Parisi potential [350, 352], the evolution of several important properties of glasses with the glass preparation [108, 353, 354], and the physics of ultrastable glasses [93, 107].

In addition, the demonstration that a very simple algorithm can speed up the equilibration dynamics of supercooled liquids can be seen as an interesting physical result in itself. If such a result appears quite natural in the context of kinetic facilitation [355, 356], it is more challenging (but possible) to interpret in the context of the random first order transition theory [223, 357, 358], where dynamics becomes highly collective at very low temperatures.

B. Franz-Parisi potential

In seminal work [359, 360], Franz and Parisi introduced a quantity now called the Franz-Parisi potential, $V(Q)$. This quantity plays the role of a Landau free energy for mean-field phase transitions, in the sense that it expresses the free energy cost of the order parameter fluctuations at the mean-field level.

For spin glass models, where the approach was first introduced, the overlap Q represents indeed the spin glass order parameter. It quantifies the degree of similarity between two configurations \mathcal{C}_0 and \mathcal{C}_1 . For liquids with continuous degrees of freedom, a practical definition of

the overlap reads:

$$Q = \frac{1}{N} \sum_{i=1}^N \sum_{j=1}^N \Theta(a - |\mathbf{r}_i^{\mathcal{C}_0} - \mathbf{r}_j^{\mathcal{C}_1}|), \quad (39)$$

where $\mathbf{r}_i^{\mathcal{C}_0}$ represents the position of particle i in configuration \mathcal{C}_0 . The overlap is close to unity when the two configurations \mathcal{C}_0 and \mathcal{C}_1 have similar density profiles, up to thermal vibrations of spatial extension a (typically, one takes a as a small fraction of the particle diameter, $a \sim 0.2\sigma$).

The Franz-Parisi potential $V(Q)$ efficiently captures all the features associated to a random first order transition. It can be defined from the probability distribution function $P(Q)$ of the overlap as $V(Q) = -(T/N) \log P(Q)$. In particular, $V(Q)$ is characterised by a single minimum near $Q = 0$ at high temperature, but develops within mean-field theory a secondary minimum at a finite $Q > 0$ when T decreases towards the Kauzmann transition, indicating that the glass phase is metastable with respect to the liquid. The free energy difference between the glass and the liquid phases in this regime is given by $TS_c(T)$, where $S_c(T)$ is the configurational entropy. Physically, this means that localising the system in a single free energy minimum in the liquid phase comes with a free energy cost of entropic nature.

In addition, Franz and Parisi introduced a field ε conjugate to the overlap Q :

$$H_{FP}[\mathcal{C}_1] = H[\mathcal{C}_1] - \varepsilon Q[\mathcal{C}_0, \mathcal{C}_1]. \quad (40)$$

This allowed them to explore an extended phase diagram by changing both T and ε [361, 362]. In this plane, the Kauzmann transition at $(T = T_K, \varepsilon = 0)$ extends as a first order transition line, which ends at a second order critical point at a position $(T_c > T_K, \varepsilon_c)$. More recent work taking into account finite dimensional fluctuations suggest that this critical point should exist also in finite dimensions, and should be in the same universality class of the random field Ising model [363].

The Franz-Parisi potential and the extended phase diagram have been studied numerically in finite dimensional models in recent years [267, 350, 352, 361, 364–368]. Taken together, these studies confirm the existence of both a first order transition line and a second order RFIM critical point in finite dimensional glass-formers.

A second important outcome of the Franz-Parisi potential is the possibility to directly estimate a configurational entropy for equilibrium glass-formers using the free energy difference between the liquid and metastable glass phase [350, 369]. This definition of the configurational entropy is conceptually closer to its mean-field definition, and does not rely on an explicit definition of metastable states for a finite dimensional system [11].

C. Point-to-set lengthscale

As mentioned in Sec. III B, assessing and measuring a growing static length scale is crucial to the glass problem. Standard probes used for second order phase transitions, such as 2-point and 4-point correlation functions, do not seem to provide any useful evidence. A possible explanation is that these correlation functions do not carry enough information to capture the relevant structural order, also termed amorphous order, and that one has to use higher-order correlation functions (see also sec. VI B). The point-to-set correlation function $C(R)$ is effectively an n -point correlation function, where n is the number of particles comprised in a sphere of radius R (the ‘set’), which can indeed be a large number.

The justification is that in order to probe amorphous order one has to proceed as in standard phase transitions: fix a suitable boundary condition and study whether it enforces a given arrangement of particles in the bulk of the system. For simple cases, such as the ferromagnetic Ising model, it is clear what type of boundary conditions are needed (all spins up or all spins down). However, for supercooled liquids this is a much harder task. The problem can be circumvented by using equilibrated configurations and freezing all particles outside a cavity of radius R . This provides the boundary conditions sought for: if the system is indeed ordering, then using cavities drawn from different equilibrium configurations will give access to different sets of appropriate boundary conditions. This method was first proposed theoretically in the context of RFOT theory [203, 370] and signal processing [371], and was transformed into a concrete numerical procedure in Refs. [17, 372]. In the last decades, measurements of the point-to-set length were progressively refined [59, 350, 351, 373–375].

Let us describe the main steps and mention some important obstacles that had to be overcome. Firstly, one needs a collection of well-equilibrated configurations \mathcal{C}_0 to start with. This is not supposed to be the hardest part, but for very low temperatures, methods such as the swap Monte Carlo algorithm are necessary.

Secondly, for each sample \mathcal{C}_0 one freezes all particles outside a cavity of radius R , then let the particles inside ergodically visit the remaining phase space, and record the configurations \mathcal{C}_1 that are sampled. For small cavities, large activation barriers make conventional molecular dynamics simulations ineffective, but this problem can be solved using parallel tempering techniques [374], in addition to swap Monte Carlo [373]. It is crucial to check that a complete sampling of the restricted configurational space has been reached inside the cavity, and careful tests have been devised to this end [373].

Thirdly, one needs to measure the overlap distribution $P(Q)$ between the quenched reference configuration \mathcal{C}_0 and the equilibrium samples \mathcal{C}_1 . This is very similar to the Franz-Parisi construction, except for the local nature of the constraint. There are two possibilities. One is that the cavity is so small that only one state (one configura-

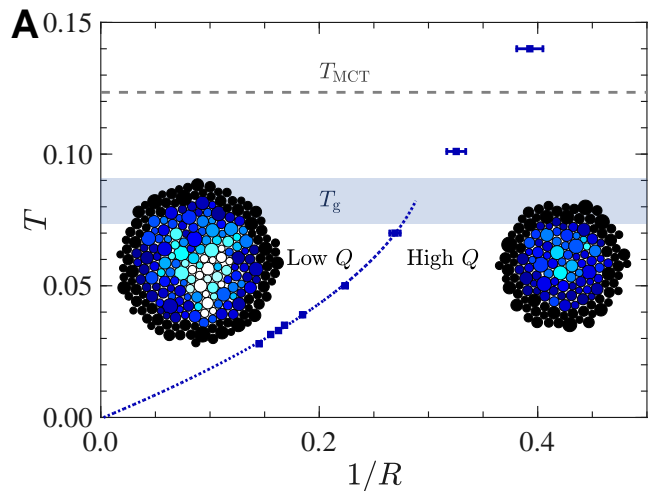


FIG. 19. From [349]. Evolution of the inverse point to set length, denoted here as $1/R$ with the temperature T . A clear growth of the point to set length up to $\xi_{PTS} \approx 6.5$ is observed. Cavities smaller (larger) than ξ_{PTS} have a large (small) overlap with the reference configuration, as illustrated in the snapshots, where the particle shade encodes the overlap value.

tion, up to vibrations) can be visited, so that the peak of $P(Q)$ is in the high-overlap range. The other is that the cavity is sufficiently large for many different states to be accessible. In that case, $P(Q)$ has a peak at low Q . In between the two cases, there is a critical value of the radius, $R \sim \xi_{PTS}$, which corresponds to the crossover, with a bimodal $P(Q)$. Since finite size cavities cannot be self-averaging, one needs to repeat the overlap measurements for many independent quenched configurations \mathcal{C}_0 , and then perform an average over these realizations of the disorder. Indeed, for $R \sim \xi_{PTS}$, large sample-to-sample variations of $P(Q)$ are observed.

There are a number of subtleties and extensions related to the overlap function that we now describe. A first subtlety is that an appropriate measure of the overlap needs to focus on the center of the spherical cavity, since boundaries always have a high overlap, and this makes the results difficult to interpret [372]. Moreover, the overlap needs to be a smooth function of the distance between configurations, and step functions are too singular to average over. A second subtlety is that for some liquids, the simple positional information does not adequately cover all the structural information. In that case, the conventional overlap needs to be completed with additional coordinates overlap, e.g. bond angles. This was used in Ref. [351] to show that hexatic order could be captured by the point-to-set correlations (see also [376]).

Let us also mention a few extensions of the method that have been proposed. In Ref. [373], the authors proposed to relax the frozen configuration constraint by letting the outside atoms vibrate, so long as they maintain a large overlap with the initial configuration: they called this reference state ‘frozen state’ (as op-

posed to frozen configuration). A second type of extension is to study various confinement geometries, as in Refs. [59, 156, 373, 377], where it was shown that the geometry of confinement needs to be carefully considered.

Thanks to the computational progress outlined above, several important results were established in the last decade. Among them: (i) clear evidence that the slowing down of the dynamics is accompanied by the growth of the point-to-set length (even though a mild one), (ii) established relation between point-to-set and configurational entropy: the former appears to be inversely proportional to the other [11], thus directly linking the growth of amorphous order to the decrease in number of metastable states—a tenet of RFOT theory, (iii) clear difference between two dimensional and three dimensional behavior: two-dimensional glass-formers display a point-to-set that appears to diverges at zero temperature, as shown in Fig. 19, thus indicating a $T_K = 0$ Kauzmann transition temperature [349]. This is in sharp contrast with the results in three dimensions, where the extrapolated T_K is larger than zero.

D. s -ensemble and large deviations

The Franz-Parisi potential is an example of a large deviation analysis. The idea behind it is that fluctuations in the overlap field play an important role for the glass transition, analog to the magnetization field in a ferromagnet. In order to investigate such fluctuations, one can then study the large deviation function (the free-energy) associated to the spatial average of the field (the order parameter). This is the usual route followed in thermodynamic analyses of second-order phase transitions. The s -ensemble is the dynamical counterpart of such a procedure. One modifies the dynamical rules, in order to be in a particular subset of the ‘dynamical states’, to probe the tendency of the original system to explore these states. This idea originates both from theoretical considerations on the large deviations of activity (rare events) predicted in KCMs [378, 379] and from considerations on efficient simulation schemes (for rare events as well) that apply more generally [380]. In practice, the s -ensemble dynamics is a particular instance of transition path sampling, where the quantity of interest is a measure of the activity of a multi-particles trajectory $\{x_i(t)\}_{i=1,\dots,N}$, cumulated over time

$$K[x(t)] = \frac{1}{N t_{obs}} \sum_{t \in [t_0, t_0 + t_{obs}]} \sum_{i \in [1, N]} (x_i(t + \Delta t) - x_i(t))^2 \quad (41)$$

where Δt (resp. t_{obs}) is chosen to be of the order of a few ballistic times (resp. a few relaxation times). In the s -ensemble, the actual relaxation time then becomes larger than t_{obs} . Here we follow the notations used in [263], where this biasing method was first applied to structural glasses (for its initial introduction in KCMs, see

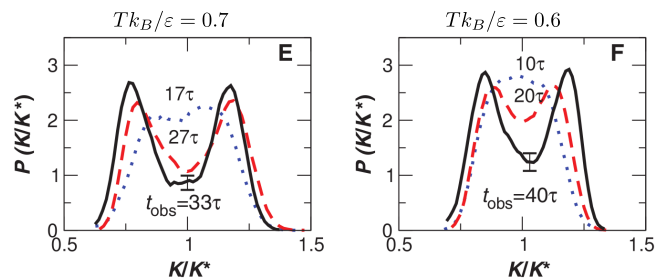


FIG. 20. From [263]. Coexistence of the active (large K) and inactive (small K) phases, as evidenced from s -ensemble biased simulations. As temperature is reduced, the distribution becomes increasingly bimodal, as expected when approaching a first order phase transition.

[246, 378, 379]). The method is called s -ensemble because the probability of a trajectory $x(t)$ is $P_0[x(t)]e^{-sK[x(t)]}$, where $P_0[x(t)]$ is the probability for the unperturbed system. This amounts to defining a ‘thermodynamics of trajectories’ which are biased (and classified) depending on their activity; s is the biasing field. In order to numerically simulate and probe such a measure, one can perform Monte-Carlo sampling in trajectory space. This method is actually so efficient at finding low-energy states that special attention must be paid to crystallisation [263].

One of the most important results obtained by the s -ensemble method is a direct evidence of a first order phase transition between an active phase (for low s) and an inactive phase (for large s) in supercooled liquids: see Fig. 20. In the $s - T$ plane this corresponds to a first order transition line $s^*(T)$ which ends in a critical point at high temperature [246, 263]. Although the method focuses on the dynamical properties, inactive states do exhibit interesting structural features. They are more stable than equilibrium samples [381]: mechanically, in terms of their lower number of low-energy modes (depletion of $D(\omega)$), and thermodynamically, in terms of a longer lived ‘melting’ transient from the glass to the liquid state. This suggests that inactive states correspond to very stable glassy state, i.e. non-equilibrium glassy states with low fictive temperatures.

The foundation of the s -ensemble relies on the dynamical behavior of KCMs. For the East model scenario it was shown [264] that configurations obtained by (i) the s -ensemble, (ii) finite-rate cooling, and (iii) quenching and long time aging, are all equivalent. This provides a concrete example where glassiness is directly related to the phase transition unveiled by the s -ensemble. Let us conclude by noticing that even systems having a RFOT display such a phase transition, the difference being that the line $s^*(T)$ reaches $s^* = 0$ for $T = T_K$ and not for $T = 0$ as for KCMs [382]. This shows that the s -ensemble is actually a general construction, which transforms the physics of metastability observed in supercooled liquids in well-defined phase transitions in the extended ensemble comprising space and time.

E. Machine Learning developments

We have mentioned the possible use of (unsupervised) Machine Learning (ML) in sec. VII C for automatic identification of LPS in supercooled liquids (see also Ref. [295]). Another set of ML techniques to be used is supervised learning: automatically defining fluid- or solid-like structures (features in ML language) by labeling them for a training set of local environments which are observed to be locally fluid- or solid-like. The general idea developed in [383] is to train a neural network (or other fitting model) to ‘predict’ the current degree of mobility or ‘instantaneous activity’ from the knowledge of structure only. This may be cast as finding the function f such that $f(\{\vec{r}\})(i, t) = y_{pred} \approx y_{true}(i, t)$, where $\{\vec{r}\}(i, t)$ is the structure of the neighborhood of particle i at time t , and $y_{true}(i, t)$ (the label) is a measure of the dynamical activity for particle i at time t . Concretely, the target label y_{true} has to encode some notion of local, instantaneous mobility [384–387], while the local structure may be defined e.g. by the (local, instantaneous) density pair correlation function $g(r)$, with the possible addition of angular variables [388, 389]. This technique has been applied with success, showing how much structure correlates with dynamics in supercooled liquids [389, 390], disordered solids [388–392], for the plasticity of amorphous materials [393, 394] and in polycrystalline materials [395].

The problem of the interpretation, which is one of the major issues with statistical learning in general, remains open: how to make use of predictions emerging from hundred-parameters models? This issue is transverse to most ML applications and is currently under active scrutiny. In terms of basic science, the conclusion of Liu and collaborators is that the predicted y_{pred} provides a new observable, called the softness field [392], which plays a key role for the dynamics.

We conclude mentioning a very recent work which introduced a new ML technique in the glass physics arena. The authors of [396] focused on the problem of predicting long-time dynamics (more precisely, the propensity field [397]) from knowledge of structure alone, by leveraging on recent progress in graph neural networks. The results are impressive: the ability to predict the propensity map is substantially better than existing numerical physics-based methods and the ML techniques described above, thus establishing a promising new way to study glassy dynamics.

X. AGING AND OFF-EQUILIBRIUM DYNAMICS

A. Why aging?

We have dedicated most of the above discussion to properties of materials approaching the glass transition at thermal equilibrium. We discussed a rich phenomenology and serious challenges for both our numerical and

analytical capabilities to account for these phenomena. For most people, however, glasses are interesting below the glass transition, so deep in the glass phase that the material seems to be frozen forever in a seemingly arrested amorphous state, endowed with enough mechanical stability for a glass to retain, say, the liquid it contains (preferably a nice red wine). Does this mean that there is no interesting physics in the glass state?

The answer is clearly ‘no’. There is still life (and physics) below the glass transition. We recall that for molecular glasses, T_g is defined as the temperature below which relaxation is too slow to occur within an experimental timescale. Much below T_g , therefore, the equilibrium relaxation timescale is so astronomically large that thermal equilibrium is out of reach. One enters therefore the realm of off-equilibrium dynamics. A full physical understanding of the non-equilibrium glassy state remains a central challenge [5, 192].

A first consequence of studying materials in a time window smaller than equilibrium relaxation timescales is that the system can, in principle, remember its complete history, a most unwanted experimental situation since all details of the experimental protocol may then matter. The simplest protocol to study aging phenomena in the glass phase is quite brutal [4]: take a system equilibrated above the glass transition and suddenly quench it at a low temperature at a ‘waiting time’ $t_w = 0$ which corresponds to the beginning of the experiment. For $t_w > 0$ the system is left unperturbed at constant temperature where it tries to slowly reach thermal equilibrium, even though it has no hope to ever get there. Aging means that the system never forgets the time t_w spent in the glass phase, its ‘age’. The evolution of one time quantities, e.g. the energy, as a function of time are not a good evidence of aging. In order to show that the system never equilibrates, two time quantities such as density-density or spin-spin correlation functions are much more useful. A typical example is presented in Fig. 21 where the self-part of the intermediate function in Eq. (5) is shown for a Lennard-Jones molecular liquid at low temperature. Immediately after the quench, the system exhibits a relatively fast relaxation: particles still move substantially. However, when the age increases, dynamics slow down and relaxation becomes much slower. When t_w becomes very large, relaxation becomes too slow to be followed in the considered time window and the system seems frozen on that particular timescale: it has become a glass. A striking feature conveyed by these data is that an aging system not only remains out-of-equilibrium for all practical purposes, but its typical relaxation time is in fact set by its age t_w . In simple cases, the effective relaxation time after waiting a time t_w scales at t_w itself, which means that since equilibration timescales have diverged, t_w is the only remaining relevant timescale in the problem.

A popular interpretation of this phenomenon is given by considering trap models [398]. In this picture, reminiscent of the Goldstein view of the glass transition men-

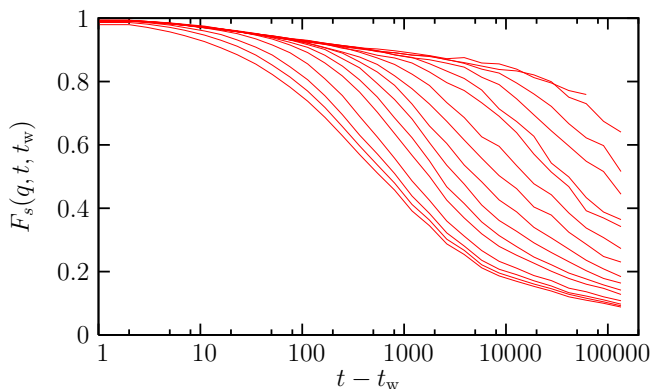


FIG. 21. Aging dynamics in a Lennard-Jones glass-forming liquid at low temperature. The system is quenched at time $t_w = 0$ at low T , where the temperature is kept constant. Two-time self-intermediate scattering functions are then measured for 20 logarithmically spaced waiting times t_w from $t_w = 1$ to $t_w = 10^5$ (from left to right). The relaxation becomes slower when t_w increases: the system ages.

tioned above [13], the system is described as a single particle evolving in a complex energy landscape with a broad distribution of trap depths—a paradigmatic mean-field approach. Aging in this perspective arises because the system visits traps that become deeper when t_w increases, corresponding to more and more stable states. It therefore takes more and more time for the system to escape, and the dynamics slow down with time, as observed in Fig. 21. This implies that any physical property of the glass becomes an age-dependent quantity in aging protocols, and more generally becomes dependent on how the glass was prepared. One can easily imagine using this property to tune mechanical or optical characteristics of a material by simply changing the way it is prepared, like how fast it is cooled to the glassy state (recall our discussion of ultrastable glasses in Sec. IV F).

A real space alternative picture was promoted in particular in the context of spin glass studies, based on the ideas of scaling and renormalization [399–401]. The physical picture is that of a coarsening process, where the system develops long-range order by growing extended domains of lengthscale $\ell(t_w)$. On lengthscales less than $\ell(t_w)$, the system has had the time to order since the quench at $t_w = 0$. The walls between domains evolve in a random environment. In order to move they have to overcome free energy barriers. It is then assumed an activated dynamic scaling which states that the typical barrier to extend the domain from linear size $\ell(t_w)$ to, say, $2\ell(t_w)$ scales as ℓ^ψ , where ψ is some ‘barrier’ exponent. Using the Arrhenius law to relate dynamics to barriers, one gets that aging corresponds to the logarithmic growth with time of spatially correlated domains, $\ell \sim (T \log t_w)^{1/\psi}$. A domain growth picture of aging in spin glasses can be directly confirmed by numerical simulations [402], only indirectly by experiments.

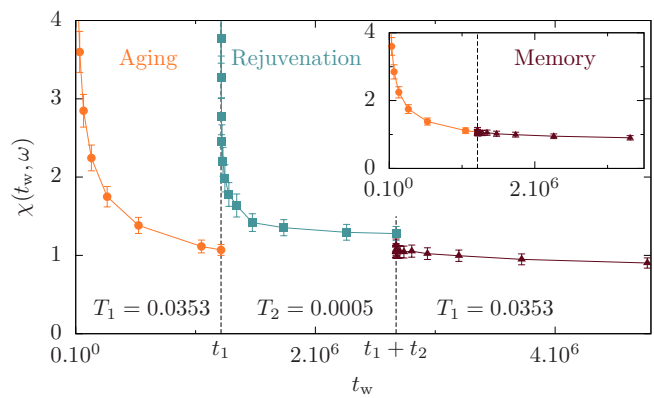


FIG. 22. Memory and rejuvenation effects obtained in the numerical simulation of a three-dimensional glass-former [303]. There is a first aging step, $0 < t_w < t_1$, during which the system slowly tries to reach thermal equilibrium at temperature T_1 . The system ‘rejuvenates’ in the second step at T_2 , $t_1 < t < t_1 + t_2$, and it restart aging (rejuvenation). Finally in the third step, temperature is back to T_1 , and memory of the first step is kept intact, as shown in the inset where relaxation during the second step of the experiment is taken away.

B. Memory and rejuvenation effects

Since the complete history of a sample in the glass phase matters, there is no reason to restrain experimental protocols to the simple aging experiment mentioned above. Indeed, experimentalists have investigated scores of more elaborated protocols that have revealed an incredibly rich, and sometimes quite unexpected, physics [5]. We restrain ourselves here to a short discussion of memory and rejuvenation effects observed during temperature cycling experiments [403] (one can imagine applying a magnetic field or a mechanical constraint, be they constant in time or sinusoidal, etc.). These two effects were first observed in spin glasses, but the protocol was then repeated in many different materials, from polymers and organic liquids to disordered ferroelectrics. After several unsuccessful attempts, similar effects are now observed in numerical work as well [404, 405]. Recent results obtained from simulations of a three-dimensional glass-former exploring the spin-glass-like Gardner phase [303] are presented in Fig. 22.

There are three steps in temperature cycling experiments [403]. The first one is a standard aging experiment, namely a sudden quench from high to low temperature at time $t_w = 0$. The system then ages for a duration t_1 at constant temperature T_1 . The system slowly relaxes towards equilibrium and its dynamics slows down: for our spin glass example (see Fig. 22) this is observed through the measurement of some dynamic susceptibility $\chi(t_w, \omega)$. Temperature is then suddenly shifted to $T_2 < T_1$ at time t_1 . There, the material restarts aging (almost) as if the first step had not taken place. This is called ‘rejuvenation effect’, because the system seems to

forget it is already ‘old’. At total time $t_1 + t_2$, temperature is then shifted back to its initial value T_1 . Then, aging is found to proceed as a quasi-perfect continuation of the first step, as if the second step had not taken place. The system has kept the ‘memory’ of the first part of the experiment, despite the rejuvenation observed in the intermediate part. The memory effect becomes more spectacular when relaxation during the second step is removed, as in the inset of Fig. 22. The third relaxation appears indeed as a perfect continuation of the first one.

On top of being elegant and quite intriguing, such protocols are relevant because they probe more deeply the dynamics of aging materials, allowing one to ask more precise questions beyond the simplistic observation that ‘this material displays aging’. Moreover, the observation of similar effects in many different glassy materials implies that these effects are intrinsic to systems with slow dynamics. Interesting also are the subtle differences observed from one material to the other.

Several experimental, numerical and theoretical papers have been devoted to this type of experiments, and these effects are not ‘mysterious’ anymore (see Ref. [192]). A clear link between memory effects and typical lengthscales over which the slow dynamics takes place has been established. Because lengthscales depend so sensitively on timescales and on the working temperature, experiments performed at two different temperatures typically probe very different lengthscales, allowing the system to store memory of its state at different temperatures over different lengthscales [405, 406]. In return, this link has been elegantly exploited to obtain a rather precise experimental estimate of dynamic lengthscales involved in the aging dynamics of spin glass materials [407], which seems to confirm the slow logarithmic growth law mentioned before.

Discussion of the rejuvenation effect is slightly more subtle. It is indeed not yet obvious that the effect as it is observed in computer simulations and reported, e.g. in Fig. 22, is exactly similar to the one observed in experiments. The difficulty comes from the fact that some seemingly innocuous details of the experimental protocol, such as the necessary use in experiments of finite cooling rates, in fact play a crucial role and influence the physics so that direct comparison between experiments and simulations is difficult. In numerical work, rejuvenation can be attributed to a gradual change with temperature of the nature of spatial correlations between spins that develop with time [404, 405]. More drastic changes are predicted to occur in disordered systems as a result of the chaotic evolution with temperature of the metastable states in a spin glass (so-called ‘chaos effect’ [408]), that could also be responsible for the observed rejuvenation effect [409].

C. Mean-field aging and effective temperatures

Theoretical studies of mean-field glassy models have provided important insights into the aging dynamics of both structural and spin glasses [410, 411]. Although such models are defined in terms of spin degrees of freedom interacting via infinite-ranged interactions, the deep connections between them and the mode-coupling theory of the glass transition make them serious candidates to investigate glassy states in general, not only thermodynamic properties at thermal equilibrium but also non-equilibrium aging dynamics. Despite their often reported ‘simplicity’, it took several years to derive a proper asymptotic solution of the long-time dynamics for a series of mean-field spin glasses (see Cugliandolo in Ref. [192]). These results have then triggered an enormous activity [412] encompassing theoretical, numerical and also experimental work trying to understand further these results, and to check in more realistic systems whether they have some reasonable range of applicability beyond mean-field.

This large activity, by itself, easily demonstrates the broad interest of these results. More recently, the derivation of the static properties of liquids and glasses in large dimensions has renewed the interest in mean-field dynamic phenomena [187]. In particular, the dynamic equations governing the equilibrium properties of supercooled liquids have now been derived [193, 413] and their consequences are being explored [414]. The study of the non-equilibrium (aging and sheared) dynamics is now under way [415–417].

In these mean-field models, thermal equilibrium is never reached, and aging proceeds by downhill motion in an increasingly flat free energy landscape [418], with subtle differences between spin glass and structural glass models. In both cases, however, time translational invariance is broken, and two-time correlation and response functions depend on both their temporal arguments. In fact, the exact dynamic solution of the equations of motion for time correlators displays behaviours in strikingly good agreement with the numerical results reported in Fig. 21.

In these systems, the equations of motion in the aging regime involve not only temporal correlations, but also time-dependent response functions. At thermal equilibrium, response and correlation are not independent, since the fluctuation-dissipation theorem (FDT) relates both quantities. In aging systems, there is no reason to expect the FDT to hold and both quantities carry, at least in principle, distinct physical information. Again, the asymptotic solution obtained for mean-field models quantitatively establishes that the FDT does not apply in the aging regime. Unexpectedly, the solution also shows that a generalized form of the FDT holds at large waiting times [410]. This is defined in terms of the two-time connected correlation function for some generic observable

$A(t)$,

$$C(t, t_w) = \langle A(t)A(t_w) \rangle - \langle A(t) \rangle \langle A(t_w) \rangle, \quad (42)$$

with $t \geq t_w$, and the corresponding two-time (impulse) response function

$$R(t, t_w) = T \left. \frac{\delta \langle A(t) \rangle}{\delta h(t_w)} \right|_{h=0}. \quad (43)$$

Here h denotes the thermodynamically conjugate field to the observable A so that the perturbation to the Hamiltonian (or energy function) is $\delta E = -hA$, and angled brackets indicate an average over initial conditions and any stochasticity in the dynamics. Note that we have absorbed the temperature T in the definition of the response, for convenience. The associated generalized FDT reads then

$$R(t, t_w) = X(t, t_w) \frac{\partial}{\partial t_w} C(t, t_w), \quad (44)$$

with $X(t, t_w)$ the so-called fluctuation-dissipation ratio (FDR). At equilibrium, correlation and response functions are time translation invariant, depending only on $\tau = t - t_w$, and equilibrium FDT imposes that $X(t, t_w) = 1$ at all times. A parametric fluctuation-dissipation (FD) plot of the step response or susceptibility

$$\chi(t, t_w) = \int_{t_w}^t dt' R(t, t'), \quad (45)$$

against

$$\Delta C(t, t_w) = C(t, t) - C(t, t_w), \quad (46)$$

is then a straight line with unit slope. These simplifications do not occur in non-equilibrium systems. But the definition of an FDR through Eq. (44) becomes significant for aging systems [410, 411]. In mean-field spin glass models the dependence of the FDR on both temporal arguments is only through the correlation function,

$$X(t, t_w) \sim X(C(t, t_w)), \quad (47)$$

valid at large waiting times, $t_w \rightarrow \infty$. For mean-field structural glass models, the simplification (47) is even more spectacular since the FDR is shown to be characterized by only two numbers instead of a function, namely $X \sim 1$ at short times (large value of the correlator) corresponding to a quasi-equilibrium regime, with a crossover to a non-trivial number, $X \sim X^\infty$ for large times (small value of the correlator). This implies that parametric FD plots are simply made of two straight lines with slope 1 and X^∞ , instead of the single straight line of slope 1 obtained at equilibrium.

Since any kind of behaviour is in principle allowed in non-equilibrium situations, getting such a simple, equilibrium-like structure for the FD relations is a remarkable result. This immediately led to the idea that

aging systems might be characterized by an effective thermodynamic behaviour and the idea of quasi-equilibration at different timescales [419]. In particular, generalized FD relations suggest to define an effective temperature, as

$$T_{\text{eff}} = \frac{T}{X(t, t_w)}, \quad (48)$$

such that mean-field glasses are characterized by a unique effective temperature, $T_{\text{eff}} = T/X^\infty$. It is thought of as the temperature at which slow modes are quasi-equilibrated. One finds in general that $0 < X^\infty < 1$, such that $T_{\text{eff}} > T$, as if the system had kept some memory of its high temperature initial state.

The name ‘temperature’ for the quantity defined in Eq. (48) is not simply the result of a dimensional analysis but has a deeper, physically appealing meaning that is revealed by asking the following questions. How does one measure temperatures in a many-body system whose relaxation involves well-separated timescales? What is a thermometer (and a temperature) in a far from equilibrium aging material? Answers are provided in Refs. [419, 420] both for mean-field models and for additional toy models with multiple relaxation timescales. The idea is to couple an additional degree of freedom, such as a harmonic oscillator, $x(t)$, which plays the role of the thermometer operating at frequency ω , to an observable of interest $A(t)$ via a linear coupling, $-\lambda x(t)A(t)$. Simple calculations show then that the thermometer ‘reads’ the following temperature,

$$\frac{1}{2} K_B T_{\text{meas}}^2 \equiv \frac{1}{2} \omega^2 \langle x^2 \rangle = \frac{\omega C'(\omega, t_w)}{2\chi''(\omega, t_w)}, \quad (49)$$

where $C'(\omega, t_w)$ is the real part of the Fourier transform of Eq. (42), and $\chi(\omega, t_w)$ the imaginary part of the Fourier transform of Eq. (43), with $h = \lambda x$. The relation (49) indicates that the bath temperature is measured, $T_{\text{meas}} = T$, if the frequency is high and FDT is satisfied, while $T_{\text{meas}} = T_{\text{eff}} > T$ if the frequency is slow enough to be tuned to that of the slow relaxation in the aging material. The link between the FDR in Eq. (44) and the effective temperature measured in Eq. (49) was numerically confirmed in the computer simulation of a glassy molecular liquid in Ref. [421].

More generally, relaxation in glassy systems occurs in well-separated time sectors [411]; it is then easy to imagine that each sector could be associated with an effective temperature [420]. A thermodynamic interpretation of effective temperatures has also been put forward, relating them to the concept of replica symmetry breaking [422]. Interestingly, the full-step or one-step replica symmetry breaking schemes needed to solve the static problem in these models have a counterpart as the FDR being a function or a number, respectively, in the aging regime. Moreover, we note that these modern concepts are related to, but make much more precise, older ideas of quasi-equilibrium and fictive temperatures in aging glasses [4].

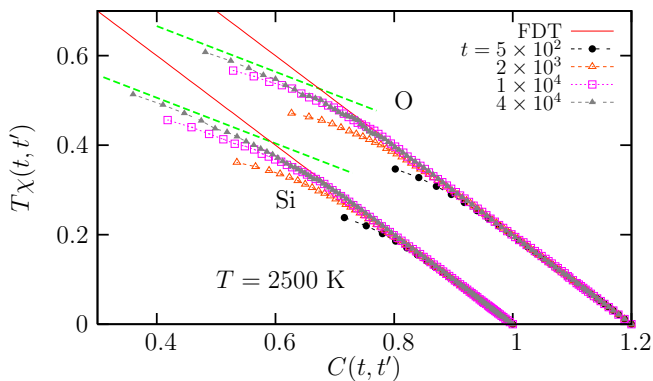


FIG. 23. Parametric correlation-response plots measured in the aging regime of a numerical model for a silica glass, SiO_2 [423]. The plots for both species smoothly converges towards a two-straight line plot of slope 1 at short times (large C values), and of slope $X^\infty \approx 0.51$ at large times (small values of C), yielding an effective temperature of about $T_{\text{eff}} = T/X^\infty \approx 4900$ K. Note that the glass transition temperature of SiO_2 is 1446K.

Taken together, these results make the mean-field description of aging very appealing, and they nicely complement the mode-coupling/RFOT description of the equilibrium glass transition described above. Moreover, they have set the agenda for a large body of numerical and experimental work, as reviewed in [412]. In Fig. 23 we present recent numerical data obtained in an aging silica glass [423], presented in the form of a parametric response-correlation plot. The measured correlation functions are the self-part of the intermediate scattering functions defined in Eq. (5), while the conjugated response functions quantify the response of particle displacements to a spatially modulated field conjugated to the density. Plots for silicon and oxygen atoms at different ages are presented. They seem to smoothly converge towards a two-straight line plot, as obtained in mean-field models (note, however, that this could be just a pre-asymptotic, finite ‘ t_w ’, effect). Moreover, the second, non-trivial part of the plot is characterized by a slope that appears to be independent of the species, and of the wavevector chosen to quantify the dynamics, in agreement with the idea of a unique asymptotic value of the FDR, possibly related to a well-defined effective temperature.

D. Beyond mean-field: Real Space

Despite successful results, such as those shown in Fig. 23, the broader applicability of the mean-field scenario of aging dynamics remains still unclear. While some experiments and simulations indeed seem to support the existence of well-behaved effective temperatures [424–426], other studies also reveal the limits of the mean-field scenario. Experiments have for instance reported anomalously large FDT violations associated

with intermittent dynamics [427–430], while theoretical studies of model systems have also found non-monotonic or even negative response functions [431–434], and ill-defined or observable-dependent FDRs [435]. In principle, these discrepancies with mean-field predictions are to be expected, since there are many systems of physical interest in which the dynamics are not of mean-field type, displaying both activated processes and spatial heterogeneity.

It is thus an important task to understand from the theoretical point of view when the mean-field concept of an FDR-related effective temperature remains viable. However, theoretically studying the interplay between relevant dynamic lengthscales and thermally activated dynamics in the non-equilibrium regime of disordered materials is clearly a challenging task. Nevertheless, this problem has been approached in different ways, as we briefly summarize in this subsection.

A first class of system that displays aging and spatial heterogeneity is given by coarsening systems. The paradigmatic situation is that of an Ising ferromagnetic model (with a transition at T_c) suddenly quenched in the ferromagnetic phase at time $t_w = 0$. For $t_w > 0$, domains of positive and negative magnetizations appear and slowly coarsen with time. The appearance of domains that grow with time proves the presence of both aging and heterogeneity.

The case where the quench is performed down to $T < T_c$ is well understood. The system becomes scale invariant [436], since the only relevant lengthscale is the growing domain size, $\ell(t_w)$. Correlation functions display aging, and scale invariance implies that $C(t, t_w) \sim f(\ell(t)/\ell(t_w))$. Response functions can be decomposed into two contributions [437, 438]: one part stems from the bulk of the domains and behaves as the equilibrium response, and a second one from the domain walls and becomes vanishingly small in the long time limit, where $\ell(t_w) \rightarrow \infty$ and the density of domain walls vanishes. This implies that for coarsening systems in $d \geq 2$, one has $X^\infty = 0$, or equivalently an infinite effective temperature, $T_{\text{eff}} = \infty$. The case $d = 1$ is special because $T_c = 0$ and the response function remains dominated by the domain walls, which yields the non-trivial value $X^\infty = 1/2$ [439, 440].

Another special case has retained attention. When the quench is performed at $T = T_c$, there is no more distinction between walls and domains and the above argument yielding $X^\infty = 0$ does not hold. Instead one studies the growth of critical fluctuations with time, with $\xi(t_w) \sim t_w^{1/z}$ the correlation length at time t_w , where z is the dynamic exponent. Both correlation and response functions become non-trivial at the critical point [441]. It proves useful in that case to consider the dynamics of the Fourier components of the magnetization fluctuations, $C_q(t, t_w) = \langle m_q(t)m_{-q}(t_w) \rangle$, and the conjugated response $R_q(t, t_w) = \frac{\delta \langle m_q(t) \rangle}{\delta h_{-q}(t_w)}$. From Eq. (44) a wavevector dependent FDR follows, $X_q(t, t_w)$, which has inter-

esting properties [442] (see [443] for a review).

In dimension $d = 1$, it is possible to compute $X_q(t, t_w)$ exactly in the aging regime at $T = T_c = 0$. An interesting scaling form is found, and numerical simulations performed for $d > 1$ confirm its validity:

$$X_q(t, t_w) = \mathcal{X}(q^2 t_w), \quad (50)$$

where the scaling function $\mathcal{X}(x)$ is $\mathcal{X}(x \rightarrow \infty) \rightarrow 1$ at small lengthscale, $q\xi \gg 1$, and $\mathcal{X}(x \rightarrow 0) \rightarrow 1/2$ (in $d = 1$) at large distance, $q\xi \ll 1$; recall that $z = 2$ in that case.

Contrary to mean-field systems where geometry played no role, here the presence of a growing correlation lengthscale plays a crucial role in the off-equilibrium regime since $\xi(t_w)$ allows one to discriminate between fluctuations that satisfy the FDT at small lengthscale, $X_q \sim 1$, and those at large lengthscale which are still far from equilibrium, $0 < X_q \sim X^\infty < 1$. These studies suggest therefore that generalized fluctuation-dissipation relations in fact have a strong lengthscale dependence—a result which is not predicted by mean-field approaches.

Another interesting result is that the FDT violation for global observables (i.e. those at $q = 0$) takes a particularly simple form, since the introduction of a single number is sufficient, the FDR at zero wavevector, $X_{q=0}(t, t_w) \equiv X^\infty = 1/2$ (in $d = 1$). This universal quantity takes non-trivial values in higher dimension, e.g. $X^\infty \approx 0.34$ is measured in $d = 2$ [442]. This shows that the study of global rather than local quantities makes the measurement of X^∞ much easier. Finally, having a non-trivial value of X^∞ for global observables suggests that the possibility to define an effective temperature remains valid, but it has become a more complicated object, related to global fluctuations on large lengthscale.

Kinetically constrained spin models represent a second class of non-mean-field systems whose off-equilibrium has been thoroughly studied recently [240]. This is quite a natural thing to do since these systems have local, finite ranged interactions, and they combine the interesting features of being defined in terms of (effective) microscopic degrees of freedom, having local dynamical rules, and displaying thermally activated and heterogeneous dynamics.

The case of the Fredrickson-Andersen model, described in Sec. VII, has been studied in great detail [240], and we summarize the main results. Here, the relevant dynamic variables are the Fourier components of the mobility field, which also correspond in that case to the fluctuations of the energy density. Surprisingly, the structure of the generalized fluctuation-dissipation relation remains once more very simple. In particular, in dimension $d > 2$, one finds a scaling form similar to (50), $X_q(t, t_w) = \mathcal{X}(q^2 t_w)$, with a well-defined limit at large distance $X_{q=0}(t, t_w) \equiv X^\infty$. The deep analogy with critical Ising models stems from the fact that mobility defects in KCMs diffuse in a way similar to domain walls in coarsening Ising models. It is in fact by exploiting this

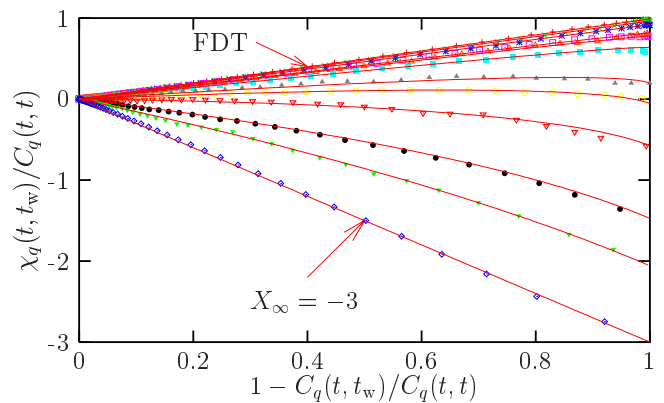


FIG. 24. Parametric response-correlation plots for the Fourier components of the mobility field in the $d = 3$ Fredrickson-Andersen model. Symbols are from simulations, lines from analytic calculations, and wavevectors decrease from top to bottom. The FDT is close to being satisfied at large q corresponding to local equilibrium. At larger distance deviations from the FDT are seen, with an asymptotic FDR which becomes negative. Finally, for energy fluctuations at $q = 0$ (bottom curve), the plot becomes a pure straight line of (negative!) slope -3 , as a result of thermally activated dynamics.

analogy that analytic results are obtained in the aging regime of the Fredrickson-Andersen model [444].

There is however a major qualitative difference between the two families of model. The (big!) surprise lies in the sign of the asymptotic FDR, since calculations show that [445]

$$X^\infty = -3, \quad d > 2. \quad (51)$$

In dimension $d = 1$, one finds $X_{q=0}(t, t_w) = f(t/t_w)$ with $X_{q=0}(t \rightarrow \infty, t_w) = \frac{3\pi}{16-6\pi} \approx -3.307$. Numerical simulations confirm these calculations. In Fig. 24, we show such a comparison between simulations (symbols) and theory (lines) in the case of the $d = 3$ Fredrickson-Andersen model [445]. Fourier components of the mobility field yield parametric FD plots that follow scaling with the variable $q^2 t_w$, as a direct result of the presence of a growing lengthscale for dynamic heterogeneity, $\xi(t_w) \sim \sqrt{t_w}$. Again, generalized fluctuation-dissipation relations explicitly depend on the spatial lengthscale considered, unlike in mean-field studies. In Fig. 24, the limit $q = 0$ corresponding to global observables is also very interesting since the plot is a pure straight line, as in equilibrium. Unlike equilibrium, however, the slope is not 1 but -3 . A negative slope in this plot means a negative FDR, and therefore suggests a negative effective temperature, a very non-intuitive result at first sight.

Negative response functions in fact directly follows from the thermally activated nature of the dynamics of these models [445]. First, one should note that the global observable shown in Fig. 24 corresponds to fluctuations of the energy, $e(t_w)$, whose conjugated field is temperature. In the aging regime the system slowly drifts towards equilibrium. Microscopic moves result from thermally ac-

tivated processes, corresponding to the local crossing of energy barriers. An infinitesimal change in temperature, $T \rightarrow T + \delta T$ with $\delta T > 0$, accelerates these barrier crossings and makes the relaxation dynamics faster. The energy response to a positive temperature pulse is therefore negative, $\delta e < 0$, which directly yields $\delta e / \delta T < 0$, which explains the negative sign of the FDR. This result does not hold in mean-field glasses, where thermal activation plays no role.

Finally, another scenario holds for local observables in some KCMs when kinetic constraints are stronger, such as the East model [240] or a bidimensional triangular plaquette model [446]. Here, relaxation is governed by a hierarchy of energy barriers that endow the systems with specific dynamic properties. In the aging regime following a quench, in particular, the hierarchy yields an energy relaxation that arises in discrete steps which take place on very different timescales, reminiscent of the ‘time sectors’ encountered in mean-field spin glasses. Surprisingly, it is found that to each of these discrete relaxations one can associate a well-defined (positive) value of the fluctuation-dissipation ratio, again reminiscent of the dynamics of mean-field spin glass models. Therefore, a physical picture seems to have some validity, even in models that are very far from the mean-field limit: in that picture, slow relaxation takes place on multiple timescales, with each timescale characterized by a different effective temperature.

E. Beyond mean-field: Energy Landscape

What the mean-field approach crucially lacks is the description of activated processes that allow the system to jump over larger and larger barriers at large times. One way to introduce this key effect is to study mean-field models at finite system size N . In fact, the mean field theory of aging is derived by first taking the limit $N \rightarrow \infty$ to study the dynamics on large but finite timescales. Instead, if one focuses on timescales that diverge exponentially with N , activated processes will occur. One can then analyze in a controlled way how jumping over barriers alters the mean-field dynamics.

This approach was pioneered numerically by Crisanti and Ritort [412, 447, 448], and more recently pursued further in [449–452]. One of the most important outcomes of their study is to show the existence of an effective temperature and its relation with the energy landscape, more precisely the complexity, even when barriers are crossed. The understanding of the dynamical evolution in this regime was reached recently by theoretical and rigorous analysis of the Random Energy Model (REM) in [449, 450, 453, 454]. It was shown that when observing the dynamics on exponentially large (in N) timescales, activated processes lead to a dynamical evolution that can be mapped on the one of the trap model [398, 455]. Again, an interesting relation with the energy landscape emerges: the exponent of the trapping time power law

describing aging dynamics at a given energy is directly linked to the slope of the configurational entropy at that energy. It is not yet clear whether this scenario goes beyond the REM and applies, for instance, to the Monte Carlo dynamics of the p -spin model. In this case the energy landscape is more complex and one needs to understand the interplay between energy and entropic barriers [456–458].

To this end, a series of recent works focused on the organization in configuration space of the barriers that can be used to escape from a given minimum for the p -spin spherical model. By using the Kac-Rice formalism, these works computed the entropy of the barriers at a given energy and at a certain distance from a given minimum [459] and obtained the dynamical instanton representing the escape from a given minimum.

Finally, another set of works performed a complementary study on finite size models of three dimensional supercooled liquids. The key idea was to focus on a size that is large enough to be representative of the bulk behavior and small enough to be able to study the dynamics in terms of energy landscape [460–462]. This led to the introduction of the notion of metabasins, a set of basins that corresponds to the same metastable state. A study of the dynamics in terms of energy barriers between metabasins was then performed. It showed in a very compelling way that the dynamics start to be activated even above the MCT cross-over in 3D systems [461, 463]. Interestingly, a strong relationship with the dynamics of the trap model was also found in this case [462].

All the results cited above provide valuable information and insights on activated dynamics. Interestingly, they show that relations between aging dynamics and energy landscape found within mean-field theory seem to hold more broadly. Many questions remain open and will hopefully be addressed in future work, such as understanding and characterizing the dynamical paths and the barrier crossings leading to relaxation during the aging regime.

F. Driven glassy materials

We have introduced aging phenomena with the argument that in a glass phase, the timescale to equilibrate becomes so long that the system always remembers its complete history. This is true in general, but one can wonder whether it is possible to invent a protocol where the material history could be erased, and the system ‘rejuvenated’ [464]. This concept has been known for decades in the field of polymer glasses, where complex thermo-mechanical histories are often used.

Let us consider an aging protocol where the system is quenched to low temperature at time $t_w = 0$, but the system is simultaneously forced by an external mechanical constraint. Experimentally one finds that a stationary state can be reached, which explicitly depends on the strength of the forcing: a system which is forced more

strongly relaxes faster than a material that is less solicited, a phenomenon called ‘shear-thinning’. The material has therefore entered a driven steady state, where memory of its age is no longer present and the dynamics have become stationary: aging is stopped.

Many studies of these driven glassy states have been performed in recent years. These studies are relevant for the rheology of supercooled liquids and glasses, and the $T \ll T_g$ limit corresponds to studies of the plasticity of amorphous solids, a broad field in itself, see Sec. VIII D. In the colloidal world, such studies are also relevant for the newly-defined field of the rheology of ‘soft glassy materials’. These materials are (somewhat tautologically) defined as those for which the non-linear rheological behaviour is believed to result precisely from the competition between intrinsically slow relaxation processes and an external forcing [465, 466]. It is believed that the rheology of dense colloidal suspensions, foams, emulsions, binary mixtures, or even biophysical systems are ruled by such a competition, which represents a broad scope for applications.

From the point of view of statmech modeling, soft glassy rheology can be naturally studied from the very same angles as the glass transition itself. As such trap models [465, 467], mean-field spin glasses [199] and the related mode-coupling theory approach [200, 201] have been explicitly extended to include an external mechanical forcing. In all these cases, one finds that a driven steady state can be reached and aging is indeed expected to stop at a level that depends on the strength of the forcing. Many of the results obtained in aging systems about the properties of an effective temperature are also shown to apply in the driven case, as shown both theoretically [199] and numerically [468]. A most interesting aspect is that the broad relaxation spectra predicted to occur in glassy materials close to a glass transition directly translate into ‘anomalous’ laws both for the linear rheological behaviour (seen experimentally in the broad spectrum of elastic, $G'(\omega)$, and loss, $G''(\omega)$, moduli), and the non-linear rheological behaviour (a strong dependence of the viscosity η upon the shear rate $\dot{\gamma}$).

XI. FUTURE DIRECTIONS

The problem of the glass transition, already very exciting in itself, has ramifications well beyond the physics of supercooled liquids. Glassy systems figure among the even larger class of ‘complex systems’. These are formed by a set of interacting degrees of freedom showing non-trivial emergent behaviour: as a whole they exhibit properties that are not already encoded in the definition of the individual parts. As a consequence the study of glass-formers as statistical mechanics models characterized by frustrated interactions is a fertile ground to develop new concepts and techniques that will likely be applied to

other physical, and more generally, scientific situations.

An example, already cited in this review, are the progress obtained in computer science and information theory [6] using techniques originally developed for spin glasses and structural glasses. There is no doubt that progress will steadily continue in the future along these interdisciplinary routes. Concerning physics, glassiness is such an ubiquitous and, yet as we showed, rather poorly understood problem that many developments are very likely to take place in the next decade.

Instead of guessing future developments of the field (and then very likely be proven wrong) we prefer to list a few problems we would like to see solved in the next years.

- Is the glass transition related to a true phase transition? If yes, a static or a dynamic one? A finite or zero temperature one?
- Do RFOT theory, defects models, or frustration-based theory form the correct starting points of ‘the’ theory of the glass transition?
- Is MCT really a useful theory for the first decades of slowing down of the dynamics? Can one find direct evidence that an avoided MCT transition exists and controls the dynamics?
- What is the correct physical picture for the low temperature phase of glass-forming liquids and spin glasses?
- Are there general principles governing off-equilibrium dynamics, and in particular aging and sheared materials?
- Do non-disordered, finite-dimensional, finite-range statmech model exist that display a thermodynamically stable amorphous phase at low temperature?

Finally, notice that we did not discuss possible interplays between glassiness, disorder and quantum fluctuations. This is a very fascinating topic that has boomed in recent years; new phenomena such as Many-Body Localization [469] and Quantum Scars [470] have been discovered, revealing new facets of slow dynamics. Models of classical glasses, such as the KCMs and the p -spin models found new applications in this arena [471, 472].

ACKNOWLEDGMENTS

We thank all the collaborators who worked with us on glass physics. This work was supported by a grant from the Simons Foundation (Grant No. 454933, L. B., Grant No. 454935, G. B.)

-
- [1] C. A. Angell, *Science* **267**, 1924 (1995).
- [2] P. G. Debenedetti and F. H. Stillinger, *Nature* **410**, 259 (2001).
- [3] L. Berthier and G. Biroli, *Reviews of Modern Physics* **83**, 587 (2011).
- [4] L. Struik, *Polymer Engineering & Science* **17**, 165 (1977).
- [5] A. P. Young, *Spin glasses and random fields*, Vol. 12 (World Scientific, 1998).
- [6] J.-P. Bouchaud, M. Mézard, and J. Dalibard, *Complex systems: lecture notes of the Les Houches Summer School 2006* (Elsevier, 2011).
- [7] R. Richert and C. Angell, *The Journal of chemical physics* **108**, 9016 (1998).
- [8] The terminology ‘strong’ and ‘fragile’ is not related to the mechanical properties of the glass but to the evolution of the short-range order close to T_g . Strong liquids, such as SiO_2 , have a locally tetrahedric structure which persists both below and above the glass transition contrary to fragile liquids whose short-range amorphous structure disappears rapidly upon heating above T_g .
- [9] H. Bässler, *Physical review letters* **58**, 767 (1987).
- [10] W. Kauzmann, *Chemical reviews* **43**, 219 (1948).
- [11] L. Berthier, M. Ozawa, and C. Scalliet, *The Journal of Chemical Physics* **150**, 160902 (2019).
- [12] R. Holyst, *Physica A: Statistical Mechanics and its Applications* **292**, 255 (2001).
- [13] M. Goldstein, *The Journal of Chemical Physics* **51**, 3728 (1969).
- [14] P. G. Debenedetti, *Metastable liquids: concepts and principles* (Princeton University Press, 1996).
- [15] N. Menon and S. R. Nagel, *Physical review letters* **74**, 1230 (1995).
- [16] L. Fernández, V. Martín-Mayor, and P. Verrocchio, *Physical Review E* **73**, 020501 (2006).
- [17] A. Cavagna, T. S. Grigera, and P. Verrocchio, *Physical review letters* **98**, 187801 (2007).
- [18] J. Wuttke, W. Petry, and S. Pouget, *The Journal of chemical physics* **105**, 5177 (1996).
- [19] K. Binder and W. Kob, *Glassy materials and disordered solids: An introduction to their statistical mechanics* (World scientific, 2011).
- [20] L. Pardo, P. Lunkenheimer, and A. Loidl, *Physical Review E* **76**, 030502 (2007).
- [21] L. Berthier and M. D. Ediger, *arXiv preprint arXiv:1512.03540* (2015).
- [22] R. G. Larson, *The structure and rheology of complex fluids*, Vol. 150 (Oxford university press New York, 1999).
- [23] P. N. Pusey and W. Van Meegen, *Nature* **320**, 340 (1986).
- [24] Z. Cheng, J. Zhu, P. M. Chaikin, S.-E. Phan, and W. B. Russel, *Physical Review E* **65**, 041405 (2002).
- [25] L. Berthier and T. A. Witten, *Physical Review E* **80**, 021502 (2009).
- [26] W. K. Kegels and A. van Blaaderen, *Science* **287**, 290 (2000).
- [27] E. R. Weeks, J. C. Crocker, A. C. Levitt, A. Schofield, and D. A. Weitz, *Science* **287**, 627 (2000).
- [28] G. Brambilla, D. El Masri, M. Pierno, L. Berthier, L. Cipelletti, G. Petekidis, and A. B. Schofield, *Physical review letters* **102**, 085703 (2009).
- [29] J. E. Hallett, F. Turci, and C. P. Royall, *Nature communications* **9**, 1 (2018).
- [30] A. Donev, S. Torquato, and F. H. Stillinger, *Physical Review E* **71**, 011105 (2005).
- [31] A. Donev, S. Torquato, F. H. Stillinger, and R. Connelly, *Journal of applied physics* **95**, 989 (2004).
- [32] A. J. Liu and S. R. Nagel, *Nature* **396**, 21 (1998).
- [33] P. Charbonneau, J. Kurchan, G. Parisi, P. Urbani, and F. Zamponi, *Annual Review of Condensed Matter Physics* **8**, 265 (2017).
- [34] H. M. Jaeger, S. R. Nagel, and R. P. Behringer, *Reviews of modern physics* **68**, 1259 (1996).
- [35] G. D’Anna and G. Grémaud, *Nature* **413**, 407 (2001).
- [36] G. Marty and O. Dauchot, *Physical review letters* **94**, 015701 (2005).
- [37] A. S. Keys, A. R. Abate, S. C. Glotzer, and D. J. Durian, *Nature physics* **3**, 260 (2007).
- [38] M. C. Marchetti, J.-F. Joanny, S. Ramaswamy, T. B. Liverpool, J. Prost, M. Rao, and R. A. Simha, *Reviews of Modern Physics* **85**, 1143 (2013).
- [39] C. Bechinger, R. Di Leonardo, H. Löwen, C. Reichhardt, G. Volpe, and G. Volpe, *Reviews of Modern Physics* **88**, 045006 (2016).
- [40] J. Deseigne, O. Dauchot, and H. Chaté, *Physical review letters* **105**, 098001 (2010).
- [41] I. Theurkauff, C. Cottin-Bizonne, J. Palacci, C. Ybert, and L. Bocquet, *Physical review letters* **108**, 268303 (2012).
- [42] I. Buttinoni, J. Bialké, F. Kümmel, H. Löwen, C. Bechinger, and T. Speck, *Physical review letters* **110**, 238301 (2013).
- [43] S. Henkes, Y. Fily, and M. C. Marchetti, *Physical Review E* **84**, 040301 (2011).
- [44] T. E. Angelini, E. Hannezo, X. Trepas, M. Marquez, J. J. Fredberg, and D. A. Weitz, *Proceedings of the National Academy of Sciences* **108**, 4714 (2011).
- [45] S. Garcia, E. Hannezo, J. Elgeti, J.-F. Joanny, P. Silberzan, and N. S. Gov, *Proceedings of the National Academy of Sciences* **112**, 15314 (2015).
- [46] A. Mongera, P. Rowghanian, H. J. Gustafson, E. Shelton, D. A. Kealhofer, E. K. Carn, F. Serwane, A. A. Lucio, J. Giammona, and O. Campàs, *Nature* **561**, 401 (2018).
- [47] N. Klongvessa, F. Ginot, C. Ybert, C. Cottin-Bizonne, and M. Leocmach, *Physical Review Letters* **123**, 248004 (2019).
- [48] L. Berthier and J. Kurchan, *Nature Physics* **9**, 310 (2013).
- [49] L. Berthier, E. Flenner, and G. Szamel, *The Journal of chemical physics* **150**, 200901 (2019).
- [50] R. Ni, M. A. C. Stuart, and M. Dijkstra, *Nature communications* **4**, 1 (2013).
- [51] L. Berthier, *Physical review letters* **112**, 220602 (2014).
- [52] R. Mandal, P. J. Bhuyan, M. Rao, and C. Dasgupta, *Soft Matter* **12**, 6268 (2016).
- [53] D. Bi, X. Yang, M. C. Marchetti, and M. L. Manning, *Physical Review X* **6** (2016), 10.1103/PhysRevX.6.021011.
- [54] L. Berthier, E. Flenner, and G. Szamel, *New Journal of Physics* **19**, 125006 (2017).

- [55] D. Matoz-Fernandez, K. Martens, R. Sknepnek, J. Barrat, and S. Henkes, *Soft matter* **13**, 3205 (2017).
- [56] P. Scheidler, W. Kob, K. Binder, and G. Parisi, *Philosophical Magazine B* **82**, 283 (2002).
- [57] K. Kim, *EPL (Europhysics Letters)* **61**, 790 (2003).
- [58] C. Cammarota and G. Biroli, *Proceedings of the National Academy of Sciences* **109**, 8850 (2012).
- [59] L. Berthier and W. Kob, *Physical Review E* **85** (2012), 10.1103/PhysRevE.85.011102.
- [60] S. Karmakar and I. Procaccia, *arXiv preprint arXiv:1105.4053* (2011).
- [61] C. Cammarota and G. Biroli, *The Journal of chemical physics* **138**, 12A547 (2013).
- [62] V. Krakoviack, *Physical Review E* **84**, 050501 (2011).
- [63] G. Szamel and E. Flenner, *EPL (Europhysics Letters)* **101**, 66005 (2013).
- [64] S. Franz and G. Parisi, *Journal of Statistical Mechanics: Theory and Experiment* **2013**, P11012 (2013).
- [65] C. Cammarota, *EPL (Europhysics Letters)* **101**, 56001 (2013).
- [66] S. Franz, G. Parisi, and F. Ricci-Tersenghi, *Journal of Statistical Mechanics: Theory and Experiment* **2013**, L02001 (2013).
- [67] V. Krakoviack, *The Journal of chemical physics* **141**, 104504 (2014).
- [68] A. D. Phan and K. S. Schweizer, *The Journal of chemical physics* **148**, 054502 (2018).
- [69] C. Cammarota and B. Seoane, *Physical Review B* **94**, 180201 (2016).
- [70] H. Ikeda, K. Miyazaki, and G. Biroli, *EPL (Europhysics Letters)* **116**, 56004 (2017).
- [71] W. Kob and L. Berthier, *Physical review letters* **110**, 245702 (2013).
- [72] P. Charbonneau and G. Tarjus, *Physical Review E* **87**, 042305 (2013).
- [73] S. Karmakar and G. Parisi, *Proceedings of the National Academy of Sciences* **110**, 2752 (2013).
- [74] S. Chakrabarty, S. Karmakar, and C. Dasgupta, *Scientific reports* **5**, 12577 (2015).
- [75] W. Kob and D. Coslovich, *Physical Review E* **90**, 052305 (2014).
- [76] R. L. Jack and C. J. Fullerton, *Physical Review E* **88**, 042304 (2013).
- [77] C. J. Fullerton and R. L. Jack, *Physical review letters* **112**, 255701 (2014).
- [78] Y.-W. Li, Y.-L. Zhu, and Z.-Y. Sun, *The Journal of chemical physics* **142**, 124507 (2015).
- [79] S. Chakrabarty, R. Das, S. Karmakar, and C. Dasgupta, *The Journal of chemical physics* **145**, 034507 (2016).
- [80] L. Angelani, M. Paoluzzi, G. Parisi, and G. Ruocco, *Proceedings of the National Academy of Sciences* **115**, 8700 (2018).
- [81] M. Ozawa, A. Ikeda, K. Miyazaki, and W. Kob, *Physical review letters* **121**, 205501 (2018).
- [82] S. Niblett, V. K. de Souza, R. Jack, and D. Wales, *The Journal of chemical physics* **149**, 114503 (2018).
- [83] S. Gokhale, K. H. Nagamanasa, R. Ganapathy, and A. Sood, *Nature communications* **5**, 4685 (2014).
- [84] S. Gokhale, A. Sood, and R. Ganapathy, *Advances in Physics* **65**, 363 (2016).
- [85] D. Ganapathi, K. H. Nagamanasa, A. Sood, and R. Ganapathy, *Nature communications* **9**, 1 (2018).
- [86] I. Williams, F. Turci, J. E. Hallett, P. Crowther, C. Cammarota, G. Biroli, and C. P. Royall, *Journal of Physics: Condensed Matter* **30**, 094003 (2018).
- [87] R. L. Jack and L. Berthier, *Physical Review E* **85**, 021120 (2012).
- [88] V. Krakoviack, *Physical Review E* **82**, 061501 (2010).
- [89] G. M. Hocky, L. Berthier, and D. R. Reichman, *The Journal of chemical physics* **141**, 224503 (2014).
- [90] F. Thalmann, C. Dasgupta, and D. Feinberg, *EPL (Europhysics Letters)* **50**, 54 (2000).
- [91] S. F. Swallen, K. L. Kearns, M. K. Mapes, Y. S. Kim, R. J. McMahon, M. D. Ediger, T. Wu, L. Yu, and S. Satija, *Science* **315**, 353 (2007).
- [92] M. D. Ediger, *The Journal of chemical physics* **147**, 210901 (2017).
- [93] L. Berthier, P. Charbonneau, E. Flenner, and F. Zamponi, *Physical review letters* **119**, 188002 (2017).
- [94] L. Zhu, C. Brian, S. Swallen, P. Straus, M. Ediger, and L. Yu, *Physical Review Letters* **106**, 256103 (2011).
- [95] K. L. Kearns, M. Ediger, H. Huth, and C. Schick, *The Journal of Physical Chemistry Letters* **1**, 388 (2010).
- [96] Z. Chen, A. Sepúlveda, M. Ediger, and R. Richert, *The Journal of chemical physics* **138**, 12A519 (2013).
- [97] T. Pérez-Castañeda, C. Rodríguez-Tinoco, J. Rodríguez-Viejo, and M. A. Ramos, *Proceedings of the National Academy of Sciences* **111**, 11275 (2014).
- [98] A. Sepúlveda, M. Tylinski, A. Guiseppi-Elie, R. Richert, and M. Ediger, *Physical review letters* **113**, 045901 (2014).
- [99] J. Ràfols-Ribé, P.-A. Will, C. Hänisch, M. Gonzalez-Silveira, S. Lenk, J. Rodríguez-Viejo, and S. Reineke, *Science advances* **4**, eaar8332 (2018).
- [100] A. Vila-Costa, J. Ràfols-Ribé, M. González-Silveira, A. Lopeandia, L. Abad-Muñoz, and J. Rodríguez-Viejo, *Physical Review Letters* **124**, 076002 (2020).
- [101] P. G. Wolynes, *Proceedings of the National Academy of Sciences* (2009).
- [102] S. Léonard and P. Harrowell, *The Journal of chemical physics* **133**, 244502 (2010).
- [103] I. Lyubimov, M. D. Ediger, and J. J. de Pablo, *The Journal of chemical physics* **139**, 144505 (2013).
- [104] R. L. Jack and L. Berthier, *The Journal of chemical physics* **144**, 244506 (2016).
- [105] R. Gutiérrez and J. P. Garrahan, *Journal of Statistical Mechanics: Theory and Experiment* **2016**, 074005 (2016).
- [106] C. J. Fullerton and L. Berthier, *EPL (Europhysics Letters)* **119**, 36003 (2017).
- [107] E. Flenner, L. Berthier, P. Charbonneau, and C. J. Fullerton, *Physical review letters* **123**, 175501 (2019).
- [108] D. Khomenko, C. Scalliet, L. Berthier, D. R. Reichman, and F. Zamponi, *arXiv preprint arXiv:1910.11168* (2019).
- [109] F. Krzakala, A. Montanari, F. Ricci-Tersenghi, G. Semerjian, and L. Zdeborová, *Proceedings of the National Academy of Sciences* **104**, 10318 (2007).
- [110] A. Anandkumar, R. Ge, D. Hsu, S. M. Kakade, and M. Telgarsky, *Journal of Machine Learning Research* **15**, 2773 (2014).
- [111] E. Richard and A. Montanari, in *Advances in Neural Information Processing Systems* (2014) pp. 2897–2905.
- [112] S. S. Mannelli, G. Biroli, C. Cammarota, F. Krzakala, P. Urbani, and L. Zdeborová, *Physical Review X* **10**, 011057 (2020).

- [162] P. G. Wolynes and V. Lubchenko, *Structural glasses and supercooled liquids: Theory, experiment, and applications* (John Wiley & Sons, 2012).
- [163] C. Crauste-Thibierge, C. Brun, F. Ladieu, D. Lhôte, G. Biroli, and J.-P. Bouchaud, *Physical review letters* **104**, 165703 (2010).
- [164] T. Bauer, P. Lunkenheimer, and A. Loidl, *Physical review letters* **111**, 225702 (2013).
- [165] C. Brun, F. Ladieu, D. Lhôte, G. Biroli, and J. Bouchaud, *Physical review letters* **109**, 175702 (2012).
- [166] R. Seyboldt, D. Merger, F. Coupette, M. Siebenbürger, M. Ballauff, M. Wilhelm, and M. Fuchs, *Soft Matter* **12**, 8825 (2016).
- [167] M. Tarzia, G. Biroli, A. Lefèvre, and J.-P. Bouchaud, *The Journal of chemical physics* **132**, 054501 (2010).
- [168] T. Speck, *Journal of Statistical Mechanics: Theory and Experiment* **2019**, 084015 (2019).
- [169] G. Adam and J. H. Gibbs, *The journal of chemical physics* **43**, 139 (1965).
- [170] M. Mézard, G. Parisi, and M. Virasoro, *Spin glass theory and beyond: An Introduction to the Replica Method and Its Applications*, Vol. 9 (World Scientific Publishing Company, 1987).
- [171] T. R. Kirkpatrick and D. Thirumalai, *Physical review letters* **58**, 2091 (1987).
- [172] T. Kirkpatrick and P. Wolynes, *Physical Review A* **35**, 3072 (1987).
- [173] G. Biroli and M. Mézard, *Physical review letters* **88**, 025501 (2001).
- [174] D. R. Nelson, *Defects and geometry in condensed matter physics* (Cambridge University Press, 2002).
- [175] R. K. Darst, D. R. Reichman, and G. Biroli, *The Journal of chemical physics* **132**, 044510 (2010).
- [176] A. Seif and T. S. Grigera, *arXiv preprint arXiv:1611.06754* (2016).
- [177] Y. Nishikawa and K. Hukushima, *arXiv preprint arXiv:2003.02872* (2020).
- [178] G. D. McCullagh, D. Cellai, A. Lawlor, and K. A. Dawson, *Physical Review E* **71**, 030102 (2005).
- [179] In order to have a well-defined thermodynamics, Bethe lattices are generated as random graphs with fixed connectivity, also called random regular graphs.
- [180] O. Rivoire, G. Biroli, O. C. Martin, and M. Mézard, *The European Physical Journal B-Condensed Matter and Complex Systems* **37**, 55 (2004).
- [181] D. J. Gross and M. Mézard, *Nuclear Physics B* **240**, 431 (1984).
- [182] T. Castellani and A. Cavagna, *Journal of Statistical Mechanics: Theory and Experiment* **2005**, P05012 (2005).
- [183] If additional symmetries are broken then one can have ergodicity breaking also in the RS phase.
- [184] A. Cavagna, *Physics Reports* **476**, 51 (2009).
- [185] J. Kurchan, G. Parisi, and F. Zamponi, *Journal of Statistical Mechanics: Theory and Experiment* **2012**, P10012 (2012).
- [186] J. Kurchan, G. Parisi, P. Urbani, and F. Zamponi, *The Journal of Physical Chemistry B* **117**, 12979 (2013).
- [187] G. Parisi, P. Urbani, and F. Zamponi, *Theory of Simple Glasses: Exact Solutions in Infinite Dimensions* (Cambridge University Press, 2020).
- [188] For large d the crystalline phase does not intervene. In fact, the amorphous and crystalline solid phases are well separated in configuration space and issues related to finite dimensions, such as the crystallization of monodisperse particles, are suppressed [473, 474].
- [189] P. Charbonneau, J. Kurchan, G. Parisi, P. Urbani, and F. Zamponi, *Journal of Statistical Mechanics: Theory and Experiment* **2014**, P10009 (2014).
- [190] There is of course no crystal state in disordered systems such as in Eq. (16). In the case of lattice glass models, there is a crystal phase but it can disappear depending whether the Bethe lattice is a Cayley tree or a random regular graph.
- [191] R. Monasson, *Physical review letters* **75**, 2847 (1995).
- [192] J.-L. Barrat, M. Feigelman, J. Kurchan, *et al.*, in *Slow Relaxations and Nonequilibrium Dynamics in Condensed Matter* (2004).
- [193] T. Maimbourg, J. Kurchan, and F. Zamponi, *Physical review letters* **116**, 015902 (2016).
- [194] E. Leutheusser, *Physical Review A* **29**, 2765 (1984).
- [195] U. Bengtzelius, W. Gotze, and A. Sjolander, *Journal of Physics C: solid state Physics* **17**, 5915 (1984).
- [196] S. P. Das and G. F. Mazenko, *Physical Review A* **34**, 2265 (1986).
- [197] G. Biroli and J.-P. Bouchaud, *EPL (Europhysics Letters)* **67**, 21 (2004).
- [198] G. Biroli, J.-P. Bouchaud, K. Miyazaki, and D. R. Reichman, *Physical review letters* **97**, 195701 (2006).
- [199] L. Berthier, J.-L. Barrat, and J. Kurchan, *Physical Review E* **61**, 5464 (2000).
- [200] K. Miyazaki and D. R. Reichman, *Physical Review E* **66**, 050501 (2002).
- [201] M. Fuchs and M. E. Cates, *Physical review letters* **89**, 248304 (2002).
- [202] T. R. Kirkpatrick, D. Thirumalai, and P. G. Wolynes, *Physical Review A* **40**, 1045 (1989).
- [203] J.-P. Bouchaud and G. Biroli, *The Journal of chemical physics* **121**, 7347 (2004).
- [204] M. Dzero, J. Schmalian, and P. G. Wolynes, *Physical Review B* **72**, 100201 (2005).
- [205] S. Franz, *EPL (Europhysics Letters)* **73**, 492 (2006).
- [206] G. Biroli and C. Cammarota, *Physical Review X* **7**, 011011 (2017).
- [207] C. A. Angell, *Journal of research of the National Institute of Standards and Technology* **102**, 171 (1997).
- [208] I. M. Hodge, *Journal of research of the National Institute of Standards and Technology* **102**, 195 (1997).
- [209] G. Johari, *The Journal of Chemical Physics* **112**, 7518 (2000).
- [210] M. Ozawa, C. Scalliet, A. Ninarello, and L. Berthier, *The Journal of chemical physics* **151**, 084504 (2019).
- [211] M. Mézard and G. Parisi, *Phys. Rev. Lett.* **82**, 747 (1999).
- [212] M. Ozawa and L. Berthier, *The Journal of Chemical Physics* **146**, 014502 (2017).
- [213] S. Franz, G. Parisi, F. Ricci-Tersenghi, and T. Rizzo, *The European Physical Journal E* **34**, 1 (2011).
- [214] This terminology was suggested to us by Jean-Philippe Bouchaud.
- [215] J. D. Stevenson, A. M. Walczak, R. W. Hall, and P. G. Wolynes, *The Journal of chemical physics* **129**, 194505 (2008).
- [216] G. Biroli, C. Cammarota, G. Tarjus, and M. Tarzia, *Physical Review B* **98**, 174205 (2018).
- [217] G. Biroli, C. Cammarota, G. Tarjus, and M. Tarzia, *Physical Review B* **98**, 174206 (2018).

- [218] T. Kirkpatrick and P. Wolynes, *Physical Review B* **36**, 8552 (1987).
- [219] T. Rizzo, *Physical Review B* **94**, 014202 (2016).
- [220] S. K. Nandi, G. Biroli, and G. Tarjus, *Physical review letters* **116**, 145701 (2016).
- [221] G. Biroli and J.-P. Bouchaud, *Structural Glasses and Supercooled Liquids: Theory, Experiment, and Applications*, 31 (2012).
- [222] L. Berthier, P. Charbonneau, and J. Kundu, arXiv preprint arXiv:1912.11510 (2019).
- [223] L. Berthier, G. Biroli, J.-P. Bouchaud, and G. Tarjus, *The Journal of Chemical Physics* **150**, 094501 (2019).
- [224] The difficulty is that the mapping to the RFIM proceeds by relating the overlap (for glasses) to the magnetization (for the RFIM). There are no natural dynamical equations for the overlap, and in the only cases where those have been established—the β -regime of MCT—these proved to be quite complex and different from the corresponding equations for the magnetization of the RFIM.
- [225] M. Castellana, A. Decelle, S. Franz, M. Mézard, and G. Parisi, *Physical review letters* **104**, 127206 (2010).
- [226] J. Yeo and M. Moore, *Physical Review E* **86**, 052501 (2012).
- [227] C. Cammarota, G. Biroli, M. Tarzia, and G. Tarjus, *Physical review letters* **106**, 115705 (2011).
- [228] M. C. Angelini and G. Biroli, *Proceedings of the National Academy of Sciences* **114**, 3328 (2017).
- [229] D. S. Fisher, *Physical review letters* **56**, 416 (1986).
- [230] D. Kivelson, S. A. Kivelson, X. Zhao, Z. Nussinov, and G. Tarjus, *Physica A: Statistical Mechanics and its Applications* **219**, 27 (1995).
- [231] J. Berges, N. Tetradis, and C. Wetterich, *Physics Reports* **363**, 223 (2002).
- [232] C. Rulquin, P. Urbani, G. Biroli, G. Tarjus, and M. Tarzia, *Journal of Statistical Mechanics: Theory and Experiment* **2016**, 023209 (2016).
- [233] W. Kob and H. C. Andersen, *Physical Review E* **48**, 4364 (1993).
- [234] F. Ritort and P. Sollich, *Advances in physics* **52**, 219 (2003).
- [235] S. Franz, R. Mulet, and G. Parisi, *Physical Review E* **65**, 021506 (2002).
- [236] C. Toninelli, G. Biroli, and D. S. Fisher, *Physical review letters* **92**, 185504 (2004).
- [237] A. C. Pan, J. P. Garrahan, and D. Chandler, *Physical Review E* **72**, 041106 (2005).
- [238] S. H. Glarum, *The Journal of Chemical Physics* **33**, 639 (1960).
- [239] G. H. Fredrickson and H. C. Andersen, *Physical review letters* **53**, 1244 (1984).
- [240] S. Léonard, P. Mayer, P. Sollich, L. Berthier, and J. P. Garrahan, *Journal of statistical mechanics: theory and experiment* **2007**, P07017 (2007).
- [241] M. H. Cohen and G. Grest, *Physical Review B* **26**, 6313 (1982).
- [242] G. H. Fredrickson and S. A. Brawer, *The Journal of chemical physics* **84**, 3351 (1986).
- [243] S. Butler and P. Harrowell, *The Journal of chemical physics* **95**, 4454 (1991).
- [244] C. Toninelli, G. Biroli, and D. S. Fisher, *Physical review letters* **96**, 035702 (2006).
- [245] Y. Elmatad, D. Chandler, and J. Garrahan, *The journal of physical chemistry. B* **113**, 5563 (2009).
- [246] Y. S. Elmatad, R. L. Jack, D. Chandler, and J. P. Garrahan, *Proceedings of the National Academy of Sciences* **107**, 12793 (2010).
- [247] Y. S. Elmatad and A. S. Keys, *Physical Review E - Statistical, Nonlinear, and Soft Matter Physics* **85** (2012), 10.1103/PhysRevE.85.061502, arXiv: 1202.5527 ISBN: 1539-3755\r1550-2376.
- [248] I. Hartarsky, L. Maréché, and C. Toninelli, arXiv preprint arXiv:1904.09145 (2019).
- [249] F. Martinelli, R. Morris, and C. Toninelli, *Communications in mathematical physics* **369**, 761 (2019).
- [250] I. Hartarsky, F. Martinelli, and C. Toninelli, arXiv preprint arXiv:1910.06782 (2019).
- [251] F. Martinelli, C. Toninelli, *et al.*, *The Annals of Probability* **47**, 324 (2019).
- [252] A. S. Keys, J. P. Garrahan, and D. Chandler, *Proceedings of the National Academy of Sciences* **110**, 4482 (2013).
- [253] A. S. Keys, L. O. Hedges, J. P. Garrahan, S. C. Glotzer, and D. Chandler, *Physical Review X* **1**, 1 (2011), arXiv: 1107.3628.
- [254] J. P. Garrahan and D. Chandler, *Physical review letters* **89**, 035704 (2002).
- [255] S. Whitelam, L. Berthier, and J. P. Garrahan, *Physical Review E* **71**, 026128 (2005).
- [256] L. Berthier and J. P. Garrahan, *The journal of physical chemistry B* **109**, 3578 (2005).
- [257] R. L. Jack, P. Mayer, and P. Sollich, *Journal of Statistical Mechanics: Theory and Experiment* **2006**, P03006 (2006).
- [258] L. Berthier, D. Chandler, and J. P. Garrahan, *EPL (Europhysics Letters)* **69**, 320 (2004).
- [259] D. Chandler, J. P. Garrahan, R. L. Jack, L. Maibaum, and A. C. Pan, *Physical Review E* **74**, 051501 (2006).
- [260] S. Whitelam, L. Berthier, and J. P. Garrahan, *Physical review letters* **92**, 185705 (2004).
- [261] A critical (different) behaviour is expected and predicted for models having a transition [244].
- [262] M. T. Downton and M. P. Kennett, *Physical Review E* **76**, 031502 (2007).
- [263] L. O. Hedges, R. L. Jack, J. P. Garrahan, and D. Chandler, *Science* **323**, 1309 (2009).
- [264] A. S. Keys, D. Chandler, and J. P. Garrahan, *Physical Review E - Statistical, Nonlinear, and Soft Matter Physics* **92**, 1 (2015), arXiv: 1401.7206v1.
- [265] M. Isobe, A. S. Keys, D. Chandler, and J. P. Garrahan, *Physical Review Letters* **117**, 1 (2016), arXiv: 1604.02621.
- [266] J. P. Garrahan, *Journal of Physics: Condensed Matter* **14**, 1571 (2002).
- [267] R. M. Turner, R. L. Jack, and J. P. Garrahan, *Physical Review E* **92** (2015), 10.1103/PhysRevE.92.022115.
- [268] R. L. Jack, L. Berthier, and J. P. Garrahan, *Physical Review E* **72**, 016103 (2005).
- [269] This type of plaquette models, and other spin models, were introduced originally [475, 476] to show how ultra-slow glassy dynamics can emerge because of growing free energy barriers.
- [270] G. Biroli, J.-P. Bouchaud, and G. Tarjus, *The Journal of chemical physics* **123**, 044510 (2005).
- [271] L. Berthier and J. P. Garrahan, *The Journal of chemical physics* **119**, 4367 (2003).
- [272] S. Whitelam and J. P. Garrahan, *The Journal of Physical Chemistry B* **108**, 6611 (2004).

- [273] R. L. Jack and J. P. Garrahan, *The Journal of chemical physics* **123**, 164508 (2005).
- [274] Most KCMs do not have a finite temperature dynamical transition and the ones displaying a transition have critical properties different from MCT.
- [275] L. Berthier, G. Biroli, D. Coslovich, W. Kob, and C. Toninelli, *Physical Review E* **86**, 031502 (2012).
- [276] F. C. Frank, *Proceedings of the Royal Society of London. Series A. Mathematical and Physical Sciences* **215**, 43 (1952).
- [277] F. Sausset, G. Tarjus, and P. Viot, *Journal of Statistical Mechanics: Theory and Experiment* **2009**, P04022 (2009).
- [278] J.-P. Vest, G. Tarjus, and P. Viot, *Molecular Physics* **112**, 1330 (2014).
- [279] J.-P. Vest, G. Tarjus, and P. Viot, *The Journal of Chemical Physics* **143**, 084505 (2015).
- [280] F. Turci, G. Tarjus, and C. P. Royall, *Physical Review Letters* **118**, 1 (2017), arXiv: 1609.03044.
- [281] D. Coslovich and G. Pastore, *The Journal of chemical physics* **127**, 124504 (2007).
- [282] D. Coslovich, *Physical Review E - Statistical, Nonlinear, and Soft Matter Physics* **83**, 1 (2011), arXiv: 1102.5663.
- [283] C. P. Royall and S. R. Williams, *Physics Reports* **560**, 1 (2015).
- [284] A. Malins, J. Eggers, C. P. Royall, S. R. Williams, and H. Tanaka, *The Journal of chemical physics* **138**, 12A535 (2013).
- [285] A. Malins, S. R. Williams, J. Eggers, and C. P. Royall, *The Journal of chemical physics* **139**, 234506 (2013).
- [286] C. P. Royall and W. Kob, *Journal of Statistical Mechanics: Theory and Experiment* **2017** (2017), 10.1088/1742-5468/aa4e92, arXiv: 1611.03314 Publisher: IOP Publishing.
- [287] F. Turci, C. P. Royall, and T. Speck, *Physical Review X* **7** (2017), 10.1103/PhysRevX.7.031028.
- [288] F. Turci, T. Speck, and C. P. Royall, *The European Physical Journal E* **41** (2018), 10.1140/epje/i2018-11662-3.
- [289] F. Turci, C. Patrick Royall, and T. Speck, *Journal of Physics: Conference Series* **1252**, 012012 (2019).
- [290] H. Tong and H. Tanaka, *Physical Review X* **8** (2018), 10.1103/PhysRevX.8.011041.
- [291] R. Shi and H. Tanaka, *Science Advances* **5**, eaav3194 (2019).
- [292] R. Pinchaipat, M. Campo, F. Turci, J. E. Hallett, T. Speck, and C. P. Royall, *Physical Review Letters* **119** (2017), 10.1103/PhysRevLett.119.028004.
- [293] S. Mossa and G. Tarjus, *Journal of Non-Crystalline Solids* **352**, 4847 (2006).
- [294] J. Paret, R. L. Jack, and D. Coslovich, *The Journal of chemical physics* **152**, 144502 (2020).
- [295] E. Boattini, S. Marín-Aguilar, S. Mitra, G. Foffi, F. Smallenburg, and L. Filion, arXiv preprint arXiv:2003.00586 (2020).
- [296] C. Scalliet, L. Berthier, and F. Zamponi, *Physical Review E* **99**, 012107 (2019).
- [297] G. Parisi and F. Slanina, *Physical Review E* **62**, 6554 (2000).
- [298] G. Parisi and F. Zamponi, *Rev. Mod. Phys.* **82**, 789 (2010).
- [299] E. Gardner, *Nuclear Physics B* **257**, 747 (1985).
- [300] L. Berthier, G. Biroli, P. Charbonneau, E. I. Corwin, S. Franz, and F. Zamponi, *The Journal of chemical physics* **151**, 010901 (2019).
- [301] C. Rainone and P. Urbani, *Journal of Statistical Mechanics: Theory and Experiment* **2016**, 053302 (2016).
- [302] S. Franz, G. Parisi, M. Sevelev, P. Urbani, and F. Zamponi, *SciPost Phys* **2**, 019 (2017).
- [303] C. Scalliet and L. Berthier, *Physical review letters* **122**, 255502 (2019).
- [304] Q. Liao and L. Berthier, *Physical Review X* **9**, 011049 (2019).
- [305] C. Scalliet, L. Berthier, and F. Zamponi, *Nature communications* **10**, 1 (2019).
- [306] L. Berthier, P. Charbonneau, Y. Jin, G. Parisi, B. Seoane, and F. Zamponi, *Proceedings of the National Academy of Sciences* **113**, 8397 (2016).
- [307] C. Scalliet, L. Berthier, and F. Zamponi, *Physical review letters* **119**, 205501 (2017).
- [308] P. Chaudhuri, L. Berthier, and S. Sastry, *Physical review letters* **104**, 165701 (2010).
- [309] A. J. Liu and S. R. Nagel, *Annu. Rev. Condens. Matter Phys.* **1**, 347 (2010).
- [310] C. S. O'Hern, S. A. Langer, A. J. Liu, and S. R. Nagel, *Physical Review Letters* **88**, 075507 (2002).
- [311] C. S. O'hern, L. E. Silbert, A. J. Liu, and S. R. Nagel, *Physical Review E* **68**, 011306 (2003).
- [312] D. J. Durian, *Physical review letters* **75**, 4780 (1995).
- [313] M. Wyart, *Physical review letters* **109**, 125502 (2012).
- [314] M. Wyart, S. R. Nagel, and T. A. Witten, *EPL (Europhysics Letters)* **72**, 486 (2005).
- [315] M. Wyart, *EPL (Europhysics Letters)* **89**, 64001 (2010).
- [316] E. Degiuli, E. Lerner, and M. Wyart, *The Journal of chemical physics* **142**, 164503 (2015).
- [317] P. Charbonneau, E. I. Corwin, G. Parisi, and F. Zamponi, *Physical review letters* **109**, 205501 (2012).
- [318] P. Charbonneau, E. I. Corwin, G. Parisi, and F. Zamponi, *Physical review letters* **114**, 125504 (2015).
- [319] E. DeGiuli, E. Lerner, C. Brito, and M. Wyart, *Proceedings of the National Academy of Sciences* **111**, 17054 (2014).
- [320] E. Lerner, G. Düring, and M. Wyart, *Soft Matter* **9**, 8252 (2013).
- [321] A. Ikeda, L. Berthier, and G. Biroli, *The Journal of chemical physics* **138**, 12A507 (2013).
- [322] C. Brito and M. Wyart, *The Journal of chemical physics* **131**, 149 (2009).
- [323] C. F. Schreck, T. Bertrand, C. S. O'Hern, and M. Shattuck, *Physical review letters* **107**, 078301 (2011).
- [324] H. Mizuno, H. Shiba, and A. Ikeda, *Proceedings of the National Academy of Sciences* **114**, E9767 (2017).
- [325] S. Franz, G. Parisi, P. Urbani, and F. Zamponi, *Proceedings of the National Academy of Sciences* **112**, 14539 (2015).
- [326] L. Berthier, H. Jacquin, and F. Zamponi, *Physical Review E* **84**, 051103 (2011).
- [327] P. Charbonneau, E. I. Corwin, G. Parisi, A. Poncet, and F. Zamponi, *Physical review letters* **117**, 045503 (2016).
- [328] E. Lerner, G. Düring, and E. Bouchbinder, *Physical review letters* **117**, 035501 (2016).
- [329] C. Rainone, P. Urbani, H. Yoshino, and F. Zamponi, *Physical review letters* **114**, 015701 (2015).
- [330] H. Yoshino and F. Zamponi, *Physical Review E* **90**, 022302 (2014).
- [331] G. Biroli and P. Urbani, *Nature physics* **12**, 1130 (2016).

- [332] P. Urbani and F. Zamponi, *Physical review letters* **118**, 038001 (2017).
- [333] I. R. Peters, S. Majumdar, and H. M. Jaeger, *Nature* **532**, 214 (2016).
- [334] G. Parisi, I. Procaccia, C. Rainone, and M. Singh, *Proceedings of the National Academy of Sciences* **114**, 5577 (2017).
- [335] J. Lin, E. Lerner, A. Rosso, and M. Wyart, *Proceedings of the National Academy of Sciences* **111**, 14382 (2014).
- [336] M. Ozawa, L. Berthier, G. Biroli, A. Rosso, and G. Tarjus, *Proceedings of the National Academy of Sciences* **115**, 6656 (2018).
- [337] L. Berthier, D. Coslovich, A. Ninarello, and M. Ozawa, *Physical Review Letters* **116** (2016), 10.1103/PhysRevLett.116.238002.
- [338] A. Ninarello, L. Berthier, and D. Coslovich, *Physical Review X* **7** (2017), 10.1103/PhysRevX.7.021039.
- [339] D. Gazzillo and G. Pastore, *Chemical Physics Letters* **159**, 388 (1989).
- [340] T. S. Grigera and G. Parisi, *Physical Review E* **63** (2001), 10.1103/PhysRevE.63.045102.
- [341] A. S. Ninarello, *Computer simulations of supercooled liquids near the experimental glass transition*, Ph.D. thesis, Montpellier (2017).
- [342] C. Brito, E. Lerner, and M. Wyart, *Physical Review X* **8** (2018), 10.1103/PhysRevX.8.031050.
- [343] G. Kapteijns, W. Ji, C. Brito, M. Wyart, and E. Lerner, *Physical Review E* **99** (2019), 10.1103/PhysRevE.99.012106.
- [344] L. Berthier, E. Flenner, C. J. Fullerton, C. Scalliet, and M. Singh, *Journal of Statistical Mechanics: Theory and Experiment* **2019**, 064004 (2019).
- [345] L. Berthier, P. Charbonneau, and J. Kundu, *Physical Review E* **99** (2019), 10.1103/PhysRevE.99.031301.
- [346] A. D. Parmar, M. Ozawa, and L. Berthier, *arXiv preprint arXiv:2002.01317* (2020).
- [347] D. Coslovich, M. Ozawa, and L. Berthier, *Journal of Physics: Condensed Matter* **30**, 144004 (2018).
- [348] M. Ozawa, G. Parisi, and L. Berthier, *The Journal of Chemical Physics* **149**, 154501 (2018).
- [349] L. Berthier, P. Charbonneau, A. Ninarello, M. Ozawa, and S. Yaida, *Nature Communications* **10** (2019), 10.1038/s41467-019-09512-3.
- [350] L. Berthier, P. Charbonneau, D. Coslovich, A. Ninarello, M. Ozawa, and S. Yaida, *Proceedings of the National Academy of Sciences* **114**, 11356 (2017).
- [351] S. Yaida, L. Berthier, P. Charbonneau, and G. Tarjus, *Physical Review E* **94** (2016), 10.1103/PhysRevE.94.032605.
- [352] B. Guiselin, L. Berthier, and G. Tarjus, *arXiv preprint arXiv:2004.10555* (2020).
- [353] L. Wang, A. Ninarello, P. Guan, L. Berthier, G. Szamel, and E. Flenner, *Nature communications* **10**, 1 (2019).
- [354] L. Wang, L. Berthier, E. Flenner, P. Guan, and G. Szamel, *Soft matter* **15**, 7018 (2019).
- [355] M. Wyart and M. E. Cates, *Physical Review Letters* **119** (2017), 10.1103/PhysRevLett.119.195501.
- [356] R. Gutierrez, J. P. Garrahan, and R. L. Jack, *arXiv:1901.07797 [cond-mat]* (2019), arXiv:1901.07797.
- [357] H. Ikeda, F. Zamponi, and A. Ikeda, *The Journal of Chemical Physics* **147**, 234506 (2017).
- [358] G. Szamel, *Physical Review E* **98** (2018), 10.1103/PhysRevE.98.050601.
- [359] S. Franz and G. Parisi, *Physical Review Letters* **79**, 2486 (1997).
- [360] S. Franz and G. Parisi, *Physica A* , 23 (1998).
- [361] M. Cardenas, S. Franz, and G. Parisi, *The Journal of Chemical Physics* **110**, 1726 (1999).
- [362] C. Donati, S. Franz, S. C. Glotzer, and G. Parisi, *Journal of Non-Crystalline Solids* **307-310**, 215 (2002).
- [363] G. Biroli, C. Cammarota, G. Tarjus, and M. Tarzia, *Physical review letters* **112**, 175701 (2014).
- [364] L. Berthier, *Physical Review E* **88** (2013), 10.1103/PhysRevE.88.022313.
- [365] L. Berthier and R. L. Jack, *Physical Review Letters* **114** (2015), 10.1103/PhysRevLett.114.205701.
- [366] R. L. Jack and J. P. Garrahan, *Physical Review Letters* **116** (2016), 10.1103/PhysRevLett.116.055702.
- [367] G. Parisi and B. Seoane, *Physical Review E* **89**, 022309 (2014).
- [368] G. Biroli, C. Rulquin, G. Tarjus, and M. Tarzia, *SciPost Physics* **1** (2016), 10.21468/SciPostPhys.1.1.007.
- [369] L. Berthier and D. Coslovich, *Proceedings of the National Academy of Sciences* **111**, 11668 (2014).
- [370] A. Montanari and G. Semerjian, *Journal of statistical physics* **125**, 23 (2006).
- [371] M. Mézard and A. Montanari, *Journal of statistical physics* **124**, 1317 (2006).
- [372] G. Biroli, J.-P. Bouchaud, A. Cavagna, T. S. Grigera, and P. Verrocchio, *Nature Physics* **4**, 771 (2008).
- [373] A. Cavagna, T. S. Grigera, and P. Verrocchio, *The Journal of Chemical Physics* **136**, 204502 (2012).
- [374] L. Berthier, P. Charbonneau, and S. Yaida, *The Journal of Chemical Physics* **144**, 024501 (2016).
- [375] P. Charbonneau, E. Dyer, J. Lee, and S. Yaida, *Journal of Statistical Mechanics: Theory and Experiment* **2016**, 074004 (2016).
- [376] J. Russo and H. Tanaka, *Proceedings of the National Academy of Sciences* **112**, 6920 (2015).
- [377] Y.-W. Li, W.-S. Xu, and Z.-Y. Sun, *The Journal of Chemical Physics* **140**, 124502 (2014).
- [378] J. P. Garrahan, R. L. Jack, V. Lecomte, E. Pitard, K. van Duijvendijk, and F. van Wijland, *Physical Review Letters* **98** (2007), 10.1103/PhysRevLett.98.195702.
- [379] J. P. Garrahan, R. L. Jack, V. Lecomte, E. Pitard, K. van Duijvendijk, and F. van Wijland, *Journal of Physics A: Mathematical and Theoretical* **42**, 075007 (2009).
- [380] F. Noe, C. Schutte, E. Vanden-Eijnden, L. Reich, and T. R. Weigl, *Proceedings of the National Academy of Sciences* **106**, 19011 (2009), ISBN: 0027-8424.
- [381] R. L. Jack, L. O. Hedges, J. P. Garrahan, and D. Chandler, *Physical Review Letters* **107** (2011), 10.1103/PhysRevLett.107.275702.
- [382] R. L. Jack and J. P. Garrahan, *Physical Review E* **81**, 011111 (2010).
- [383] S. S. Schoenholz, in *Journal of Physics: Conference Series*, Vol. 1036 (IOP Publishing, 2018) p. 012021.
- [384] R. Candelier, O. Dauchot, and G. Biroli, *Physical Review Letters* **102**, 1 (2009), arXiv: 0811.0201 ISBN: 0031-9007.
- [385] R. Candelier, A. Widmer-Cooper, J. K. Kummerfeld, O. Dauchot, G. Biroli, P. Harrowell, and D. R. Reichman, *Physical Review Letters* **105**, 135702 (2010),

- arXiv: 0912.0193 ISBN: 0031-9007\n1079-7114.
- [386] R. Candelier, O. Dauchot, and G. Biroli, *EPL (Europhysics Letters)* **92**, 24003 (2010), arXiv: 0912.0472 ISBN: 0295-5075\n1286-4854.
- [387] R. Candelier, A. Widmer-Cooper, J. K. Kummerfeld, O. Dauchot, G. Biroli, P. Harrowell, and D. R. Reichman, *Physical Review Letters* **105** (2010), 10.1103/PhysRevLett.105.135702, arXiv: 0912.0193.
- [388] E. D. Cubuk, S. S. Schoenholz, E. Kaxiras, and A. J. Liu, *Journal of Physical Chemistry B* **120**, 6139 (2016), ISBN: 1520-5207 (Electronic) 1520-5207 (Linking).
- [389] S. S. Schoenholz, E. D. Cubuk, E. Kaxiras, and A. J. Liu, *Proceedings of the National Academy of Sciences* **114**, 263 (2016), arXiv: 1607.06969.
- [390] F. P. Landes, G. Biroli, O. Dauchot, A. J. Liu, and D. R. Reichman, *Physical Review E* **101**, 010602 (2020).
- [391] E. D. Cubuk, S. S. Schoenholz, J. M. Rieser, B. D. Malone, J. Rottler, D. J. Durian, E. Kaxiras, and A. J. Liu, *Physical Review Letters* **114**, 1 (2015), arXiv: 1409.6820.
- [392] S. S. Schoenholz, E. D. Cubuk, D. M. Sussman, E. Kaxiras, and A. J. Liu, *Nature Physics* **12**, 469 (2015), arXiv: 1506.07772 ISBN: 1745-2473.
- [393] R. Ivancic, E. Cubuk, S. Schoenholz, D. Strickland, D. Gianola, and A. Liu, *Bulletin of the American Physical Society* **62** (2017).
- [394] E. D. Cubuk, R. J. S. Ivancic, S. S. Schoenholz, D. J. Strickland, A. Basu, Z. S. Davidson, J. Fontaine, J. L. Hor, Y.-R. Huang, Y. Jiang, N. C. Keim, K. D. Koshigan, J. A. Lefever, T. Liu, X.-G. Ma, D. J. Magagnosc, E. Morrow, C. P. Ortiz, J. M. Rieser, A. Shavit, T. Still, Y. Xu, Y. Zhang, K. N. Nordstrom, P. E. Arratia, R. W. Carpick, D. J. Durian, Z. Fakhraai, D. J. Jerolmack, D. Lee, J. Li, R. Riggelman, K. T. Turner, A. G. Yodh, D. S. Gianola, and A. J. Liu, *Science* **358**, 1033 (2017), ISBN: 3487716170192.
- [395] T. A. Sharp, S. L. Thomas, E. D. Cubuk, S. S. Schoenholz, D. J. Srolovitz, and A. J. Liu, *Proceedings of the National Academy of Sciences* **115**, 10943 (2018).
- [396] V. Bapst, T. Keck, A. Grabska-Barwińska, C. Donner, E. D. Cubuk, S. Schoenholz, A. Obika, A. Nelson, T. Back, D. Hassabis, *et al.*, *Nature Physics* **16**, 448 (2020).
- [397] A. Widmer-Cooper and P. Harrowell, *Physical review letters* **96**, 185701 (2006).
- [398] J.-P. Bouchaud, *Journal de Physique I* **2**, 1705 (1992).
- [399] A. Bray and M. Moore, *Journal of Physics C: Solid State Physics* **17**, L463 (1984).
- [400] J. van Hemmen and I. Morgenstern, in *Lecture Notes in Physics, Berlin Springer Verlag*, Vol. 275 (1987).
- [401] D. S. Fisher and D. A. Huse, *Physical review letters* **56**, 1601 (1986).
- [402] J. Kisker, L. Santen, M. Schreckenberg, and H. Rieger, *Physical Review B* **53**, 6418 (1996).
- [403] P. Refregier, E. Vincent, J. Hammann, and M. Ocio, *Journal De Physique* **48**, 1533 (1987).
- [404] L. Berthier and A. Young, *Physical Review B* **71**, 214429 (2005).
- [405] L. Berthier and J.-P. Bouchaud, *Physical Review B* **66**, 054404 (2002).
- [406] J.-P. Bouchaud, V. Dupuis, J. Hammann, and E. Vincent, *Physical review B* **65**, 024439 (2001).
- [407] F. Bert, V. Dupuis, E. Vincent, J. Hammann, and J.-P. Bouchaud, *Physical review letters* **92**, 167203 (2004).
- [408] A. Bray and M. Moore, *Physical review letters* **58**, 57 (1987).
- [409] P. Jönsson, R. Mathieu, P. Nordblad, H. Yoshino, H. A. Katori, and A. Ito, *Physical Review B* **70**, 174402 (2004).
- [410] L. F. Cugliandolo and J. Kurchan, *Physical Review Letters* **71**, 173 (1993).
- [411] L. F. Cugliandolo and J. Kurchan, *Journal of Physics A: Mathematical and General* **27**, 5749 (1994).
- [412] A. Crisanti and F. Ritort, *Journal of Physics A: Mathematical and General* **36**, R181 (2003).
- [413] J. Kurchan, T. Maimbourg, and F. Zamponi, *Journal of Statistical Mechanics: Theory and Experiment* **2016**, 033210 (2016).
- [414] A. Manacorda, G. Schehr, and F. Zamponi, *The Journal of Chemical Physics* **152**, 164506 (2020).
- [415] E. Agoritsas, G. Biroli, P. Urbani, and F. Zamponi, *Journal of Physics A: Mathematical and Theoretical* **51**, 085002 (2018).
- [416] E. Agoritsas, T. Maimbourg, and F. Zamponi, *Journal of Physics A: Mathematical and Theoretical* **52**, 144002 (2019).
- [417] A. Altieri, G. Biroli, and C. Cammarota, arXiv preprint arXiv:2005.05118 (2020).
- [418] J. Kurchan and L. Laloux, *Journal of Physics A: Mathematical and General* **29**, 1929 (1996).
- [419] L. F. Cugliandolo, J. Kurchan, and L. Peliti, *Physical Review E* **55**, 3898 (1997).
- [420] J. Kurchan, *Nature* **433**, 222 (2005).
- [421] L. Berthier and J.-L. Barrat, *Physical review letters* **89**, 095702 (2002).
- [422] S. Franz, M. Mézard, G. Parisi, and L. Peliti, *Physical Review Letters* **81**, 1758 (1998).
- [423] L. Berthier, *Physical review letters* **98**, 220601 (2007).
- [424] T. S. Grigera and N. Israeloff, *Physical Review Letters* **83**, 5038 (1999).
- [425] B. Abou and F. Gallet, *Physical Review Letters* **93**, 160603 (2004).
- [426] P. Wang, C. Song, and H. A. Makse, *Nature Physics* **2**, 526 (2006).
- [427] L. Bellon, S. Ciliberto, and C. Laroche, *EPL (Europhysics Letters)* **53**, 511 (2001).
- [428] L. Bellon and S. Ciliberto, *Physica D: Nonlinear Phenomena* **168**, 325 (2002).
- [429] L. Buisson, L. Bellon, and S. Ciliberto, *Journal of Physics: Condensed Matter* **15**, S1163 (2003).
- [430] L. Buisson, S. Ciliberto, and A. Garcimartin, *EPL (Europhysics Letters)* **63**, 603 (2003).
- [431] J. Talbot, G. Tarjus, and P. Viot, *Journal of Physics A: Mathematical and General* **36**, 9009 (2003).
- [432] M. Nicodemi, *Physical review letters* **82**, 3734 (1999).
- [433] F. Krzkalá, *Physical review letters* **94**, 077204 (2005).
- [434] M. Depken and R. Stinchcombe, *Physical Review E* **71**, 065102 (2005).
- [435] S. Fielding and P. Sollich, *Physical review letters* **88**, 050603 (2002).
- [436] A. Bray, *Advances in Physics* **43**, 357 (1994).
- [437] A. Barrat, *Physical Review E* **57**, 3629 (1998).
- [438] L. Berthier, J.-L. Barrat, and J. Kurchan, *The European Physical Journal B-Condensed Matter and Complex Systems* **11**, 635 (1999).
- [439] C. Godrèche and J. Luck, *Journal of Physics A: Mathematical and General* **33**, 1151 (2000).

- [440] E. Lippiello and M. Zannetti, *Physical Review E* **61**, 3369 (2000).
- [441] C. Godreche and J. Luck, *Journal of Physics A: Mathematical and General* **33**, 9141 (2000).
- [442] P. Mayer, L. Berthier, J. P. Garrahan, and P. Sollich, *Physical Review E* **68**, 016116 (2003).
- [443] P. Calabrese and A. Gambassi, *Journal of Physics A: Mathematical and General* **38**, R133 (2005).
- [444] P. Mayer and P. Sollich, *Journal of Physics A: Mathematical and Theoretical* **40**, 5823 (2007).
- [445] P. Mayer, S. Léonard, L. Berthier, J. P. Garrahan, and P. Sollich, *Physical review letters* **96**, 030602 (2006).
- [446] R. L. Jack, L. Berthier, and J. P. Garrahan, *Journal of Statistical Mechanics: Theory and Experiment* **2006**, P12005 (2006).
- [447] A. Crisanti and F. Ritort, *EPL (Europhysics Letters)* **51**, 147 (2000).
- [448] A. Crisanti and F. Ritort, *EPL (Europhysics Letters)* **52**, 640 (2000).
- [449] M. Baity-Jesi, A. Achard-de Lustrac, and G. Biroli, *Physical Review E* **98**, 012133 (2018).
- [450] M. Baity-Jesi, G. Biroli, and C. Cammarota, *Journal of Statistical Mechanics: Theory and Experiment* **2018**, 013301 (2018).
- [451] A. Billoire, L. Giomi, and E. Marinari, *EPL (Europhysics Letters)* **71**, 824 (2005).
- [452] D. A. Stariolo and L. F. Cugliandolo, *EPL (Europhysics Letters)* **127**, 16002 (2019).
- [453] G. B. Arous, A. Bovier, and V. Gaynard, *Physical review letters* **88**, 087201 (2002).
- [454] V. Gaynard, *Probability Theory and Related Fields* **174**, 501 (2019).
- [455] J. C. Dyre, *Physical review letters* **58**, 792 (1987).
- [456] A. Barrat and M. Mézard, *Journal de Physique I* **5**, 941 (1995).
- [457] C. Cammarota and E. Marinari, *Journal of Statistical Mechanics: Theory and Experiment* **2018**, 043303 (2018).
- [458] C. Cammarota and E. Marinari, *Physical Review E* **92**, 010301 (2015).
- [459] V. Ros, G. Biroli, and C. Cammarota, *EPL (Europhysics Letters)* **126**, 20003 (2019).
- [460] S. Büchner and A. Heuer, *Physical Review E* **60**, 6507 (1999).
- [461] B. Doliwa and A. Heuer, *Physical Review E* **67**, 030501 (2003).
- [462] A. Heuer, *Journal of Physics: Condensed Matter* **20**, 373101 (2008).
- [463] R. A. Denny, D. R. Reichman, and J.-P. Bouchaud, *Physical review letters* **90**, 025503 (2003).
- [464] G. McKenna and A. Kovacs, *Polymer Engineering & Science* **24**, 1138 (1984).
- [465] P. Sollich, F. Lequeux, P. Hébraud, and M. E. Cates, *Physical review letters* **78**, 2020 (1997).
- [466] A. Ikeda, L. Berthier, and P. Sollich, *Physical review letters* **109**, 018301 (2012).
- [467] P. Sollich, *Physical Review E* **58**, 738 (1998).
- [468] L. Berthier and J.-L. Barrat, *The Journal of Chemical Physics* **116**, 6228 (2002).
- [469] R. Nandkishore and D. A. Huse, *Annu. Rev. Condens. Matter Phys.* **6**, 15 (2015).
- [470] C. J. Turner, A. A. Michailidis, D. A. Abanin, M. Serbyn, and Z. Papić, *Nature Physics* **14**, 745 (2018).
- [471] N. Pancotti, G. Giudice, J. I. Cirac, J. P. Garrahan, and M. C. Bañuls, *Physical Review X* **10**, 021051 (2020).
- [472] D. Facoetti, G. Biroli, J. Kurchan, and D. R. Reichman, *Physical Review B* **100**, 205108 (2019).
- [473] M. Skoge, A. Donev, F. H. Stillinger, and S. Torquato, *Physical Review E* **74**, 041127 (2006).
- [474] J. A. van Meel, B. Charbonneau, A. Fortini, and P. Charbonneau, *Physical Review E* **80**, 061110 (2009).
- [475] A. Lipowski, D. Johnston, and D. Espriu, *Physical Review E* **62**, 3404 (2000).
- [476] J. P. Sethna, J. D. Shore, and M. Huang, *Physical Review B* **44**, 4943 (1991).